Indian J Chem
APRIL 1992

CODEN : IJOCAP 31A(4) 215-290 (1992)
ISSN : 0376-4710

INDIAN JOURNAL OF CHEMISTRY

SECTION A

(Inorganic, Bio-inorganic, Physical, Theoretical & Analytical Chemistry)

Published by
PUBLICATIONS & INFORMATION DIRECTORATE, CSIR, NEW DELHI
in association with
THE INDIAN NATIONAL SCIENCE ACADEMY, NEW DELHI

GOLDEN OFFER

You can now book your copies of the popular science titles under

CSIR GOLDEN JUBILEE SERIES

in advance

Titles now available

BODY'S BATTLES

BY BAL PHONDKE

This attractive and lavishly illustrated book unfolds the dramatic story of our inner defence organisation, the diversity and specificity of its armament, and the methodical way in which it maintains round the clock vigil to meet squarely every imaginable threat to the human body and also how it wins the Body's Battles most of the time.

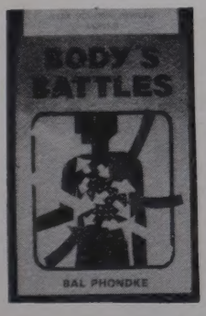

ISBN-81-85038-99-6
(Paperback)
84 pages, price Rs. 9.00
ISBN-81-7236-003-7
(Hardcover)
84 pages, price Rs. 18.00

HIS MASTER'S SLAVE

BY TAPAN BHATTACHARYA

This book, full of illustrations, explains even to the non-specialist the core concepts of computers. Against the backdrop of a canvas rich in detail is revealed the riveting story of modern day genie of the bottle, the PC.

ISBN 81-7236-018-5
(Paperback)
88 pages, price Rs. 10.00
ISBN 81-7236-019-3
(Hardcover)
88 pages, price Rs. 18.00

MINING THE OCEAN

BY T.K.S. MURTHY

This well illustrated book written especially for the non-specialist, reveals the timeless secrets of the seas. It unfolds in exquisite detail the bounty that seas hold in reserve and highlights man's attempts at mining the oceans.

ISBN 81-7236-014-2
(Paperback)
106 pages,
price Rs. 12.00
ISBN 81-7236-015-0
(Hardcover)
106 pages,
price Rs. 20.00

INSIDE STARS

BY BIMAN BASU

This attractive and lavishly illustrated book written especially for the non-specialist provides a privileged glimpse into star nurseries, tracking their luminescent trail to an ultimate fiery senescence and death. It reveals the mysteries and marvels that reign inside stars.

ISBN 81-7236-022-3
(Paperback)
90 pages,
price Rs. 10.00
ISBN 81-7236-023-1
(Hardcover)
90 pages,
price Rs. 18.00

FORTHCOMING TITLES

- PLASTIC FEAST
- ARTIFICIAL INTELLIGENCE
- VERSATILE CERAMICS
- HARDY COMPOSITES
- ALTERNATIVE ENERGY
- DESIGNER MOLECULES

You may place order for all the 10 titles by sending Rs.120.00 (for paperback) or Rs.200 (for hardcover) including postage, by Demand Draft/M.O. payable to "Publications and Information Directorate". Each title will be sent to you by post as soon as it is published, one every month. The titles already published will be sent to you as soon as the payment is received by us.

For further information write to:

Senior Sales and Distribution Officer
Publications & Information Directorate (CSIR)
Dr K.S. Krishnan Marg
New Delhi - 110 012.

INDIAN JOURNAL OF CHEMISTRY

Section A: Inorganic, Bio-inorganic, Physical, Theoretical & Analytical Chemistry

Editors : Dr B.C. Sharma, Dr S. Sivakamasundari and Dr S.K. Bhasin
Sr. Scientific Assistant : Geeta Mahadevan

Published by the Publications & Information Directorate (CSIR), Hillside Road, New Delhi 110 012
Director: Dr G P Phondke

The Indian Journal of Chemistry is issued monthly in two sections: A and B. Communications regarding contributions for publication in the journal should be addressed to the Editor, Indian Journal of Chemistry, Publications & Information Directorate, Hillside Road, New Delhi 110 012.

Correspondence regarding subscriptions and advertisements should be addressed to the Sales & Distribution Officer, Publications & Information Directorate, Hillside Road, New Delhi 110 012.

The Publications & Information Directorate (CSIR) assumes no responsibility for the statements and opinions advanced by contributors. The Editorial Board in its work of examining papers received for publication is assisted, in an honorary capacity by a large number of distinguished scientists, working in various parts of India.

Annual Subscription: Rs. 400.00 £ 100.00 $ 150.00; 50% discount admissible to research workers and students and 25% discount to non-research individuals on annual subscription.

Single Copy: Rs. 40.00 £ 10.00 $ 15.00

Payments in respect of subscriptions and advertisements may be sent by cheque, bank draft, money order or postal order marked payable to Publications & Information Directorate, Hillside Road, New Delhi 110 012.

Claims for missing numbers of the journal will be allowed only if received within 3 months of the date of issue of the journal plus the time normally required for postal delivery of the journals and the claim.

Author Index

Indian Journal of Chemistry

Sect. A: Inorganic, Bio-inorganic, Physical, Theoretical & Analytical

VOL. 31A NUMBER 4 APRIL 1992

CONTENTS

Notes

(*contd.*)

CONTENTS

Authors for correspondence are indicated by (*)

Indian Journal of chemistry
Vol. 31A, April 1992, pp. 215-218

A theoretical investigation of the lowest B_u state of *trans*-butadiene

Sachchida N Rai*
Department of Chemistry, North-Eastern Hill University, Shillong 793 003, India
and
Robert J Buenker
Fachbereich 9-Theoretische Chemie, Bergische Universität GH Wuppertal, Gaussstrasse 20, D-5600 Wuppertal 1, Germany

Received 3 October 1991; revised and accepted 17 January 1992

Results of an *ab initio* CI study of the lowest singlet B_u state of *trans*-butadiene are presented. It is found that a minimum exists for the $1\ ^1B_u$ state of the present system in a geometry in which all C−C bond lengths are equal and both terminal CH_2 groups are rotated by 10°. An attempt is made to provide an interpretation of the appearance of the broad intense π-π* band in the spectrum of *trans*-butadiene.

The electronic spectrum of *trans*-butadiene has been an object of numerous studies by means of both experimental and theoretical techniques[1]. However, one major question still remaining is the assignment of a broad intense band observed in its optical[2-6] and electron impact spectra[7-13] stretching from 5.7 eV to 6.3 eV. The broad band shows three peaks at 5.76, 5.92 and 6.05 eV, of which the most intense peak is the 5.92 eV peak.

Several theoretical investigations on the low-lying state of *trans*-butadiene have been reported. However, extended *ab initio* calculations using DZ AO basis sets augmented by various diffuse functions performed by Shih *et al.*[14] and Hosteny *et al.*[15] have predicted the lowest ^1B_u state to possess so much Rydberg character that it was difficult to assign it to the intense broad absorption system. Shih *et al.*[14] suggested that the most probable transitions to this species are distinctly nonvertical. Buenker *et al.*[16] used a DZ AO basis augmented with Rydberg functions on the C atoms and performed an all-valence electron CI treatment which suggested that the valence like feature in the absorption system cannot be satisfactorily explained on the basis of a strictly vertical treatment. Nascimento and Goddard[17,18] also suggested that the ^1B_u states possess both Rydberg and valence characters and are complicated.

Lasaga *et al.*[19] calculated the excitation energy for the 1^1B_u state to be 5.51 eV. Bonačič-Koutecky *et al.*[20] predicted that the lowest singlet excited state energy surface exhibits a minimum at an intermediate twist angle in addition to the one at the 90° twist. Dinur *et al.*[21] suggested that the 1^1B_u state may have a nonplanar minimum but the twist around a terminal bond is not larger than 30°. Aoyagi *et al.*[22] showed that the 1^1B_u state has a local minimum at a planar conformation in which three C−C bond lengths are nearly equal to that in benzene (1.399Å) in agreement with results of an experimental analysis performed by Granville *et al.*[23].

Cave and Davidson[24] found that the value for the excitation energy for the 1^1B_u state is 6.23 eV which is only 0.3 eV above the experimental intensity maximum. However, they noticed that the 1^1B_u state contains significantly more Rydberg character and suggested the possibility of the 1^1B_u (π-π*) transition being nonvertical. Another possibility considered by Cave and Davidson[24] was that the excited state is of lower symmetry than the ground state as reported by Buenker *et al.*[16] and Chadwick *et al.*[25]. Kitao and Nakatsuji[26] also found results in near agreement with those of Cave and Davidson[24]. Cave and Davidson[27] performed another *ab initio* calculation and found greater difference between the vertical and O−O transition energies (0.49 eV) than that found experimentally (0.18 eV). Aoyagi and Osamura[28] and Szalay *et al.*[29] suggested that in the lowest lying non-planar excited singlet state one terminal CH_2-group is rotated by 90°.

The above analysis of various investigations on butadiene suggests that the 1^1B_u transition is nonvertical. The C−C bond lengths change in the excited state which is also of lower symmetry than the ground state. Though significant contributions to the excitation spectra are expected to come from planar geometries of varying chain lengths, sufficient indications are there for non-planar structures of the low-lying excited states. Twisting of only one terminal CH_2 group by 90° gives an excitation energy which lies below the π-π* excitation band and

seemingly does not correspond to it. There exists the possibility that rotation of the terminal CH_2 group is by an angle less than 90° (ref. 20) or even less than 30° (ref. 21). Also, simultaneous rotations of both terminal CH_2 groups with varying chain lengths may result in lowering of the excitation energies for the low-lying excited states. However, none of the theoretical investigations cited above has considered these possibilities. In an attempt to understand the 1^1B_u (π-π^*) state of *trans*-butadiene more clearly we have carried out *ab initio* CI calculations of 1^1B_u states, first in the high symmetry of the ground state and then in an optimized geometry of low symmetry in the excited states in which both terminal CH_2 groups are rotated. The results of this study are presented here.

Theoretical

For the purpose of the present study, the equilibrium geometry for *trans*-butadiene was taken from the work of Buenker and Whitten[30]. Two basis sets, one containing a total of 56 (ref. 31) and the other 86 (ref. 32) AO's were employed. In the smaller basis set, four *s* and two *p* AO's at each C atom, two *s* AO's at each H atom and one *s* and one *p* function were placed at the midpoint of the middle C – C bond as bond functions. In the larger basis set one *d* function was additionally placed at each C atom and the midpoint of the middle C – C bond.

For the excited state geometry optimization, the smaller basis set was used. In the present CI treatment four carbon 1*s* and four carbon 2*s* shells were retained as fixed core and corresponding four 1*s* species were distributed over 44 MO's in all CI calculations.

The CI calculations for the electronic ground state ^1A_g and the excited states 1^1B_u and 2^1B_u of *trans*-butadiene were carried out with the aid of the multireference singles- and doubles-excitation (MRD-) CI method[33,34], which makes use of the Table CI algorithm[35-37]. The one-electron basis for the CI calculations consisted of the SCF orbitals of each of these electronic states. The extrapolated MRD-CI eigenvalues were then modified using the multireference analogue of the Davidson correction[38-39] in order to get an accurate estimate of the full CI energies at the AO basis limit. The latter results were then used throughout the present study to analyze the 1^1B_u state.

Geometry optimization was done in two steps. In the first step we optimized the C – C bond lengths. For this purpose we define a parameter γ such that,

$$T_\gamma = (1-\gamma)T_0 + \gamma M_0, \text{ and}$$

$$M_\gamma = (1-\gamma)M_0 + \gamma T_0$$

where T_γ and M_γ are bond lengths of terminal and middle C – C bonds, respectively. T_0 and M_0 are the corresponding bond lengths when the terminal bonds are double bonds and the middle bond is single bond. At $\gamma = 0.5$ all the three C – C bond lengths become equal. In the second step we optimized the angle ω by which both terminal CH_2 groups are rotated simultaneously along the C – C bond.

The big basis set was employed to obtain the energies of the ground and excited states at the equilibrium and optimized geometries. Similar to the CI treatment using the small basis set, 14 active electrons were considered in CI calculations employing big basis set also.

Results and Discussion

Excitation energies for the 1^1B_u and 2^1B_u states of *trans*-butadiene reported by previous investigators are given in Table 1.

A series of CI calculations has been carried out for the 1^1A_g, 1^1B_u states of *trans*-butadiene in the manner described above. Some details of calculations are summarized in Table 2. Excitation energies for the 1^1B_u and 2^1B_u states obtained from various CI treatments performed in the present investigation are given in Table 3 alongwith corresponding Franck-Condon factors(f).

The geometry optimization for excited state indicates that a minimum exists for the 1^1B_u state of *trans*-butadiene at $\gamma = 0.5$ and $\omega = 10°$ which corresponds to the geometry in which all C – C bond lengths are equal and both terminal CH_2 groups are rotated by 10°, thus sending the four terminal H atoms out of molecular plane. In addition to the fact that the experimental evidence exists for the change in bond lengths[6] and distortion of planar structure[25] of *trans*-butadiene in excited state, it is also natural to expect a slight change in planar structure due to the lengthening or shortening of the C – C bonds.

Table 1—Vertical excitation energies (in electron volts) for the 1^1B_u and 2^1B_u states of *trans*-butadiene obtained from different calculations and experimental values

Calculation	Ref.	1^1B_u	2^1B_u
Shih *et al.*	14	6.60	7.98
Hosteny *et al.*,	15	7.05	8.06
Buenker *et al.*	16	6.67	7.67
Nascimento & Goddard	17,18	6.67	7.97
Aoyagi *et al.*	22	6.88	8.08
Cave & Davidson	24	6.23	7.16
Kitao & Nakatsuji	26	6.39	7.05
Experimental	40	5.92	6.64

Table 2—Details of the present CI calculations of the ground, 1^1B_u and 2^1B_u states of *trans*-butadiene

State	γ	ω	Basis	No. of mains/ roots	Secular Eqs generated/solved	Estimated full CI energy (hartree)
^1A_g(GS)	0	0	56	5M1R	119401/2762	−155.0855
	0	0	86	5M1R	384127/5270	−155.2298
1^1B_u	0	0	56	4M3R	72020/10226	−154.8383
	0	0	86	9M3R	650459/14902	−154.9866
	0.5	10°	56	8M4R	348912/13644	−154.8567
	0.5	10°	86	12M4R	1547872/15369	−155.0067
2^1B_u	0	0	56	4M3R	72020/10226	−154.8079
	0	0	86	9M3R	650459/14902	−154.9588
	0.5	10°	56	8M4R	348912/13644	−154.8262
	0.5	10°	86	12M4R	1547872/15369	−155.9652

Table 3—Vertical and nonvertical excitation energies (in electron volts) for the 1^1B_u and 2^1B_u states of *trans*-butadiene obtained from various CI treatment in the present work. Frank-Condon factors (f) are given in parentheses

State	γ = 0		ω = 0		γ = 0.5	ω = 10°
	Small basis		Large basis		Small basis	Large basis
1^1B_u	6.73(0.25)	6.67(0.7)	6.61(0.38)		6.23(0.41)	6.07(0.82)
2^1B_u	7.55(0.73)	7.67(0.99)	7.37(0.56)		7.06(0.47)	7.20(0.04)

Rotation of CH_2 groups by 10° falls within the 30° limit set by Dinur *et al.*[21] for the twist around a terminal bond. Also, it may correspond to the intermediate twist angle (in addition to the one at 30°) indicated by Bonačič-Koutecký[20].

Results presented in Table 3 indicate that the 1^1B_u state of *trans*-butadiene is very sensitive to the geometry of the molecule as well as to the various levels of CI treatment. The calculated f values for the vertical excitation of 1^1B_u state reveal its mixed valence and Rydberg character. Though the valence character increases with the size of the basis set, the lowest state still remains diffuse. However, f values caculated for the nonvertical excitation of 1^1B_u increase rapidly in going from the smaller basis set (0.41) to the larger basis set (0.82).

For the analysis of the broad intense band (π-π*) in the butadiene spectrum, it is helpful to make use of results of similar studies on comparable systems such as C_2H_4. Experience with ethylene[41,42] indicates that typically calculated value for the π-π* excitation energy is 8.0-8.1 eV and the upper state is semidiffuse. Like butadiene, the ethylene spectrum is also very broad. Analysis of C_2H_4 spectrum has led to the suggestion that the vertical electronic energy difference is not necessarily equal to the energy corresponding to the intensity maximum. This suggestion is based on the following observations.

Since the upper state has a energy maximum, it is possible that the vibrational level reached during the excitation is below the energy of the excited state at the equilibrium geometry of the ground state. Also, zero-point effects cause a shift in the location of the intensity maximum. The ground state has one more double bond and one less single bond than the excited state at vertical geometry. In addition to this, torsion is large in the ground state and practically nil in the excited state. Based on these points one expects at least 0.1 eV greater zero point energy in the ground state which will shift the location of the intensity maximum from the vertical energy difference. Finally, the appearance of the broad spectrum itself indicates that nonadiabatic effects are important near the intensity maximum. For ethylene, bending vibrations were found to be important for this effect. However, the present calculations show that γ vibration (C−C stretching) is more important for butadiene and if the stretching is asymmetric the system will pass through a point of low symmetry causing avoided crossing and lowering the vertical transition energy. On the basis of these points it is expected that the calculated vertical energy difference will be 0.2-0.3 eV or even bigger compared to the energy corresponding to the intensity maximum.

In addition to the above points the geometry relaxation effects are also to be taken into account. Both, present calculations as well as those of Cave and Davidson[27] indicate an energy difference of $\Delta E \sim 0.5$ eV between the vertical and O−O transitions. We do not expect to find the absolute minimum in the energy for O−O transition because calculations of Bonačič-Koutecký *et al.*[20] and Szalay *et al.*[29] show that these geometries are out of Franck-

Condon region; but as in the case of C_2H_4 one might see the vibration. So a good interpretation of the calculations is that the relaxation energy of 0.5 eV is closer to the ΔE between lowest observable level (in our relaxed C_4H_6 structure) and the one at vertical geometry. By this line of reasoning, if T_0 is 5.73 eV then the vertical level should be 0.5 eV higher, i.e., 6.2-6.3 eV without any zero point or nonadiabatic effects. If these effects are also included, the vertical level should be at 6.3-6.5 eV. This means that the exact solution of Born-Oppenheimer Schrödinger equation for the vertical geometry might actually yield this value. The value of 6.23 eV obtained by Cave and Davidson[24] is a little low but well within the expected error bars. Our results (6.61 eV) are on the higher side but still within the error limits. Our value for the relaxed geometry is 6.07 eV which is also high compared to the experimental value of 5.73 eV, which is consistent, whereas Cave and Davidson[24] have calculated a value of 5.74 eV without taking into consideration effects discussed above. Kitao and Nakatsuji[26] have calculated a value for the vertical electronic energy difference of 6.39 eV (6.34 eV) which is in very good agreement with our estimation. However, we think that the present interpretation of the butadiene spectrum is preferable to doing calculations for the vertical excitation energy by neglecting nonadiabatic, zero points, and other effects.

Considering the fact that the 1^1B_u state is sensitive to the level of CI treatment, we find it a worthwhile future investigation to carry out calculations for the present system by employing a larger basis set and taking all valence electrons into consideration. We hope to analyze the spectrum with more clarity when such calculations are performed.

Acknowledgement

The present work has been carried out within the framework of the Sonder-Forschungsbereich 42 with the financial support of the Deutsche Forschungsgemeinschaft. The computations were carried out on a Perkin Elmer 3242 computer of the SFB 42 in Wuppertal.

References

1 Hudson B S, Kohler B E & Schulton K, in *Excited sates*, Vol. 6, edited by E C Lim (Academic Press, New York) 1982, 1.
2 McDiarmid R, *J chem Phys*, 64 (1976) 514.
3 McDiarmid R, *Chem Phys Lett*, 34 (1975) 130.
4 Wiberg K B, Peters K S, Ellison G B & Dehmer J L, *J chem Phys*, 66 (1977) 2224.
5 Vaida V & McClelland G M, *Chem Phys Lett*, 71 (1980) 436.
6 Hemley R J, Dawson J I & Vaida V, *J chem Phys*, 78 (1983) 2915.
7 Mosher O A, Flicker W M & Kuppermann A, *J chem Phys*, 59 (1973) 6502.
8 Doering J P, *J chem Phys*, 70 (1979) 3902.
9 McDiarmid R, *J chem Phys*, 79 (1983) 9.
10 Doering J P & McDiarmid R, *J chem Phys*, 73 (1980) 3617.
11 Doering J P & McDiarmid R, *J chem Phys*, 75 (1981) 2477.
12 McDiarmid R & Doering J P, *Chem Phys Lett*, 88 (1982) 602.
13 Reddish T, Wallbank B & Comer J, *J chem Phys*, 108 (1986) 159.
14 Shih S, Buenker R J & Peyerimhoff S D, *Chem Phys Lett*, 16 (1972) 244.
15 Hosteny R P, Dunning (Jr) T H, Gilman R R, Pipano A & Shavitt I, *J chem Phys*, 62 (1975) 4764.
16 Buenker R J, Shih S & Peyerimhoff S D, *Chem Phys Lett*, 44 (1976) 385.
17 Nascimento M A C & Goddard (III) W A, *Chem Phys*, 36 (1979) 147.
18 Nascimento M A C & Goddard (III) W A, *Chem Phys*, 53 (1980) 251.
19 Lasaga A C, Areni R J & Karplus M, *J chem Phys*, 73 (1980) 5230.
20 Bonačič-Koutecký V, Persico M, Döhnert D & Sevin A, *J Am chem Soc*, 104 (1982) 6900.
21 Dinur U, Hemley R J & Karplus M, *J phys Chem*, 87 (1983) 924.
22 Aoyagi M, Osamura Y & Iwata S, *J chem Phys*, 83 (1985) 1140.
23 Granville M F, Kohler B E & Snow J B, *J chem Phys*, 75 (1981) 3765.
24 Cave R J & Davidson E R, *J phys Chem*, 91 (1987) 4481.
25 Chadwick R R, Gerrity D P & Hudson B S, *Chem Phys Lett*, 115 (1985) 24.
26 Kitao O & Nakatsuji H, *Chem Phys Lett*, 143 (1988) 528.
27 Cave R J & Davidson E R, *Chem Phys Lett*, 148 (1988) 190.
28 Aoyagi M & Osamura Y, *J Am chem Soc*, 111 (1989) 470.
29 Szalay P G, Karpfen A & Lischka H, *Chem Phys*, 130 (1989) 219.
30 Buenker R J & Whitten J L, *J chem Phys*, 49 (1968) 5381.
31 Huzinaga S, *J chem Phys*, 42 (1965) 1293.
32 Dunning (Jr) T H, *J chem Phys*, 55 (1971) 3958.
33 Buenker R J & Peyerimhoff S D, *Theoret chim Acta*, 35 (1974) 33; 39 (1975) 217.
34 Buenker R J, Peyerimhoff S D & Butscher W, *Molec Phys*, 35 (1978) 771.
35 Buenker R J, in *Proceedings of workshop on quantum chemistry & molecular physics*, Wollongong, Australia, edited by P Burton (University Press, Wollongong) 1980.
36 Buenker R J, in *Studies in physical & theoretical chemistry*, Vol. 21. *Current aspects of quantum chemistry*, edited by R Carbo (Elsevier, Amsterdam) 1981, 17.
37 Buenker R J & Phillips R A, *J Molec Struct Theochem*, 123 (1985) 291.
38 Longhoff S R & Davidson E R, *Intern J Quantum Chem*, 8 (1974) 61.
39 Buenker R J, Peyerimhoff S D & Bruna P J, in *Computational theoretical organic chemistry*, edited by I G Csizmadia & R Daudel (Reidel, Dordrecht) 1981, 55.
40 Flicker W W, Mosher O A & Kuppermann A, *J chem Phys*, 59 (1973) 6502; *Chem Phys*, 30 (1978) 307.
41 Petrongolo C, Buenker R J & Peyerimhoff S D, *J chem Phys*, 76 (1982) 3655.
42 McMurchie L E & Davidson E R, *J chem Phys*, 67 (1977) 5613.

Indian Journal of chemistry
Vol. 31A, April 1992, pp. 219-226

Thermal properties of ABA and BAB triblock copolymers

Sukumar Maiti* & Subhas Chandra Shit

Polymer Division, Materials Science Centre, Indian Institute of Technology, Kharagpur 721 302

Received 30 August 1991; revised and accepted 16 December 1991

Thermal studies (TGA and DSC) of various ABA and BAB copolymers have been made and the crosslinking and swelling behavior of the polymers have been reported in order to establish the suitability of these polymers for their application as thermoplastic elastomers. From the thermal recycling and outdoor stability studies it is concluded that the ABA copolymers having polyester as the hard block and butadiene based rubber as the soft block would be suitable for use as thermoplastic elastomers. Addition of appropriate antioxidants increases the outdoor stability and thermal recycle ability of these block copolymers.

ABA triblock copolymers[1] represent an important class of materials, known commercially as thermoplastic rubbers or elastomers[2]. The unique behavior of these polymers mostly depends on the difference in the response to thermal energy of the two block segments present in ABA copolymers. The thermal performance depends on the microstructure and crystallizability of the two blocks present in such copolymers[3]. Thermal properties of ABA copolymers are, therefore, important both for understanding their nature and for assessment of their commercial applications. In this paper we report the results of investigation on the glass transition behavior, thermal stability, crosslinking and thermal recycling properties of a few triblock copolymers, synthesis of which was reported earlier[4-8].

Materials and Methods

ABA or BAB type copolymers were synthesized from two types of the block segments, viz., (1) a hard segment (A) consisting of polyester or polyesteramide or polyether sulfone, and (2) a soft segment (B) consisting of butadiene-acrylonitrile copolymer or polybutadiene or butadiene-polyethylene glycol-acrylonitrile copolymer. The synthesis and characterization of these triblock copolymers were reported earlier[4-8].

Solvents such as N-methylpyrrolidone (NMP), hexamethyl phosphoric triamide (HMPA), and 1,4-dioxane were purified by the standard procedure.

Thermal measurements

Sample preparation—The polymers were powdered, washed with either alcohol or *n*-hexane: benzene mixture and dried at about 40°C for 24 h under vacuum.

Thermogravimetric analysis (TGA) of copolymer samples was made with a DuPont thermal analyzer, Model 990, in air at a heating rate of 10°C/min.

Differential scanning calorimetry (DSC) of the powdered dry samples was run by Mettler Tc 10A system at a heating rate of 20°C/min in air.

Crosslinking reaction

Crosslinking of the polymers was studied by heating the polymer samples at different temperatures for different time intervals. The sample (2.0g) was placed on a glass plate and kept in a closed container under N_2 and heated at the specified temperature for a fixed period. The percentage of crosslinking was determined by Sol-Gel analysis.

Analysis of sol-gel fraction

The crosslinked polymer sample was subjected to soxhlet extraction by NMP or HMPA or 1,4-dioxane solvent (whichever was found suitable to dissolve the uncrosslinked fraction of the sample) for 96 h. The insoluble product was dried to constant weight.

Swelling behavior of crosslinked copolymers

Swelling behavior of a sample was determined gravimetrically by the quantity of solvent taken by a crosslinked polymer by the following relation

$$S_W = \frac{M_S - M_D}{M_D} \times 100$$

where M_S is the weight of the wet swollen crosslinked sample after 7 days' immersion in the solvent at 30°C (washed with diethyl ether and blotted by filter paper and weighed quickly), and M_D the corresponding weight of the dry sample.

IR spectroscopy of copolymers

IR spectra of the copolymers were recorded with a Perkin-Elmer, Model 237 spectrophotometer on KBr discs.

Thermal recycling behavior of copolymers

The copolymers without antioxidant were repeatedly heated upto their respective softening temperature and cooled down to room temperature and heated again for a total period of 6 h. Similarly, samples containing an antioxidant were treated as above. The heat treated samples were dissolved in respective solvents to judge whether crosslinking occurs or not.

Outdoor stability

Copolymer samples were kept at room temperature in the outdoor environment for about 2 months.

Results and Discussion

The structures of the repeat unit of various copolymers (ABA or BAB) investigated in this study are shown in Table 1.

Four types of hard segments i.e., polyethylene isophthalate (PEI), polyethylene terephthalate (PET), polyether sulfone (PES) and polyesteramide (PEA), and three types of soft rubbery blocks i.e., poly(butadiene-co-acrylonitrile) (CTBN), polybutadiene (CTB), and CTBN-polyethylene glycol-CTBN (CTBN-PEG-CTBN) have been used in the synthesis of these ABA or BAB copolymers. The number average molecular weight, $\bar{M}_n$, of the hard blocks ranges from as low as about 1000 to 9000 while the corresponding values for the three soft blocks are fixed: 3200, 4200 and 6840 for CTBN, CTB and CTBN-PEG-CTBN, respectively. The details of synthesis and characterization of these copolymers and the prepolymer blocks were reported elsewhere[4-8].

Table 1—The structure and molecular weight of ABA and BAB copolymers

Polymer	ABA Structure[a]	$\bar{M}_n$ (Theoret.)
I	PEI-CTBN-PEI (998-3,200-998)	5,196
II	PEI-CTBN-PEI (1,344-3,200-1,344)	5,888
III	PEI-CTBN-PEI (2,000-3,200-2,000)	7,200
IV	PEI-CTB-PEI (2,000-4,200-2,000)	8,200
V	PEI-CTBN/PEG/CTBN-PEI (2,000-6,840-2,000)	10,840
VI	PET-CTBN-PET (1,248-3,200-1,248)	5,696
VII	PET-CTBN-PET (1,342-3,200-1,342)	5,884
VIII	PET-CTBN-PET (2,112-3,200-2,112)	7,424
IX	PET-CTBN-PET (2,880-3,200-2,880)	8,960
X	PET-CTB-PET (2,880-4,200-2,880)	9,960
XI	PET-CTBN/PEG/CTBN-PET (2,880-6,840-2,880)	12,600
XII	PES-CTBN-PES (1,768-3,200-1,768)	6,736
XIII	PES-CTBN-PES (1,768-3,200-1,768)	6,736
XIV	PES-CTBN-PES (2,120-3,200-2,120)	7,440
XV	PES-CTBN-PES (2,870-3,200-2,870)	8,940
XVI	PES-CTB-PES (2,870-4,200-2,870)	9,940
XVII	PES-CTBN/PES/CTBN-PES (3,870-6,864-3,870)	12,580
XVIII	PEA-CTBN-PEA (999-3,200-999)	5,198
XIX	PEA-CTBN-PEA (1,477-3,200-1,477)	6,154
XX	PEA-CTBN-PEA (4,106-3,200-4,106)	11,412
XXI	PEA-CTBN-PEA (8,408-3,200-8,408)	20,016
XXII	PEA-CTB-PEA (6,900-4,200-6,900)	18,000
XXIII	PEA-CTBN/PEG/CTBN-PEA (9,000-6,840-9,000)	24,840
XXIV	CTBN-PEI-CTBN (3,200-972-3,200)	7,372
XXV	CTBN-PEI-CTBN (3,200-1,216-3,200)	7,616
XXVI	CTBN-PEI-CTBN (3,200-1,940-3,200)	8,340
XXVII	CTB-PEI-CTB (4,200-3,940-4,200)	10,340
XXVIII	CTBN/PEG/CTBN-PEI-CTBN/PEG CTBN (6,840-1,940-6,840)	15,620

[a]The figures in the parentheses indicate $\bar{M}_n$ of the respective block segments of the copolymer. (PEI = polyethylene isophthalate block, PET = polyethylene terephthalate block, PES = polyether sulfone block, PEA = polyesteramide block, CTBN = carboxy terminated butadiene-acrylonitrile rubber block, CTB = carboxy terminated butadiene rubber block and PEG = polyethylene glycol)

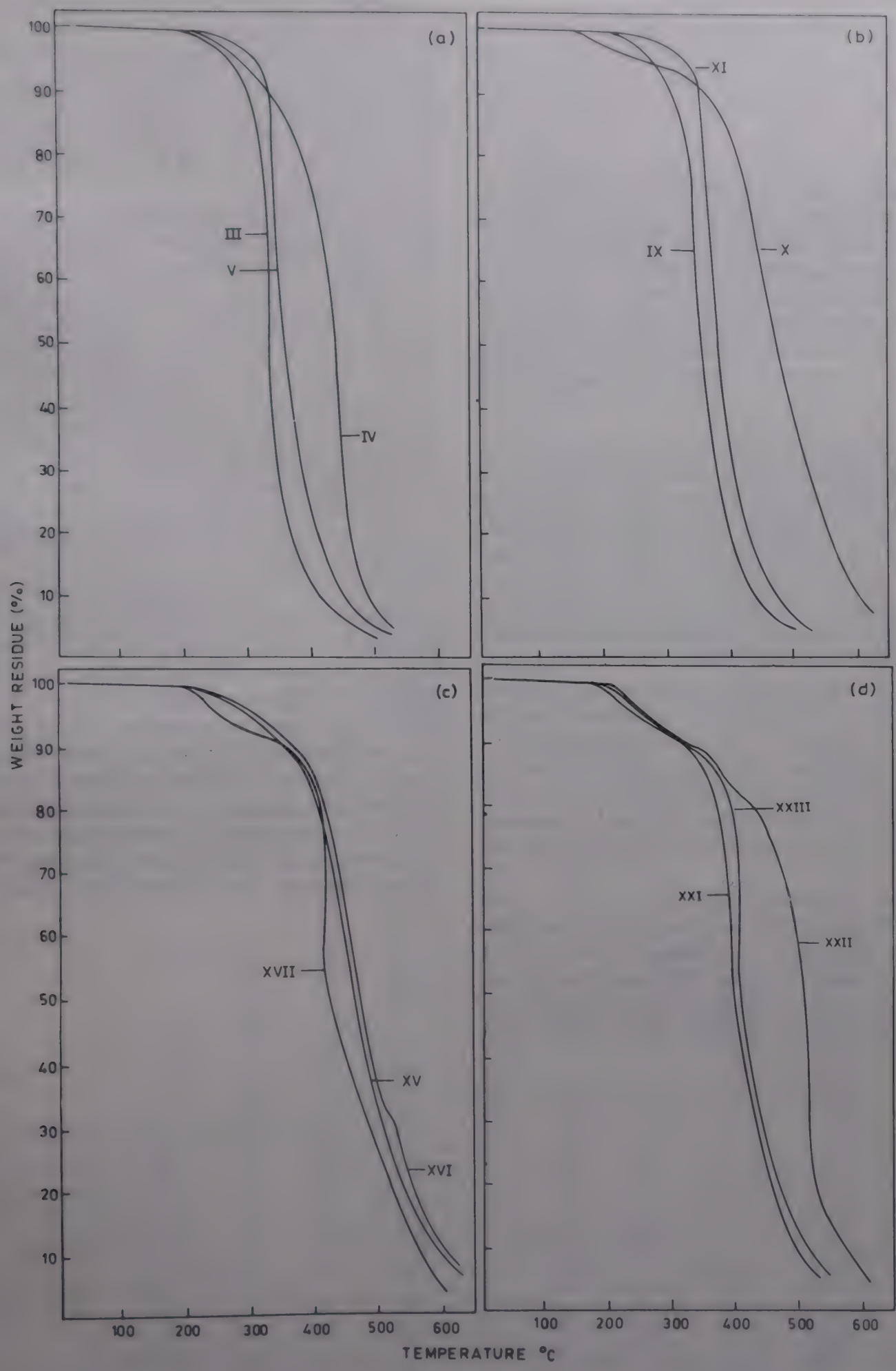

Fig. 1—TGA curves of ABA and BAB copolymers

(a) ABA copolymers III-V; (b) ABA copolymers IX-XI; (c) ABA copolymers XV-XVII; and (d) BAB copolymers XXI-XXIII

Thermal behavior of copolymers

TGA curves of copolymers III, IV and V are shown in Fig. 1(a), those of copolymers IX, X and XI in Fig. 1(b), those of copolymers XV, XVI and XVII in Fig. 1(c) and those of copolymers XXI, XXII and XXIII in Fig. 1(d). Thus, Fig. 1 offers a comparative evaluation of the contribution of CTBN, CTB and CTBN-PEG-CTBN soft (B) segments to the thermal stability of the copolymers vis-a-vis those of the different hard (A) terminal blocks: PEI, PET, PES and PEA, respectively. It is clear that the ABA copolymers having CTBN central blocks degrade faster than those with CTB block segments, which in turn are found to be less thermostable than those with CTBN-PEG-CTBN as the middle block (B).

Polymers having PEI and PET hard terminal segments degrade by one step (curves V and XI) while those with PES (curve XVII) and PEA (curves XXI-XXIII) segments degrade by two stages. This is perhaps due to the fact that in polyarylether sulfone and polyesteramide based copolymers the initial weight loss step indicates the degradation of its rubber content[9,10]. The improved thermal stability of PES block segment is due to its higher aromatic ring content in the polymer structure, while that of PEA segment is due to its high crystalline structure[11] and the presence of strong sites for interchain interaction. Such sites for strong interchain interaction are not present in the polyester (PEI and PET) segments although both of them are also crystalline, and consequently the latter are not so thermostable as the former.

However, the initial weight loss occurs in both PES and PEA segments containing block copolymers earlier than those containing polyester block segments probably because PES and PEA do not get mixed well with the rubbery B blocks of the respective chain as it happens in PET or PEI based copolymers. It has been found that copolymers having almost same percentage of rubber (soft) segments but of different molecular weights differ in thermal behavior; the higher the molecular weight the higher is the thermal stability (i.e., V is more thermostable than II). The thermal stability of the copolymers increases with increase in chain length of either segments.

For all the samples the maximum weight loss occurs in the range of 300-500°C. The BAB copolymers having soft rubbery segments as the endblocks and PEI as the central block are less thermostable than the corresponding ABA copolymers where rubber segments are present as the central block.

DSC curves of the prepolymers constituting the hard segments of the ABA or BAB copolymers are shown in Fig. 2. It was found that both T_g and T_m increase with increase in molecular weight. Both these endothermic transitions become sharper and more distinct with increase in $\bar{M}_n$. No T_m was observed in the case of polyarylether sulfone possibly due to its amorphous nature.

DSC curves of the copolymers (Fig. 3) show the two phase nature of the block copolymers[13]. In copolymers II, VI and VII the T_g of the A segment, i.e., polyester segments (PEI and PET) is somewhat less distinct and difficult to assign (not shown in Fig. 3). On the other hand, in copolymers XV and XVII the T_g (near 160°C) of the polyarylether sulfone segment is prominent. In all the copolymers studied the T_g of the soft segments, i.e., CTBN or CTB comes almost at the same position. Since increase in length of A segment, i.e., PEA block does not change the T_g of the soft segment (curve XX, M_n of A block 4,106

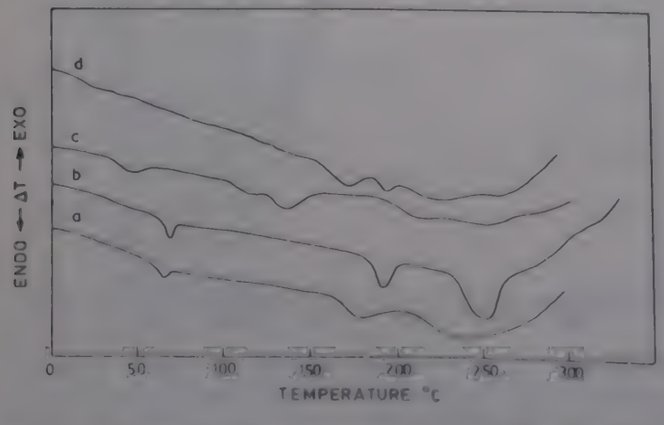

Fig. 2—DSC curves of the prepolymers: a: PET ($\bar{M}_n$ = 2,000); b: PET ($\bar{M}_n$ = 2,800); c: PEI ($\bar{M}_n$ = 2,000); d: PES ($\bar{M}_n$ = 2,870).

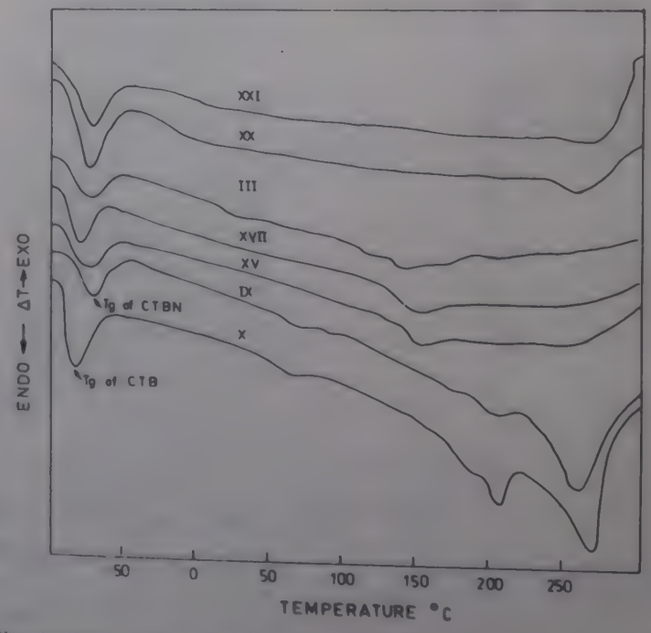

Fig. 3—DSC curves of ABA copolymers. The curve numbers correspond to the number of Table 1.

versus curve XXI. $\bar{M}_n$ of A block 8,408), it is reasonable to assume that anchoring effect by the hard segment[13,14] is nil in XXI copolymer. Further, the difference between T_g of A and B blocks in copolymers XX and XXI is very large (~ 330°C); thus one melts before the other starts melting. This is also observed in copolymers XV and XVII containing PES hard segments. Due to increase in the length of soft segment (B) in copolymer XVII its T_g decreases[15]. The T_g of the soft block in CTBN based copolymer XV is decreased by two degrees when CTBN is substituted by CTBN-PEG-CTBN in copolymer XVII.

Since the difference between T_g of A and B segments is very large in PES (e.g. curves XV and XVII) and PEA (e.g. curves XX and XXI) based copolymers, their processing becomes difficult, because at the processing temperature above T_g of their hard (A) blocks the rubber (B) blocks get crosslinked and thereby a thermoplastic material is converted to a thermoset. On the other hand, although there is a phase separation (i.e., two phase behavior) observed from the DSC studies in the case of copolymers III, IX and X, there would be some processing advantage at temperatures above T_g of the hard segment because the difference between T_g of A and B blocks ranges from about 100-150°C. Two T_gs for both block segments were also observed in the case of BAB copolymers (not shown in Fig. 3).

Crosslinking behavior of ABA copolymers

Crosslinking reaction of the copolymers was carried out at 100, 150 and 200°C for time intervals of 2 h, 4 h and 6 h (Table 2). The extent of crosslinking reaction depends on the nature and percentage of the hard and soft segments of the copolymers as well as on the temperature and time of heating. For example, copolymers (I-V) at 150°C for 6 h heating the percentage of crosslinking increases from 27-40 and from 65-80 at 200°C for 6 h heating. In PEI (I-V) and PET (VI-XI) based copolymers the degree of cross linking increases gradually with increasing percentage of the rubber segment. But in the case of polyarylether sulfone (XII-XVII) and polyesteramide (XVIII-XXIII) based copolymers the extent of crosslinking is almost quantitative at 200°C for 6 h heating. Since the T_g of PET and PEI are not as high as that of PSU (polyarylether sulfone) and PEA (polyesteramide), their segmental motion is not res-

Table 2—Crosslinking of ABA copolymers

Copolymer	Percentage of crosslinked copolymers after heating at									Solvent used	% of A segment
	100°C			150°C			200°C				
	2h	4h	6h	2h	4h	6h	2h	4h	6h		
I	—	—	10	20	29	40	45	58	80	NMP	38
II	—	—	6	15	27	38	40	52	70	NMP	45
III	—	—	5	10	17	27	30	50	65	NMP	54
IV	—	10	20	25	30	40	45	56	78	NMP	49
V	—	—	10	25	30	38	42	54	78	NMP	40
VI	—	—	10	15	25	36	42	50	70	NMP	42
VII	—	—	10	15	22	32	40	45	67	NMP	45
VIII	—	—	5	10	15	25	36	39	60	NMP	56
IX	—	—	4	10	15	25	32	40	60	NMP	64
X	—	6	12	15	25	38	42	52	72	NMP	58
XI	—	—	10	15	25	36	40	60	72	NMP	42
XII	5	10	15	30	35	46	58	67	98	NMP	51
XIII	5	8	12	30	36	42	58	68	95	NMP	50
XIV	4	6	10	25	30	38	48	65	90	NMP	54
XV	3	5	20	25	30	36	45	92	88	NMP	66
XVI	10	20	26	30	35	45	50	70	98	NMP	46
XVII	5	10	16	35	40	48	53	70	96	NMP	48
XVIII	10	20	30	35	40	50	56	70	98	1,4-Dioxane	34
XIX	8	14	26	30	34	48	55	68	92	NMP	47
XX	5	10	16	30	36	44	52	62	82	HMPA	72
XXI	4	8	12	25	32	42	48	60	80	HMPA	92
XXVI[a]	10	20	25	50	55	80	88	90	98	1,4-Dioxane	21

[a]BAB copolymer

tricted and thus good phase mixing is possible in polyester based copolymers. On the other hand, in PEA or PSU based copolymers the soft segments are within the soft domain even at above 150°C because of the high T_g of the PEA or PSU segment. This allows easy crosslinking of the rubber segments in the copolymer having PSU or PEA hard segments. The PET based copolymers are not easily crosslinked and 80% crosslinking occurs at 200°C after 8 h. The percentage of crosslinked product with BAB copolymer is more than that with ABA of nearly same molecular weight, since the former contains higher percentage of rubber.

Swelling behavior of the crosslinked copolymers

The virgin copolymers containing unsaturation in the soft block are soluble in highly polar solvents such as NMP, DMF, DMAC. The swelling is possible due to the fact that irreversible covalent crosslinks in polymers are much stronger force than polarity or other secondary valence forces, which make crosslinked polymers insoluble even in highly polar solvents[16-18]. The percentage swelling of various copolymers (I-XXIII) depends on the nature of the solvent. For example, the % swelling in *n*-hexane, benzene, 1,4-dioxane, MEK, DMF, DMAC and NMP ranges from 98-110, 120-150, 130-160, 130-180, 130-200, 140-200 and 140-200, respectively. With the increase in the percentage of PEI in the PEI-based copolymers (I-V) swelling in nonpolar solvents such as *n*-hexane and benzene decreases. On the other hand, in polar solvents e.g., 1,4-dioxane, MEK, DMF, DMAC and NMP swelling increases except in copolymers (IV) containing CTB as the middle segment. When the percentage of PET is increased in PET based copolymers (VI-XI) the change in swelling is not much significant except in the case of X. Rather when the percentage of polyarylether sulfone (PSU) is increased in polyarylether sulfone based copolymers swelling in polar solvents is prominent and it increases gradually as the solvent polarity increases. It has been found that swelling of

Table 3—Thermal recycling behavior of ABA copolymers

Copolymers	T_g		Softening range (°C)	Recyclable upto temperature	
	A segment	B segment		Without antioxidant	With antioxidant
I	—	−78	90-100	100	120
II	44	−78	90-110	110	130
III	48	−78	90-110	110	130
IV	48	−82	90-110	110	130
V	48	−80	90-100	100	120
VI	56	−78	100-110	110	120
VII	58	−78	100-110	110	125
VIII	58	−78	105-115	115	125
IX	68	−78	110-125	120	130
X	68	−82	110-125	110	125
XI	68	−80	100-110	100	120
XII[a]	155	−78	—	—	—
XIII[a]	155	−78	—	—	—
XIV[a]	157	−78	—	—	—
XV[a]	159	−78	—	—	—
XVI[a]	159	−82	—	—	—
XVII[a]	159	−80	—	—	—
XVIII[a]	—	−78	—	—	—
XIX[a]	—	−78	—	—	—
XX[a]	—	−78	—	—	—
XXI[a]	—	78	—	—	—
XXII[a]	—	−82	—	—	—
XXIII[a]	—	80	—	—	—
XXIV[b]	48	78	80-90	90	95

[a]Infusible melt was observed

[b]BAB copolymer

the copolymer is maximum in those solvents whose solubility parameter values coincide with the copolymer's solubility parameter value[19]. The extent of swelling is minimum in the PEA-based copolymers, and as the percentage of polyesteramide block is increased in the copolymers, the swelling decreases significantly. This is due to the highly crystalline nature of PEA homopolymer[20].

IR spectroscopy of the copolymers

The IR spectra of the copolymers showed the absorption peaks characteristic of the groups present, viz. 1740 cm^{-1} (ester group), 3400 cm^{-1} (OH), 1600 cm^{-1} (aromatic double bond), 1620 cm^{-1} (CH=CH), 2240-2250 cm^{-1} (C≡N), 1315 cm^{-1} (SO_2, asymmetric), 1152 cm^{-1} (SO_2 symmetric), 1248 cm^{-1} (Ar-O-Ar), 3300-3580 cm^{-1} (phenolic OH and/or=NH), 1150 cm^{-1} (CH_2-O-CH_2) and 1710 cm^{-1} (−COOH). But in the crosslinked copolymer samples, absorption peaks other than the peak for aliphatic double bonds for the rubbery soft segment at 1620 cm^{-1} are present. This indicates that the double bonds of the rubber segments are involved in crosslinking reaction of the copolymers.

Thermal recycling behavior of the ABA copolymers

To become a successful thermoplastic elastomer the ABA copolymers should exhibit a certain degree of phase separation i.e., a significant degree of immiscibility between the two types of block segments (hard and soft blocks) should exist. Since these copolymers contain segments having higher glass transition (plastic block) as well as lower glass transition (elastomeric block), the thermoplastic elastomeric behavior of these copolymers is expected[2], provided that the blocks do not interact with each other. But it has been found both from TGA and crosslinking studies that there is a lack of proper phase mixing (thermally homogeneous[21] i.e. a single-phase material results due to the mobility of both the segments) at temperatures above T_g of the hard segment of polyesteramide and polyarylether sulfone based copolymers. When these copolymers are heated upto 140°C which is below the T_g of the hard block, the soft block which is molten at that temperature cannot diffuse into the hard segment as the latter is still infusible at 140°C[22]; and therefore a non-uniform physical mixture results. And when the temperature is raised to 170°C i.e., above the T_g of PES, the crosslinking reaction occurs in the rubbery phase converting the soft block into a hard infusible mass. So, at higher temperature also an inhomogeneous product will be obtained as the molten hard segment fails to diffuse into the crosslinked infusible rubber block. Thus at the temperature above the T_g of the hard segment, the PES and PEA based ABA copolymers could not be processed.

Polyester (PEI and PET) based copolymers become fluid at a temperature just above the T_g of PEI or PET which are comparatively lower than the T_g of PEA or PES segments. And since the temperature is lower, the crosslinking of the rubber block does not occur and consequently a thermally homogeneous material will result. This has been corroborated by the present study. The important criteria of thermoplastic elastomers should be such that A and B blocks should not be miscible in the normal state but miscible in the melt[23].

It has been found (Table 3) that the copolymers (I-XI) can be thermally recycled with or without antioxidant. However, the presence of antioxidant in the copolymers exhibits better service temperature than those without it. The copolymers having higher percentage of polyester (PEI or PET) retain thermoplasticity upto higher temperature than that containing lower amount of polyester segment.

BAB copolymers (PEI based) can be recycled upto 90°C and above this temperature they start crosslinking after five cycles of heating.

Outdoor stability

When the ABA copolymers (I-XI) were kept without antioxidant in air they easily undergo crosslinking or oxidative degradation after 15 days. But when they are left with antioxidant (N-isopropyl-N-phenyl phenylenediamine) the copolymers do not undergo crosslinking even after 45 days. It is also observed that copolymers containing higher percentage of polybutadiene ($-CH_2-CH=CH-CH_2-$) block exhibit more facile crosslinking reaction than others.

Acknowledgement

Authors thank the Department of Science and Technology, New Delhi for partial support of this investigation and the B.F. Goodrich Company, USA for a gift of CTBN and CTB reactive rubber samples.

References

1 Noshay A & McGrath J E, *Block copolymers, overview and critical survey*, (Academic Press, New York), 1977, 53.
2 Walker B M, *Handbook of thermoplastic elastomers*, (Van Nostrand-Reinhold, New York) 1979, 79.
3 Ref. 1, p. 63.
4 Shit S C, Mahato B M, Maiti M M & Maiti S, *J appl polym Sci*, 31 (1986) 55.
5 Shit S C & Maiti S, *J polym Sci polym Lett*, 24 (1986) 383.
6 Shit S C, Ph.D. Thesis, IIT, Kharagpur, 1987.

7 Shit S C & Maiti S, *J polym Mater*, 8 (1991) 197.
8 Maiti S & Shit S C, *J polym Mater*, 8 (1991) 361.
9 Sung C K, *J Korean chem Soc*, 7 (1963) 96; *Chem Abstr*, 61 (1964) 5761.
10 Baer M, *J polym Sci*, A2 (1964) 417.
11 Deanin R D, *Polymer structure, properties and applications*, (Cahners Book, Boston), 1972, 341.
12 Seefried C G, Jr., Koleske J V & Critchfield F E, *J appl polym Sci*, 19 (1975) 2493, 3185.
13 Sangen O, Oxada T, Ishii T & Yamamoto Y, *Kobunshi*, 36 (1979) 783; *Chem Abstr*, 92 (1980) 77790.
14 Hesketh T R, Van Bogart J W C & Cooper S L, *Polym eng Sci*, 20 (1980) 1907.
15 Ref. 12, p. 2503.
16 Bear E, *Engineering design for plastics*, (Reinhold, New York) 1964, 1041.
17 McFarlane S B, *Technology of synthetic fibers*, (Fair Child Publication, New York) 1953, 84.
18 Ref. 11, p. 324.
19 Maiti S & Ray A, *Angew makromol Chem*, 116 (1983) 193.
20 De La Mare H E & Shaw A W (to Shell Oil), U.S. Patent 3,670,054 (1972)
21 Ref. 2, p. 85.
22 Manson J A & Sperling L H, *Polymer blends and composites*, (Plenum Press, New York) 1976, 149.
23 Morton M, *Rubber Chem Technol*, 56 (1983) 1096.

Indian Journal of chemistry
Vol. 31A, April 1992, pp. 227-231

Solvation behaviour of cupric chloride in non-aqueous solvents

Prem P Singh*, Manjula Soni & S Maken
Department of Chemistry, Maharshi Dayanand University, Rohtak 124 001

Received 17 June 1991; revised 28 October 1991; accepted 18 November 1991

Electromotive force measurements have been made at 303.15K on the cell $Cu_xHg/CuCl_2(m)$ (in solvent S; S = FD, W or DMF)/AgCl/Ag where FD = formamide, W = water and DMF = dimethylformamide. The data obtained suggest that while FD and W favour deposition of Cu^{2+} from the solution onto the copper amalgam electrode in the order FD > W, DMF favours dissolution of metallic copper in the concentration range $0 < m < 0.0056$ (the effect becomes more pronounced as $m \rightarrow 0$), but it favours deposition of Cu^{2+} ions from the solution onto the copper amalgam when $m > 0.0056$. This has been explained on the basis of kinetics of electrode processes. Equilibrium constants for the dissociation processes as also the respective degrees of dissociation have been obtained by iterative procedure. The standard electrode data of the above cell have also been evaluated in FD, W and DMF and the same have been utilized to evaluate standard molar Gibbs free energy of transfer of $CuCl_2$ from W → FD or DMF. The data have been considered in terms of solute-solvent interactions.

Solvation of an ion in a solvent depends, among other things, on electron pair donation (measured by Gutmann donor number[1,2]) and acceptance (as indicated by electron pair acceptance polarity index[3]), structural[4] (categorized by stiffness, openness and ordering) and self-association characteristics of the solvent molecules. If solvation of an ion in a solvent is the net effect of the formation of definite solvates[5], then as the solvation of an ion in any solvent involves its transfer from its ideal standard state into its standard state in solution[4(a)], the solute particles undergo drastic changes in its internal degree of freedom, so that the thermodynamic quantities of transfer do not truly reflect solute-solvent interactions.

The thermodynamic quantities of transfer would be a good measure of solute-solvent interactions only if the solute is transferred from one solvent to another solvent[4(a)]. In that situation the thermodynamic quantities of transfer from water to another solvent should yield meaningful insight into the influence of cation-solvent, anion-solvent and solvent-solvent interactions on the dissolutional behaviour of a solute in water in the presence of a co-solvent. Further, though 2:1 electrolytes ionize in water as[6]: $MX_2 \rightleftharpoons (MX)^+ + X^-$; $(MX)^+ \rightleftharpoons M^{2+} + X^-$, yet very few equilibrium constant data are available about these equilibria in medium other than water. Moreover, very scant information is available about their activity coefficients in media other than water. Again, as lower amides are suitable model compounds[7] of proteins, the dissolutional behaviour of 2:1 electrolytes in W, and lower amides should be of considerable biochemical interest. These considerations prompted us to study the solvation behaviour of $CuCl_2$ in water, formamide (FD) and N,N-dimethylformamide (DMF).

Materials and Methods

Formamide (BDH, AR grade 98%) and N,N-dimethylformamide (Loba, AR grade 99%) were purified and their purities checked as described earlier[8]. Deionized double distilled (from all-glass apparatus) water was used for preparing stock solutions.

Cupric chloride dihydrate (Loba, AR grade 98%) was dehydrated[8] by heating it in an oven at 130°C for 18 h. The anhydrous $CuCl_2$ was found (by complexometric[8] determination of its copper content[9]) to contain 98.5% of $CuCl_2$. Required sets of solutions of cupric chloride in each solvent (water or S) were prepared by mass dilution from a stock solution prepared from weighed amounts of the anhydrous salt and solvent; the aqua-molality of the stock solution was 0.00894 while the molalities of the stock solutions of cupric chloride in FD and DMF were 0.008 and 0.01394 *m* respectively. All solutions were deaerated with nitrogen.

Molar Gibbs free energy of transfer of $CuCl_2$ from water to S were evaluated from emf measurements on the cell (1):

$Cu_xHg/Cu(II)Cl_2$ (*m*, in water or solvent S)/AgCl/Ag

(Cell 1)

The Ag/AgCl electrode was prepared[10] by anodic polarization of Ag electrode at a current density of 0.4 mA cm^{-2} in 0.1 *N* HCl for 30 min. The copper amalgam was prepared by vigorous shaking of freshly prepared atomic copper[11] with distilled mercury in a separating funnel and the amount of atomic copper was so adjusted that the percentage of copper(II) in the amalgam was about 0.0042% (by complexometric[9] determination of its copper content). Under these conditions, the emf of the copper-amalgam electrode is reported[12] to be independent of the amount of copper in the amalgam.

The cell (1) was maintained at 303.15 ± 0.02K in a water thermostat and a Vernier potentiometer (OSAW, India) coupled with a spot reflecting galvanometer (Toshniwal, India) was used to measure the emf of the cell (1) (after thermal equilibrium) to an accuracy of ± 0.1 mV.

Results

The cell reaction is given by Eq. 1,

$$Cu(Hg) + 2\,AgCl \rightleftharpoons Cu^{2+} + 2Cl^- + Ag \qquad \ldots (1)$$

The emf of the cell would then be given[12] by Eq. 2,

$$E = E^\circ - \frac{RT}{2F} \ln\{m_{(Cu^{2+})}\, m^2_{(Cl^-)}\, \gamma^3_\pm\} \qquad \ldots (2)$$

where m and $\gamma_\pm$ are the true molality and the mean molar activity coefficient respectively of copper(II) chloride and E° is the standard potential of the cell 1 (in the solvent S(S = FD, DMF or W). If $CuCl_2$ ionizes completely, like[13] $CdCl_2$, and if log $\gamma_\pm$ is expressed[13] as $(-A\sqrt{m} + Bm)$ where A is the limiting slope of the Debye-Huckel theory, then one obtains[13] (for cell 1),

$$E' = E + k \log 4m^3 - 3k\, A\sqrt{m} = E^\circ - 3k\, Bm$$

where $k = 2.303\ RT/2F$. Accordingly, if $CuCl_2$ were a completely dissociated electrolyte, E' should be a linear function of m in dilute solutions. The E' vs m plots (Fig. 1) clearly show that E' is not a linear function of m and so suggest that $CuCl_2$ is incompletely dissociated in the present solvents. If $CuCl_2$ is assumed to ionize in the present solvents in the manner represented by the equilibria 3 and 4,

$$CuCl_2 \overset{K_1}{\rightleftharpoons} (CuCl)^+ + Cl^- \qquad \ldots (3)$$

$$(CuCl)^+ \overset{K_2}{\rightleftharpoons} Cu^{2+} + Cl \qquad \ldots (4)$$

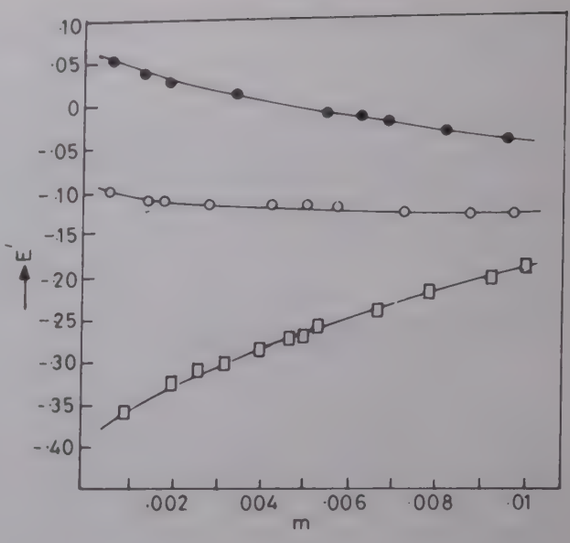

Fig. 1—Variation of E' with m at 303.15 K (○, water; □, FD; ●, DMF)

and if α_1 and α_2 denote the degree of dissociation of $CuCl_2$ and $(CuCl)^+$ respectively, then these are related to the corresponding equilibrium constants K_1 and K_2 by Eqs 5 and 6,

$$\alpha_1 = 0.5[-p' + (p'^2 + 4p')^{0.5}] \qquad \ldots (5)$$

$$\alpha_2 = 0.5[-(1+Q) + (1+Q)^2 + 4Q)^{0.5}] \qquad \ldots (6)$$

where

$$p' = K_1/m(1-\alpha_2)^2\gamma^2_{Cl^-} \qquad \ldots (7)$$

and

$$Q = K_2/\alpha_1 m\gamma_{Cu^{2+}} \qquad \ldots (8)$$

In deriving Eqs 5 and 6, it has been assumed[14,15(a)] that $\gamma_{Cl^-} = \gamma_{(CuCl)^+}$, and $\gamma_{Cu^{2+}}$ is the real activity coefficient of Cu^{2+} ion with actual concentration being given by m. This would then mean[14] that $\gamma_{Cu^{2+}}$ and γ_{Cl^-} should have values[15(b)] comparable to that found for a typical strong electrolyte and should be expressible in a medium of dielectric constant ε and at an actual ionic strength I by,

$$\log \gamma_i = -A\, Z_i^2\, I^{0.5}/(1 + I^{0.5}) + BI \qquad \ldots (9)$$

where Z_i represents the valency of Cu^{2+} or Cl^- ion,

$$A^{15(a)} = 1.823 \times 10^6/(\varepsilon T)^{1.5} \qquad \ldots (10)$$

$$B^{15(a)} = 35.56\ a^\circ/(\varepsilon T)^{0.5} \qquad \ldots (11)$$

and a° is the distance of closest approach of the ions of the electrolyte in Å and which for a 2:1 electrolyte has been taken[15(c)] to be 5Å. Further, if the mean molar activity coefficient of $CuCl_2$ at any ionic strength $I = 0.5, \Sigma\, C_i Z_i^2$ is given by

$$\log \gamma_\pm = -A' I_i^{0.5}/(1 + I_i^{0.5}) + BI_i)$$

Table 1—Measured emf (E) of cell (1) as functions of the molality m of $CuCl_2$. Also recorded are the equilibrium constants K_1 and K_2 of the equilibria 3 and 4, standard cell potential $E°$, activity coefficient $\gamma_\pm$, degree of dissociation α_1 and α_2, regression coefficient r and the slope s, of the plot of LHS of Eq. 12 vs I_1 at 303.15K

$CuCl_2$ in Water

m	E(volt)	$\gamma_\pm$	α_1	α_2
0.0006	−0.0998	0.9048	0.7964	0.6253
0.0015	−0.1113	0.8774	0.6325	0.5092
0.0019	−0.1112	0.8698	0.5892	0.4832
0.0029	−0.1130	0.8558	0.5143	0.4414
0.0044	−0.1148	0.8312	0.4453	0.4060
0.0052	−0.1150	0.8352	0.4193	0.3935
0.0059	−0.1156	0.8305	0.4000	0.3845
0.0074	−0.1185	0.8220	0.3675	0.3698
0.0089	−0.1217	0.8149	0.3420	0.3589
0.0098	−0.1219	0.8111	0.3292	0.3537

$K_1 = 0.001$; $K_2 = 0.001$; $r = 0.9747$; $s = 11.1355$; $E° = -0.3985$V

$CuCl_2$ in DMF

m	E(volt)			
0.0014	0.0502	0.7208	0.3162	0.7010
0.0020	0.0411	0.6921	0.2842	0.6963
0.0028	0.0308	0.6616	0.2591	0.6962
0.0035	0.0248	0.6396	0.2451	0.6987
0.0043	0.0179	0.6171	0.2338	0.7027
0.0056	0.0041	0.5864	0.2215	0.7105
0.0064	−0.0009	0.5698	0.2162	0.7156
0.0070	−0.0059	0.5583	0.2129	0.7193
0.0083	−0.0159	0.5357	0.2074	0.7274
0.0097	−0.0256	0.5140	0.2030	0.7357

$K_1 = 0.00005$; $K_2 = 0.0005$; $r = 0.9417$; $s = -4.8879$; $E° = -0.2255$V

$CuCl_2$ in FD

0.0010	−0.3625	0.9388	0.6864	0.5314
0.0021	−0.3208	0.9288	0.5395	0.4408
0.0027	−0.3087	0.9255	0.4909	0.4129
0.0033	−0.2984	0.9230	0.4533	0.3920
0.0041	−0.2886	0.9204	0.4137	0.3708
0.0047	−0.2730	0.9188	0.3895	0.3582
0.0051	−0.2694	0.9178	0.3754	0.3509
0.0054	−0.2576	0.9172	0.3656	0.3459
0.0068	−0.2400	0.9147	0.3270	0.3267
0.0080	−0.2200	0.9131	0.3008	0.3140
0.0094	−0.2071	0.9116	0.2756	0.3021
0.0101	−0.1862	0.9110	0.2646	0.2970

$K_1 = 0.001$; $K_2 = 0.001$; $r = 0.9945$; $s = 75.9178$; $E° = -0.7497$

where

$A'^{15(d)} = \nu^{-1}(\Sigma \nu_j Z_j^2)\, 1.29 \times 10^6/(\varepsilon T)^{1.5}$

$I_1 = (2\alpha_1 + 1)m$ and B is given by Eq. 11, then the cell emf E would be related to $E°$ by Eq. 12,

$$E^{(b)} = E + \frac{2.303\,RT}{2F}\left[\log \alpha_2 \alpha_1^2 (1+\alpha_2)^2 m^3 - \frac{3AI_1^{0.5}}{1+I_1^{0.5}}\right] = E° - YI_1 \quad \ldots (12)$$

Iterative procedure[15(a)] were then employed to evaluate K_1, K_2, α_1 and α_2.

For this purpose, $\gamma_{Cu^{2+}}$ and γ_{Cl^-} were first evaluated at any ionic strength I($I_{Cu^{2+}} = 2m$, $I_{Cl^-} = m$) from Eq. 9 employing the values of A and B as given by Eqs 10 and 11. Then, for certain assumed values of K_2 and taking $\alpha_1 = 1$, α_2 was evaluated from Eq. 6. This value of α_2 was next utilized to calculate a value of α_1 from Eq. 5 for some assumed value of K_1. This process was repeated till the new value of α_2 did not differ from the previous α_2 by more than 0.2%. $\gamma_{Cu^{2+}}$ and γ_{Cl^-} in the particular solvent were next evaluated from Eq. 9 by replacing $I_{Cu^{2+}} = 2m$ by $I_{Cu^{2+}} = (2\alpha_1\alpha_2 m)$ and $I_{Cl^-} = m$ by $I_{Cl^-} = 0.5\alpha_1(1+\alpha_2)m$ and the entire process of evaluating α_1 and α_2 for the same assumed values of K_1 and K_2 was repeated till it gave α_1 and α_2 data that did not differ from the previous α_1 and α_2 data by more than 0.2%. If the correct values of K_1 and K_2 had been used in the above mentioned process, then $E^{(b)}$ should be a linear function of I_1 with intercept $E°$. It was observed that this procedure did yield linear plots (with regression coefficient $r \geqslant 0.94$) of $E^{(b)}$ vs I_1 for $CuCl_2$ in W, NND and FD. The relevant best K_1, K_2, α_1, α_2 and $E°$ data for $CuCl_2$ in W, NND and FD are recorded in Table 1. All the calculations were performed on a Casio XT programmable calculator; the regression coefficient r and the slope s and intercept $E°$ of the $E^{(b)}$ vs I_1 plots are also recorded in Table 1.

Discussion

We are unaware of any $E°$ data at 303.15 K of cell 1 with which to compare our present $E°$ data. The K_1 and K_2 data for the dissociation of $CuCl_2$ and $(CuCl)^+$ in W, FD and DMF show that while $CuCl_2$ and $(CuCl)^+$ both ionize (as per the equilibria 3 and 4) to the same extent in W and FD, the dissociation of $CuCl_2$ to yield $(CuCl)^+$ in DMF is 10 times smaller than the dissociation of $(CuCl)^+$ to yield Cu^{2+} ion. The emf data of cell 1 further reveals that though E(FD) (emf of cell 1 with $CuCl_2$ in FD) and

E(W) data are both negative, yet E(FD) data are more negative than the corresponding E(W) data. Again E(DMF) data are positive in the concentration range $0 < m < 0.0056$ but become negative thereafter.

If the cell reaction for positive emf is $Cu + 2AgCl \rightleftharpoons Cu^{2+} + 2Cl^- + Ag$, then the present emf data suggest that while FD and W as solvents for $CuCl_2$ favour deposition of Cu^{2+} ions from the solution onto the copper amalgam electrode (and this effect should be more marked in FD than in W) over the entire $CuCl_2$ concentration range investigated in the present study, DMF should favour dissolution of metallic copper in the concentration range $0 < m < 0.0056$ only (and the effect should become more pronounced as $m \rightarrow 0$). In the range $m > 0.0056$, even DMF should favour deposition of Cu^{2+} ions from the solution onto the copper amalgam electrode and the effect should become more marked with increase in the concentration of $CuCl_2$. This is as it should be. The two phase copper amalgam electrode in contact with Cu^{2+} ions in the solvent S(S = FD, W or DMF) would be characterized by[16] (i) its tendency to cause Cu to pass into solution as Cu^{2+} ions and (ii) by the tendency of Cu^{2+} ions (from the solution) to be discharged onto the amalgam electrode, i.e., via the equilibrium,

$$[Cu(S)_x]^{2+} + 2e \rightleftharpoons Cu + xS \qquad \ldots (13)$$

Since the Gutman donor number (defined[1,2] as the negative of the molar enthalpy in kcal mol^{-1} of reaction of the solvent in a dilute solution of 1,2-dichloroethane with antimony pentachloride) varies[1,2] as: FD(36) > W(33) > DMF (26.6), the tendency of these solvents to coordinate/solvate with Cu^{2+} ions and to shift the equilibrium represented by Eq. 13 to the right should vary as FD > W > DMF. The shift of equilibrium 13 to the right would leave[16] free electrons on the solution side of the electrode and positive Cu^{2+} ions would accumulate on the copper amalgam electrode. Since Cu^{2+} ions would have greater tendency to coordinate/solvate than the Ag^+ ion with the present solvents, the above arguments would require that the tendency of the Ag/AgCl electrode to acquire negative charge in these solvents should vary as FD > W > DMF. The setting up of double layer around the electrodes would then require that the tendency of Cu^{2+} ions (in FD, W and DMF) to be deposited onto the copper amalgam electrode should vary as FD > W > DMF. Again, the dielectric constant at 303.15K of these solvents varies[4] as FD (107.40) > W(78.20) > DMF (38.82). The lowest dielectric constant of DMF coupled with its lowest Gutman donor number[1,2] (as compared to that of FD and W) would then require, as the concentration of $CuCl_2$ is raised and as the tendency of $CuCl_2$ to yield free Cu^{2+} ions is very small ($K_2 = 5 \times 10^{-4}$), the shifting of equilibrium 13 to the right; this would evidently favour the deposition of Cu^{2+} ions from the solution onto the amalgam electrode. The above arguments would then require that while the emf of cell 1 should be negative when FD and W are used as solvents for $CuCl_2$ {and E(FD) should be more negative than E(W)}, it should be positive in the range $m \rightarrow 0$ when $CuCl_2$ is dissolved in DMF (and should become less positive and eventually become negative as the concentration of $CuCl_2$ is raised). This is indeed true of the present emf data.

The E° data in Table 1 were next employed to compute the standard molar Gibbs free energy of transfer of $CuCl_2$ from W to FD or DMF utilizing the relationship[17],

$$\Delta G^\circ(tr)[CuCl_2, W \rightarrow S'(S' = FD \text{ or } DMF)] = -2F[(E^\circ)_{S'} - (E^\circ)_w] - 3RT \ln(M_S/M_W)$$

where M_S, etc., denote the molecular mass of the solvent S'.

The $\Delta G^\circ(tr)(CuCl_2, W \rightarrow FD) = 60.90$ kJ mol^{-1} and $\Delta G^\circ(tr)(CuCl_2 W \rightarrow DMF) = -43.98$ kJ mol^{-1} data at 303.15K then suggest that though the transfer of $CuCl_2$ from W to FD is energetically not favourable, yet the transfer of $CuCl_2$ from W to DMF is energetically favourable. This is as it should be. The process of transfer of an electrolyte from W to S' actually involves the transfer of charged species from W to S'. The $\Delta G^\circ(tr)(CuCl_2, W \rightarrow S')$ term should, therefore, be composed of (a) an electrostatic component $\Delta G^\circ(tr)(el)$, that takes cognizance of the change in dielectric constant of the medium and (b) a chemical component $\Delta G^\circ(tr)(chem)$, that arises from cation-solvent and anion-solvent interactions. Following Roy *et al.*[18], $\Delta G^\circ(tr)(CuCl_2, W \rightarrow S')$ may then be expressed as,

$$\Delta G^\circ(tr)(CuCl_2, W \rightarrow S') = \Delta G^\circ(tr)(el) + \Delta G^\circ(tr)(chem)$$

If the electrostatic component of $\Delta G^\circ(tr)$ is assumed to be well described by Born-model of ion solvation, then for $CuCl_2$ it should be expressible[19] by,

$$\Delta G^\circ(tr)(el) = 0.5\, Ne^2[(1/\varepsilon_{s'}) - (1/\varepsilon_w)](1/r_+ + 2/r_-)$$

Where while $\varepsilon_{s'}$ and r_+, etc., denote respectively the dielectric constant of the medium S' and the radius of the cation, N is Avogadro's number, and e is the electronic charge. The $\Delta G^\circ(tr)(chem)$ $(CuCl_2, W \rightarrow S')$ should then be a good measure of ion-solvent interactions. The $\Delta G^\circ(tr)(chem)$ $(CuCl_2, W \rightarrow FD) = 61.50$ kJ mol^{-1} and $G^\circ(tr)(chem)(CuCl_2, W \rightarrow DMF) = -45.06$ kJ mol^{-1} at 303.15K (the

relevant ε_S, S and r_+, etc., data were taken from the literature[4,20]), then clearly shows that ions of $CuCl_2$ undergo better ion-solvent interactions in DMF than that in FD, and that ion-solvent interactions play a very important role in the transfer of $CuCl_2$ from W to FD and DMF.

Acknowledgement

The authors express their thanks to the UGC, New Delhi for financial assistance.

References

1 Gutmann V & Wychera E, *Inorg nucl Chem Lett*, 2 (1966) 257.
2 Gutmann V, *Coord Chem Rev*, 18 (1976) 225.
3 Reichardt C & Harbusch-Goernem E, *Liebigs Ann Chem*, (1983) 721.
4 Marcus Y, in *Ion solvation* (John Wiley, Chichester) 1985, (a) p. 146 & p. 150; (b) 131-144.
5 Furter W F, in *Thermodynamic behaviour of electrolytes in mixed solvents* (Amer Chem Soc, Washington, DC) 1976, 26-35.
6 Harned H S & Fitzgerald M E, *J Am chem Soc*, 58 (1936) 2624.
7 Assarson P, Chen N Y & Eirich F R in *Colloidal dispersions and micellar behaviour* edited by K L Mittal (ACS symposium series 9, Am. Chem. Soc., Washington D.C.), (1975), 25.
8 Singh P P & Bhatia M, *J chem Soc Faraday Trans I*, 85 (1989) 3797.
9 Vogel A I, *A text book of quantitative inorganic analysis* (Longmans, London) 3rd Edn. 1961, 445.
10 Hornibrook W J, Janz G J & Gordon A R, *J Am chem Soc*, 64 (1942) 573.
11 Brewster R O & Groening T, *Org Syn CollVol* 3, 2 (1943) 446.
12 Ahrland S & Rawsthrone, *Acta chem scand*, 24 (1978) 157.

Indian Journal of chemistry
Vol. 31A, April 1992, pp. 232-236

Studies on solute-solvent interactions in aqueous solution of isomeric mono-hydroxybenzoate salts

D K Chatterjee & B K Seal*
Department of Chemistry, University of Burdwan, Burdwan 713 104, India

Received 31 May 1991; revised 23 September 1991; rerevised and accepted 1 January 1992

Measurements of the relative viscosities of aqueous solutions of sodium salts of *o*-, *m*- and *p*-hydroxybenzoic acids in the temperature range 298-308 K have revealed that among the three salts, *o*-hydroxybenzoate has the smallest B-coefficient and it behaves as a structure breaker while the *meta*- and *para*-isomers act as water structure makers, the structure forming capacity of the latter two being almost the same. The energy of activation data support the above conclusions. The smaller B-coefficient of *o*-hydroxybenzoate ion may be due to involvement of the *ortho*-hydroxyl group in intra- and inter-molecular hydrogen bonding with the carboxylate group and the solvent water respectively. Since the probability of intra-molecular hydrogen bonding is absent in the case of *meta*- and *para*-hydroxybenzoates, these have B-values higher than that of the *o*-isomer. A comparison of B-coefficients of the three isomeric *mono*-hydroxybenzoate salts with that of sodium benzoate at 298 and 308 K shows that introduction of an hydroxyl group destroys partly the hydrophobic character of the benzene ring in the benzoic acid molecule.

The majority of viscosity B-coefficients so far reported are for simple inorganic electrolytes and the fluidity of electrolytes with organic skeleton has been much less studied except for the quaternary ammonium salts[1], amino acids[2] and salts of several aliphatic acids[3,4]. A study of the viscosity behaviour of benzoic acid and alkali metal benzoates has revealed that benzoic acid, benzoate salts and benzoate ion are all structure makers and the ionic B-coefficient is higher than the molecular B-values. Yashuda *et al.*[5] have determined the B-coefficients of several substituted benzoate salts and have noted a positive effect of substituent on solute-solvent interaction. A systematic study of substituent effect on water-structure has been carried out by the present authors[6-8] using isomeric mono-nitro- and mono-amino-benzoate salts as solutes employing high precision viscometric technique. Encouraged by the results obtained on nitro- and amino-benzoates, we have undertaken a systematic viscometric investigation on alkali metal salts of isomeric mono- and di-hydroxybenzoic acids in order to understand the effect of substitution at different positions of the aromatic ring. In the present communication we report the results of investigations on the viscosity behaviour of *o*-, *m*- and *p*-hydroxybenzoates of sodium.

Materials and Methods

Sodium salts of hydroxybenzoic acids were prepared by mixing equivalent amounts of the crystallised acid and sodium carbonate (AR) in the minimum volume of water to obtain a clear solution (sometimes a slight warming was necessary for dissolution) from which the salt was slowly crystallised out. The repeatedly crystallised salt was finally washed several times with distilled ether and dried. Stock solutions of the salts were prepared by weighing. Solutions of varying concentrations were prepared from the stock solution by dilution.

The densities of the solutions were measured by a calibrated Weld-type pycnometer (40 ml) provided with a graduated stem fitted with a standard joint stopper at its upper end and placed in a constant temperature bath controlled to 0.01°C. A specially designed long flow-time Ostwald viscometer placed in a thermostat (regulated to ±0.01°C) was used to measure the viscosities of solutions. Efflux times (at least three) of solutions measured by a 0.1 sec stop watch with timings reproducible to ±0.2 sec were averaged. For calibration of the viscometer the observed flow times for freshly prepared triply distilled water at two different temperatures, viz., 303 and 308 K were 867.8 and 785.5 sec respectively. The viscometer constants were determined according to Eq. 1,

$$\frac{\eta}{d} = A' t - \frac{B'}{t} \qquad \ldots (1)$$

where η (cp) is the viscosity, d, the density (g ml^{-1}) and t, the flow-time in sec. The viscometer constants

Table 1—B-coefficients of isomeric monohydroxy sodium benzoates, *o*- and *p*-anisates and their anions at different temperatures and energy of activation for viscous flow for the anions at 298 K

Solute	B_{salt}			B_{anion}			A-coefficient at 298 K		$\Delta E^{\neq}$ 298 K (kJ mol^{-1})
	298 K	303 K	308 K	298 K	303 K	308 K	Calc.	Obs.	
Sodium *o*-hydroxybenzoate	0.368 (±0.023)	0.379 (±0.017)	0.394 (±0.011)	0.282	0.293	0.309	0.009	0.011 (±0.0026)	−1.288
Sodium *m*-hydroxybenzoate	0.483 (±0.008)	0.469 (±0.013)	0.446 (±0.011)	0.397	0.383	0.361	0.0095	0.003 (±0.0016)	1.372
Sodium *p*-hydroxybenzoate	0.466 (±0.025)	0.462 (±0.008)	0.444 (±0.019)	0.380	0.377	0.359	0.0096	0.010 (±0.003)	0.297
Sodium benzoate	0.541*	—	0.500 (±0.014)	0.454	—	0.415		0.005	1.890
Sodium *p*-anisate	0.583 (±0.022)	0.500 (±0.033)	—	0.497	0.415	—	—	−0.015 (±0.003)	7.780
Sodium *o*-anisate	0.593 (±0.014)	—	0.549 (±0.013)	0.509	—	0.464	—	0.00 (±0.002)	2.030

*Taken from Ph.D. Thesis submitted by Dr. P. K. Mandal, p 122 (University of Burdwan, 1973); standard errors are given in the parentheses.

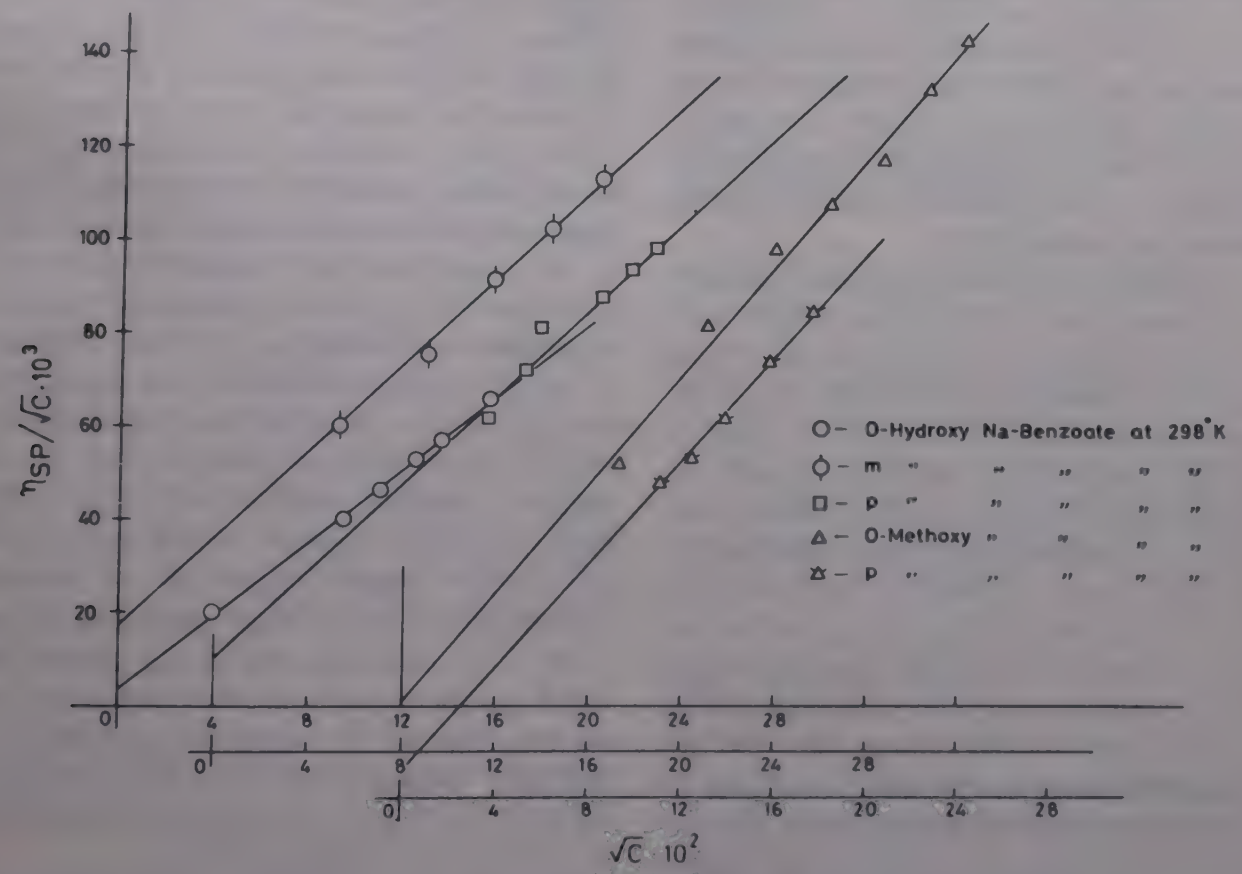

Fig. 1—Plot of $\eta_{sp}/\sqrt{C}$ vs $\sqrt{C}$

A′ and B′ were found to be 9.299×10^{-4} and 5.2111 respectively.

Results and Discussion

Experimental results of the relative viscosities of aqueous solutions of the solutes have been analysed by Jones-Dole equation[9] (Eq. 2),

$$\frac{\eta_{sp}}{\sqrt{C}} = A + B\sqrt{C} \qquad \ldots (2)$$

where $\eta_{sp} = \eta/\eta_0 - 1$, η and η_0 are the viscosities of the solution and the solvent respectively, and C is the molar concentration. A and B are constants characteristic of ion-ion and ion-solvent interactions respectively. The B-coefficient, which depends on ion-size and ion-structure, cannot be calculated *a priori*. The plots of $\eta_{sp}/C^{1/2}$ vs $C^{1/2}$ for the electrolytes were found to be linear with least scatter in the concentration range studied. Some typical plots are presented in Fig. 1. The regression coefficients for

Table 2—Partial molal volume, hydration number and radii of anions at 298 K

Solute	ϕ_v^0 (ml mol^{-1})	$\eta_{H,O}$	Hydration no. of anion	R^a (Å)	R^b (Å)
Sodium *o*-hydroxybenzoate	92.76	3.08	−0.92	3.55	3.32
Sodium *m*-hydroxybenzoate	80.00	6.27	2.27	3.98	3.18
Sodium *p*-hydroxybenzoate	88.80	5.40	1.40	3.92	3.29
Sodium benzoate	87.17[c]	7.15	3.15	4.15	3.26
Sodium *p*-anisate	107.00	7.00	3.00	4.28	3.50
Sodium *o*-anisate	101.21	7.60	3.60	4.32	3.42

(a) *R* calculated from *B*
(b) *R* calculated from ionic partial molal volume
(c) Data from Mohanty R K & Bhowmik S, *Indian J Chem*, **22A** (1983) 518

the plots of $\eta_{sp}/C^{1/2}$ vs $C^{1/2}$ lie in the range 0.994-0.992. The constants A and B were obtained as intercepts and slopes of the Jones-Dole plots. The B values of the salts obtained at three different temperatures are recorded in Table 1 where the A coefficients at 25°C only have been shown. The theoretical values of A calculated from the Falkenhagen-Vernon equation have also been recorded in the same table where the standard errors in A and B have been given. Such data may now be employed to suggest qualitatively the structure making/breaking ability of the solutes investigated.

The B-coefficients of the isomeric mono-hydroxybenzoates, as seen from Table 1, are positive and fairly large when compared with those of simple electrolytes. For *ortho*-hydroxybenzoate the B-value increases with increase in temperature, while it decreases in the case of *meta*- and *para*-isomers. To obtain better insight into solute-solvent interactions, splitting of the B-coefficient into ionic components is desirable. Ionic B values obtained by the method of Kaminsky[10] are shown in Table 1. B_{anion} values exhibit the same trend as the B's of the electrolytes with respect to temperature. This observation suggests that while *o*-hydroxybenzoate salt and the corresponding anion act as structure breakers, the *m*- and *p*-isomers are structure promoters. The negative value of the energy of activation for viscous flow of the *o*-isomer supports its structure disrupting property.

For the *m*- and *p*-isomers the activation energy is positive—a characteristic of structure makers. Table 1 shows that the structure making ability of the *m*- and *p*-isomers is almost the same. These results suggest that ion-solvent interaction depends on the mutual positions of the $-OH$ and $-COO^-$ groups. The works of Yasuda *et al.*[5] support this conclusion. The smaller B value of the *o*-hydroxybenzoate ion compared to those of the *meta*-and *para*-isomers is probably due to simultaneous involvement of the *ortho*-hydroxyl group in intramolecular hydrogen bonding with the carboxylate site and intermolecular interaction with the surrounding water molecules. As a result, the electrostrictive action of the carboxylate group and hence its structure making ability is reduced. The second mechanism suggests that the hydroxyl group cleaves the cage of the water structure present around the benzene ring where the hydration may be expected to be hydrophobic due to its large size[11]. That the hydrophobic hydration surrounding a large ion is reduced due to the presence of an hydroxyl group in the ion-structure has been demonstrated by Wen and Saito[11] in their work on tetra-(2-hydroxyethyl)-ammonium ion which has a B value lower than that of tetrapropylammonium ion of similar size. Since intramolecular hydrogen bonding between the carboxylate and hydroxyl group is absent in the *meta*- and *para*-isomers, they have B values higher than that of the *ortho*-isomer. This is further corroborated by the fluidity behaviour of sodium *ortho*-methoxybenzoate in the temperature range 25-35°C. It is observed that at any given temperature the B-coefficient of *o*-methoxybenzoate ion is greater than that of the *o*-hydroxybenzoate ion and the thermal dependence of B-coefficient of *o*-methoxybenzoate ion is similar to that of the *meta*- and *para*-hydroxybenzoate ions.

From Table 1 it appears that the B values of sodium benzoate and sodium *p*-anisate are greater than those of *p*-hydroxybenzoate at the temperatures studied. The results clearly suggest that in *p*-hydroxybenzoate the hydroxyl group cleaves the structure of water molecules causing thereby a decrease in its B-value compared to that of benzoate.

Hydration of solute

The number of water molecules ($n_{H,O}$) bound per mole of the solute has been calculated from the following equation[12],

Table 3—Free energy of activation of solute and its anion for viscous flow at different temperatures

Solute	$\Delta\mu_3^{0\neq}$ (kJ mol^{-1})			$\Delta\mu_{3(-)}^{0\neq}$		
	298 K	303 K	308 K	298 K	303 K	308 K
Sodium *o*-hydroxybenzoate	69.75	72.57	75.26	51.35	54.26	56.97
Sodium *m*-hydroxybenzoate	83.93	82.96	82.85	65.53	64.65	64.56
Sodium *p*-hydroxybenzoate	82.81	82.26	82.18	64.41	63.95	63.89
Sodium *p*-anisate	98.60	91.87	—	80.20	73.56	—
Sodium *o*-anisate	101.76	—	99.63	83.36	—	55.12
Solvent[a]	9.21	9.04	8.94			

(a) *J chem Soc Faraday Trans I*, **72** (1976) 656.

Table 4—Enthalpy and entropy of activation for viscous flow of solutes and their anions at 298 K

Solute	$\Delta H_3^{0\neq}$ (kJ mol^{-1})	$T\Delta S_3^{0\neq}$ (kJ mol^{-1})	$\Delta H_{3(-)}^{0\neq}$ (kJ mol^{-1})	$T\Delta S_{3(-)}^{0\neq}$ (kJ mol^{-1})
Sodium *o*-hydroxybenzoate	−94.54	−164.29	−116.40	−167.75
Sodium *m*-hydroxybenzoate	116.23	32.30	94.38	28.85
Sodium *p*-hydroxybenzoate	101.55	18.74	79.69	15.29
Sodium *p*-anisate	499.71	401.11	475.94	395.75
Sodium *o*-anisate	946.89	845.13	925.03	841.67

$$B = 2.5.10^{-3} M_2(\phi_v^0/M_2 + \omega_1/d_0) \quad \ldots(3)$$

where ϕ°_v is the partial molal volume of the solute at infinite dilution, M_2 is the solute molecular weight, ω_1 is the weight of water per unit weight of the solute and d_0 is the density of water. The values of n_{H_2O} are shown in Table 2. The hydration number is lowest for sodium salicylate, while *m*-and *p*-hydroxybenzoates of sodium have nearly the same solvation number. The hydration numbers of anions have also been shown in Table 2. For salicylate ion, it is negative—a characteristic of structure breakers[13], and for the *m*- and *p*-isomers the values are positive—a property associated with structure making behaviour.

Radii of anions

The radii of the anions have been calculated using the following equation[14]:

$$B_{anion} = 2.5\ \bar{V} = 2.5 \times \frac{4}{3}\pi\frac{R^3N}{1000} \quad \ldots(4)$$

assuming the ion to behave like a rigid sphere with an effective radius R moving in a continuum. The values of R calculated from the above equation as well as from partial anionic molal volumes are recorded in Table 2. The values are fairly close to each other.

Viscosity data have also been analysed on the basis of the transition state theory of the relative viscosity of electrolyte solutions as suggested by Feakins *et al*[15]. The B-coefficient, according to Feakins, is expressed by the equation,

$$B = \frac{\bar{V}_1^0 - \bar{V}_3^0}{1000} + \frac{\bar{V}_1^0}{1000}\left(\frac{\Delta\mu_3^{0\neq} - \Delta\mu_1^{0\neq}}{RT}\right) \quad \ldots(5)$$

where $\bar{V}_1^0$ and $\bar{V}_3^0$ are the partial molal volumes of the solvent and solute respectively, $\Delta\mu_3^{0\neq}$ is the contribution per mole of the solute to the free energy of activation for viscous flow of the solution. $\Delta\mu_1^{0\neq}$, the free energy of activation per mole of the pure solvent, is given[16] by Eq. 6,

$$\Delta\mu_1^{0\neq} = RT \ln\left(\frac{\eta_1 V_1}{hN}\right) \quad \ldots(6)$$

The free energies of activation for viscous flow for the electrolytes, anions and pure solvent are presented in Table 3.

According to Feakins *et al.*[15], $\Delta\mu_3^{0\neq} > \Delta\mu_1^{0\neq}$ for the solutes having positive B-values. The greater the value of $\Delta\mu_3^{0\neq}$, the greater is the structure making ability of the solute. On the basis of this viewpoint it is concluded from the results shown in Table 3 that while the *para*-anisate ion is an efficient structure maker, the salicylate ion is least so. According to Feakin's model, $\Delta\mu_3^{0\neq}$ increases with temperature for solutes having positive values of dB/dT. This is nicely shown in the case of salicylate ion which acts as a structure breaker.

The magnitude and sign of $\Delta\mu_3^{0\neq}$ depend on the relative values and signs of $\Delta H_3^{0\neq}$ and $T\Delta S_3^{0\neq}$. The values of $\Delta H_3^{0\neq}$ and $T\Delta S_3^{0\neq}$ for the salts as well as their anions have been calculated at a particular temperature, viz., 298 K and the results are shown in Table 4. It is observed that while $\Delta H_3^{0\neq}$ and $\Delta S_3^{0\neq}$ are negative for salicylate ion, they are positive for the *m*- and *p*-salicylates as well as for *ortho*- and *para*-anisates. The negative values of enthalpy and entropy of activation for viscous flow suggest that for salicylate the solute-solvent interactions are strong in the transition state solvent, as observed by Feakins for several structure breakers in aqueous solution. In the case of *m*- and *p*-hydroxybenzoates as well as of *o*- and *p*-anisates both the enthalpy and entropy of activation are positive and $\Delta H_3^{0\neq} > T\Delta S_3^{0\neq}$, suggesting that solute-solvent interaction for these anions is nearly complete in the ground state. Similar observations have been made by Feakins *et al.*[17] in aqueous solution of LiCl.

References

1 Kay R L, Vituccio T, Zawoyski C & Evans D F, *J phys Chem*, 70 (1966) 2336.

2 Devine W & Lowe B M, *J chem Soc (A)*, (1971) 2113.

3 Lawrence V D & Wolfenden J H, *J chem Soc*, (1934) 1114.

4 Patil K J, Patil P V & Thakara O B, *Indian J Chem*, 17A (1979) 177.

5 Yasuda M & Mizutani K, *Bull chem Soc (Jpn)*, 46 (1973) 1973.

6 Mandal P K, Chatterjee D K, Seal B K & Basu A S, *J sol Chem*, 7 (1979) 57.

7 Seal B K, Chatterjee D K, Chatterjee R & Mandal P K, *Acta chim Acad scient hung Tomns*, 111(1) 88 (1983) 37.

8 Seal B K, Chatterjee D K & Mandal P K, *Indian J Chem*, 21A (1982) 509.

9 Jones G & Dole M, *J Am chem Soc*, 51 (1929) 2950.

10 Kaminsky M, *Discuss Faraday Soc*, 24 (1957) 171.

11 Wen W Y & Saito S, *J phys Chem*, 68 (1964) 2639.

12 Patil R I, Patil K J & Kanland M V Z, *Z physik Chem (NF)*, 86 (1973) 67.

13 Woldan M, *Z physik Chemie (Leipzig)*, 269, 6S (1988) 628.

14 Einstein A, *Ann physik*, 19 (1906) 289.

15 Feakins D, Freemantle D J & Lawrence K G, *J chem Soc Faraday Trans I*, 70 (1974) 795.

16 Glasstone S, Laidler K J & Eyring H, *The theory of rate processes* (McGraw Hill, N.Y.), 1941, 477.

17 Feakins D, Waghorne W E & Lawrence K G, *J chem Soc Faraday Trans I*, 82 (1986) 563.

Indian Journal of chemistry
Vol. 31A, April 1992, pp. 237-242

Investigations on electrochemical oxidation of 2-mercaptobenzothiazole

R N Goyal* & Anoop Kumar
Department of Chemistry, University of Roorkee, Roorkee 247 667

Received 27 August 1991; revised and accepted 17 December 1991

The electrochemical oxidation of 2-mercaptobenzothiazole (2-MBT) at pyrolytic graphite electrode has been studied in phosphate buffers of *p*H range 2.31-10.3. It is observed that oxidation of 2-MBT does not stop at disulphide stage but further oxidation followed by desulphurization gives elemental sulphur and mono sulphide as the final products of oxidation. A tentative mechanism for formation of products has been proposed.

Benzothiazoles have been a subject of investigation for a long time due to their importance in physiological systems. 2-Mercaptobenzothiazole (2-MBT) has many useful applications[1-7].

The importance of oxidation reactions in biological systems has made the redox chemistry of 2-mercaptobenzothiazole (2-MBT) a subject of much interest. Chemical oxidation of 2-MBT has been studied by various workers using different reagents and it has been suggested that oxidation of 2-MBT depends on the nature of oxidising agent as well as reaction conditions[8-10]. Electrode reactions of 2-MBT have also been studied to some extent[11-14].

In a recent report from our laboratory[15], electrochemical oxidation of 2-mercaptobenzothiazole was reported at PGE. In cyclic voltammetry, electrooxidation of 2-MBT exhibited two oxidation peaks and a mechanism corresponding to peak Ia (at less positive potential) was reported. In this paper some interesting results corresponding to peak IIa are presented.

Materials and Methods

2-Mercaptobenzothiazole (2-MBT) was obtained from Aldrich Chemical Co., USA and was used as received. 2,2′-Dithiobis(benzothiazole) and 2,2′-thiobis(benzothiazole) were synthesized in our laboratory by the method reported in literature[16] and their purity was ascertained by repeated crystallisation, TLC and melting point. All other chemicals used were of AR grade. All the experiments were carried out in phosphate buffers[17] of ionic strength 0.5 mol dm^{-3}.

Equipment used for electrochemical studies has been described elsewhere[18]. Pyrolytic graphite electrode (PGE) used as working electrode was prepared in the laboratory by the reported method[19]. It had an area of ~2.0 mm^2. IR spectra of products were recorded in KBr on a Perkin-Elmer FT-IR 1600 spectrophotometer. Mass spectra of the samples were monitored at 70 eV using a Hewlett-Packard 5985-B instrument.

Stock solution (2 mmol) of 2-MBT was prepared by dissolving the required amount in minimum amount of methanol (10%) followed by the addition of doubly distilled water. For recording cyclic voltammograms, 5 ml of the stock solution was mixed with 5 ml of phosphate buffer (ionic strength, 1.0 *M*) of appropriate *p*H so that overall ionic strength of the working solutions was maintained as 0.5 mol dm^{-3}. A purified stream of nitrogen was passed through the solution for about 8-10 min to deaerate the solution before recording the voltammograms. Coulometric studies were carried out in a conventional three comparment cell using pyrolytic graphite plate (area 5.8 cm^2) as working, platinum gauze as auxillary and SCE as reference electrode. The n value, number of electrons involved in electrooxidation process, was calculated by graphical integration of the current time curve as reported by Lingane[20].

For the product identification, 4-5 mg of 2-MBT was electrooxidised at a potential 100 mV more positive than peak IIa and the course of electrolysis was monitored by recording cyclic voltammograms at different time intervals. When peak IIa decreased to about 95%, electrolysis was stopped and the electrolysed solution was removed from the cell and lyopholised. The dried material obtained was dissolved in 1-2 ml of distilled water and was passed through a glass column packed with Sephadex G-10 (bead size 40-120 μ) using doubly distilled water as the eluting solvent. The flow rate was 8-10 ml/hr and 5 ml fractions were collected using SICO (FRAC-711) fraction collector. The absorbance of each fraction was measured at 210 nm using a Beck-

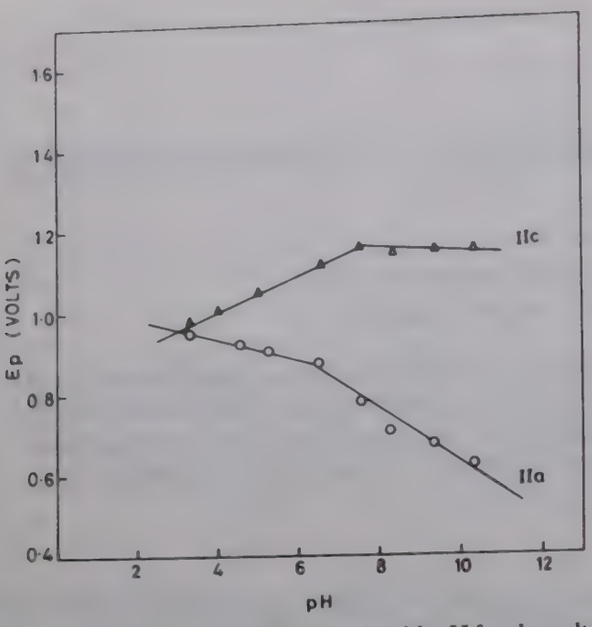

Fig. 1—Variation of the peak potentials with *p*H for the voltammetric oxidation of 2-MBT.

mann Du-6 spectrophotometer. The absorbance versus volume plot showed two peaks [110-170; 180-250 ml]. The peak in the region 110-170 ml was due to phosphate and hence this fraction was discarded. This arrangement gave separation of phosphate from oxidation products. The fractions in volume range 180-250 ml was lyophilised and freeze dried material obtained was analysed by m.p., IR and mass spectra. TLC was carried out using silica gel for TLC as adsorbent and benzene-methanol (80:20) as eluent.

Results and Discussion

Cyclic voltammetry

In cyclic voltammetry at sweep rate of 200 mV s^{-1}, 2-MBT was electrooxidised in two well-defined oxidation peaks Ia and IIa in the *p*H range 2.31-10.3. As characteristics of peak Ia have been described earlier[15], the results on peak IIa only are described here. Peak potential of oxidation peak IIa was dependent on *p*H and shifted towards less positive potential with increase in *p*H. E_p versus *p*H plot exhibited a break at around *p*H 6.4 indicating pK_a of the species generated in peak Ia reaction [2,2'-dithiobis(benzothiazole)] (Fig. 1). The linear dependence of E_p on *p*H can be represented by the following equations,

$$E_p(2.3\text{-}6.4) = [1.04\text{-}0.025\ pH]\ V\ (\text{versus SCE})$$

$$E_p(6.5\text{-}10.3) = [1.27\text{-}0.066\ pH]\ V\ (\text{versus SCE})$$

Peak clipping experiments indicated that peak IIc is related to peak IIa and thus the product formed in Ia is reduced in Ic and oxidized in IIa to a species reduced in IIc. The peak potential of peak IIc was also

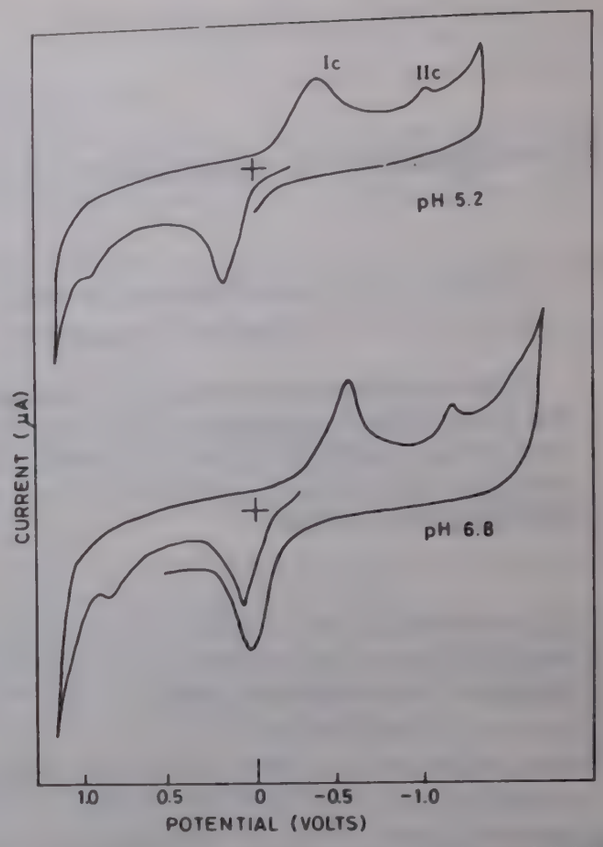

Fig. 2—Typical cyclic voltammograms of 0.5 mmol 2-MBT in phosphate buffers of different *p*H [sweep rate 200 mV/s].

dependent on *p*H and shifted towards more negative potential with increase in *p*H (Fig. 2). The $E_p(II)_c = f(pH)$ indicates that at *p*H greater than about 7.5, peak potential becomes practically *p*H-independent. This indicates that the product of oxidation in E_p(IIa) undergoes an acid-base equilibrium which is sufficiently rapidly established up to *p*H 7.5. At *p*H > 7.5, the conjugate base is reduced.

The effect of concentration of 2-MBT on peak current of oxidation peak IIa was studied in the concentration range 0.1-2.0 mmol. At higher concentration (> 2.5 mmol) peak IIa turned to a bump which probably indicated adsorption complications associated with PGE. In the concentration range 0.1-2.0 mmol, peak currents of peaks IIa and IIc increased linearly with concentration indicating that 2-MBT can be safely estimated in this concentration range at PGE.

Adsorption of 2-MBT at PGE was further confirmed by the plot of peak current function (i_p/ $ACV^{1/2}$) against log of sweep rate. The peak current function for peak IIa increased with increase in sweep rate indicating thereby strong adsorption of 2-MBT at the surface of PGE.

Coulometry

The value of n, number of electrons involved in electrooxidation corresponding to peak IIa, was de-

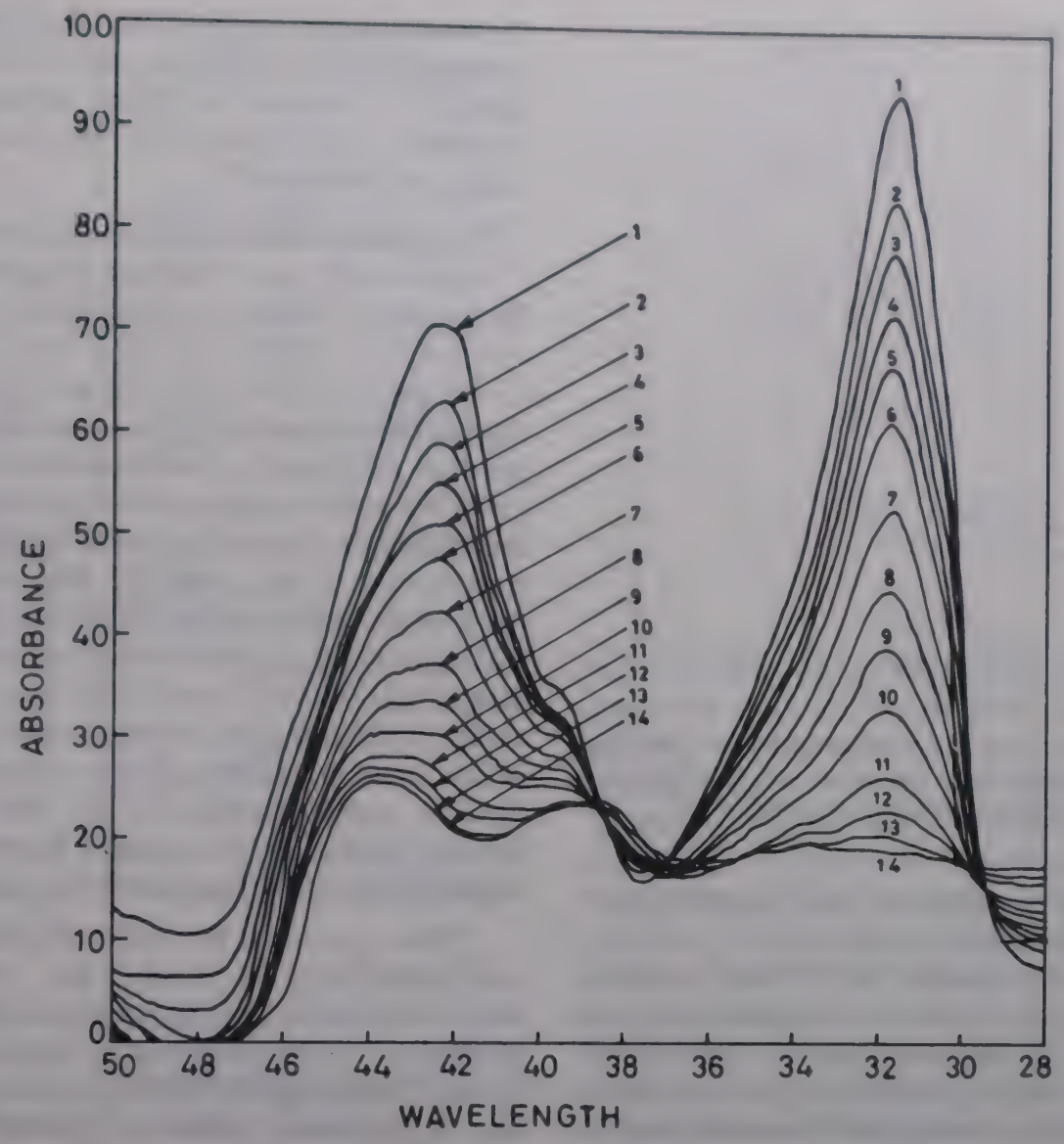

Fig. 3—Observed spectral changes for 0.01 mmol 2-MBT undergoing electrooxidation at peak IIa potential (curves 1-14 were recorded at intervals of 10 min).

Table 1—Observed coulometric n-values for the electrooxidation of 2-mercaptobenzothiazole

*p*H	Conc. (mmol)	Potential* (V)	Exp. n-value†
3.28	0.5	1.0	0.65
4.50	0.5	1.1	0.68
5.20	0.5	1.1	0.62
6.20	0.5	1.1	0.58
8.50	0.5	1.1	0.60
9.30	0.5	1.1	0.65
10.30	0.5	1.1	0.60

*The potential was switched to higher value when the electrolysis at peak Ia potentials was completed.
†Average of at least two replicate determinations.

termined at different concentrations of 2-MBT and at different *p*H. It was found to be 0.60 ± 0.06. The n value observed was less than 1.0 probably because of large background corrections required. The plot $\log i_p = f(t)$ for oxidation at peak IIa potential was a straight line for first 10 min of electrolysis and thereafter a large deviation was observed. This indicated that oxidation followed a single path only for first 10 min and thereafter follow up chemical reactions played a significant role as suggested by Cauquis *et al.*[21]. A 0.2 mmol solution of 2-MBT generally took around 4 hr for complete electrolysis. The values of n calculated by graphical integration of current time curves are presented in Table 1. Progress of electrolysis was monitored by recording cyclic voltammograms at different time intervals. At *p*H 7.2 when 1 mmol solution of 2-MBT was electrooxidised corresponding to peak IIa, the peak current for peak IIa systematically decreased whereas peak current for peak IIc remained practically constant and hence indicated that product of oxidation in IIa undergoes a bulk chemical reaction. After 5 hr of electrolysis, peak IIa completely disappeared whereas peak IIc was clearly visible in completely electrolysed solution indicating electroactive nature of the products formed. Thus, cyclic voltammogram of electrolysed solution did not change after several hours of electrolysis indicating that electrooxidised

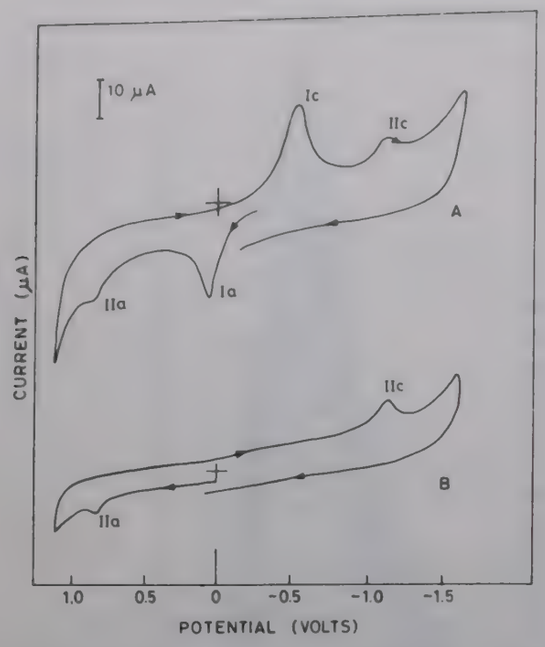

Fig. 4—A comparison of cyclic voltammograms of 2-MBT and 2,2′-dithiobis(benzothiazole) at the sweep rate of 100 mVs^{-1} [(A) 2-MBT (B) 2,2′-dithiobis(benzothiazole)].

product is stable in solutions. An identical behaviour was observed at *p*H 3.2 and 9.3.

UV/Vis spectral changes for 2-MBT were recorded by applying potential corresponding to peak IIa. At *p*H 7.0, 0.01 mmol solution of 2-MBT exhibited λ_{max} at 236 and 318 nm. When potential corresponding to peak IIa was applied, the absorbance at λ_{max} 236 and 318 nm systematically decreased (Fig. 3 curves 1-14). A systematic increase in absorbance in the range 255-270 nm was observed. After 3 hr of electrolysis the absorbance at λ_{max} reached a minimal value and two absorption bands in the region 220-230 and 255-270 nm were clearly visible (Fig. 3). Almost similar behaviour was observed for peak IIa at *p*H 3.2 and 10.3.

Product characterization

Products of electrooxidation of 2-MBT corresponding to peak IIa were identified at *p*H 3.2, 7.0 and 9.3. For this purpose about 5-6 mg of 2-MBT was electrooxidised at potential 100 mV positive to peak IIa. It was very interesting to observe that after 15 min of electrolysis, a yellowish white precipitate started appearing at the surface of PGE which was scratched at the end of electrolysis. The remaining solution was lyopholised. The freeze-dried material was passed through the Sephadex G-10 column (see experimental). The volume collected between 180 and 250 ml was lyopholised and the dried material exhibited one spot in TLC (R_f 0.60). This indicated the presence of only one product in the solution. Yellowish white material collected from scratching the electrode was analysed by TLC. The R_f value of compound using *n*-heptane as developing reagent was 0.70. This value was found similar to that of the authentic sulphur sample as reported for elemental sulphur in literature[22].

The product obtained for the fraction from 180 to 250 ml with R_f value 0.06 had a m.p. 98°C. The FT-IR spectrum of this product gave bands at 2940 (−C=C−), 1580 (−C=N), 765 (phenyl ring C−H) and 730 cm^{-1} (C−S) as reported for 2,2′-thiobis(benzothiazole). The mass spectrum of this product exhibited a clear molecular ion peak at $m/z = 300$ and thus indicated the loss of one sulphur in the disulphide formed in peak Ia oxidation. Hence, a comparison of m.p. and IR data was made with those of the authentic 2,2′-thiobis(benzothiazole). It was interesting to observe that m.p. of the authentic sample was 98-99°C and the IR observed was practically superimposable on the observed IR spectrum of the material. Hence, it was concluded that the product corresponding to R_f 0.60 is 2,2′-thiobis(benzothiazole). No attempt, however, has been made to explain the fragmentation pattern.

Thus, products of electrooxidation of 2-MBT corresponding to peak IIa are 2,2′-thiobis(benzothiazole) and elemental sulphur. As monosulphide is electro-inactive in nature, peak IIc in cyclic voltammogram should be due to the reduction of elemental sulphur to H_2S by the following process.

$$S + 2H^+ + 2e^- \rightarrow H_2S$$

The formation of H_2S during oxidation of 2-MBT was observed when potential in exhaustively electrolysed solution of 2-MBT at peak IIa potential was switched to negative potential corresponding to peak IIc. When a paper dipped in lead acetate was exposed at the mouth of the cell it immediately turned black. Thus, it was concluded that peak IIc is due to the reduction of elemental sulphur to H_2S. To further confirm the formation of 2,2′-thiobis(benzothiazole) in peak IIa oxidation of 2-MBT, electrochemical oxidation of 2,2′-dithiobis(benzothiazole) was studied at different *p*H. A comparison of cyclic voltammograms of 2-mercaptobenzothiazole and 2,2′-dithiobis(benzothiazole) is presented in Fig. 4 which indicates that 2,2′-dithiobis(benzothiazole) undergoes oxidation at a potential similar to that of peak IIa of 2-mercaptobenzothiazole. Hence, the products of electrooxidation of 2,2′-dithiobis(benzothiazole) were also identified at *p*H 7.2 and were found to be elemental sulphur and 2,2′-thiobis(benzothiazole). Therefore, it was concluded that the peak IIa products of 2-mercaptob-

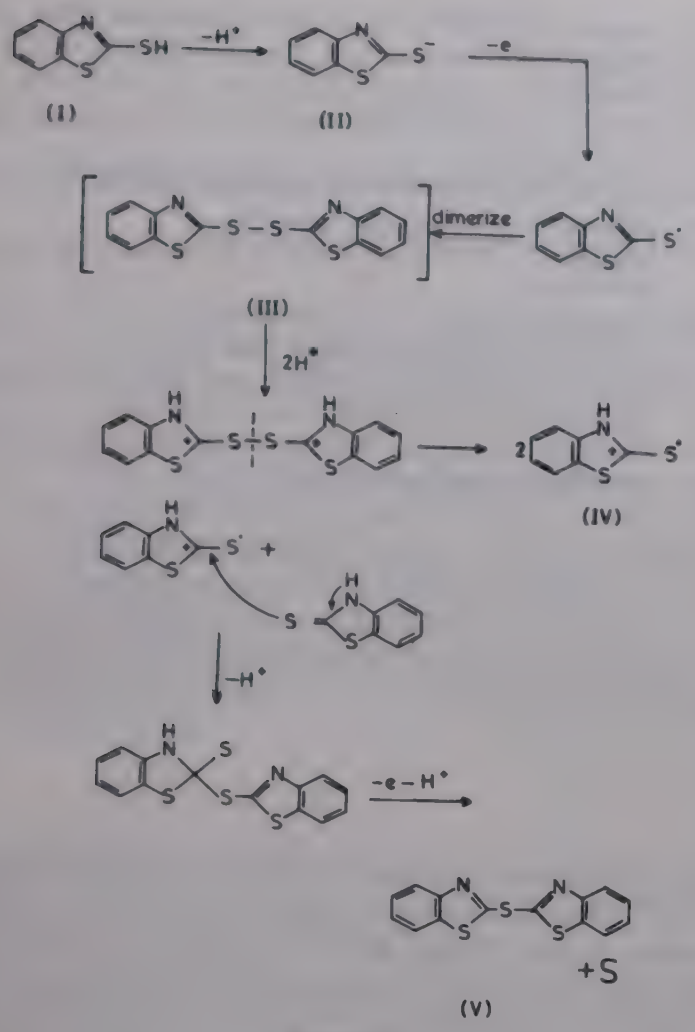

Scheme-1

enzothiazole are 2,2′-thiobis(benzothiazole) and elemental sulphur.

Electrode reaction

On the basis of evidences presented above, it is clear that 2-mercaptobenzothiazole undergoes electrooxidation in two well-defined peaks. The mechanism shown in Scheme 1 can be proposed to account for the experimental observations. As anion (II) is the electroactive species of 2-MBT, 2,2′-dithiobis(benzothiazole) (III) is formed in peak Ia oxidation as reported earlier[15]. The disulphide (III) has been reported[23] to be stable in acetonitrile. However, in phosphate buffers and at pyrolytic graphite electrode the disulphide (III) is found to be unstable and rapidly gives a cationic free radical (IV) as shown in Scheme 1. The cationic free radical (IV) is then attacked by a molecule of 2-mercaptobenzothiazole and gives monosulphide (V) and elemental sulphur as products of oxidation. As elemental sulphur can undergo reduction, peak IIc is observed in cyclic voltammetry due to the formation of H_2S. Thus, it can be safely concluded that initial formation of disulphide in peak Ia reaction is followed by oxidative desulphurisation to give compound (V) and elemental sulphur as the final products of oxidation. The possibility of an alternative route to

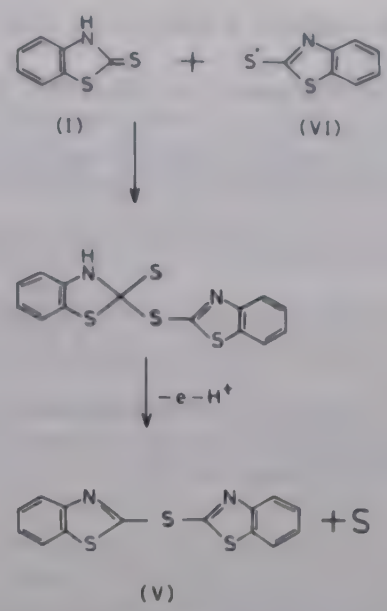

Scheme-2

the formation of monosulphide, which does not require the oxidative cleavage of disulphide (Scheme 2), was ruled out on the basis that when products corresponding to peak IIa were identified, only monosulphide and sulphur were obtained. If monosulphide (V) had formed according to Scheme 2, the disulphide should have also been obtained in the products. Hence, it is proposed that oxidative cleavage of disulphide is involved in the formation of monosulphide.

It is apparent from the present experimental data that electrooxidation of 2-mercaptobenzothiazole occurs in two steps as shown by two well defined peaks. In contrast to the earlier work on platinum electrode, at which 2,2′-dithiobis(benzothiazole) was reported to be non-oxidisable, a further oxidation occurs in peak IIa reaction followed by desulphurisation at the pyrolytic graphite electrode resulting in monosulphide and elemental sulphur as the final products. The proposed mechanism explains all the observed experimental data. The facile desulphurisation of organic disulphides by phosphine has already been reported in the literature[16].

Acknowledgement

The authors are thankful to Dr Rajeshwari for her help in preliminary studies. One of the authors (AK) is grateful to the CSIR, New Delhi for the award of a Research Associateship.

References

1 Liebermeister K, *Z Naturforsch*, 5b (1950) 79.
2 Roda B, Holbova E, Milkulasek S, Sidoova E & Gvodjakova A, *Acta Virol*, 23 (1979) 203.
3 Schraufstatter E, *Z Naturforsch*, 5b (1950) 190.
4 Cech J, *Colln Czech Chem Commun*, 14 (1949) 555.
5 Bandyopadhyay P K & Banerjee S, *J appl polym Sci*, 23 (1979) 185.
6 Prajapathi S N, Soni K P & Bhatt I M, *J electrochem Soc India*, 27 (1978) 177.

7 Patel N K, Franco J & Patel I S, *J Indian Chem Soc*, 58 (1977) 815.
8 Gibbs E M & Robinson F A, *J chem Soc*, (1945) 925.
9 Mathes R A & Beber A J, *J Am chem Soc*, 70 (1948) 1451.
10 Ostrovskaya V M & Shunskaya I A, *Khim Promst Ser React Osobo Christ Veshchestva*, 2 (1980) 14; *Chem Abstr*, 92: 41523r.
11 Bruno M M & Stoddard E, *Nuclear Science Abstr*, 13 (1959) 13217.
12 Sartori G, Liberti A & Calzolari C, *Comite Intern Thermodynm et Cinet Electrochim Compt Rend reunion* (1950) 301.
13 Sartori G & Liberti A, *J electrochem Soc*, 97 (1950) 20.
14 Chandrasekaran M & Krishnan V, *Trans SAEST*, 21 (1986) 25.
15 Goyal R N & Rajeshwari, *Indian J Chem*, 29A (1990) 46.
16 Harpp D N & Gleason J G, *J Am chem Soc*, 93 (1971) 2437.
17 Wopschall R H & Shain I, *Anal Chem*, 39 (1967) 1514.
18 Goyal R N, Bhushan R & Agarwal A, *J electroanal Chem*, 171 (1984) 281.
19 Goyal R N, Srivastava S K & Agarwal R, *Bull Soc chim Fr*, 4 (1985) 656.
20 Lingane J J, Swan C G & Fields M, *J Am chem Soc*, 65 (1950) 1427.
21 Cauquis G & Parker V D, *Organic electrochemistry*, Edited by M M Baizer (Marcel Dekker, New York) 1973, 134.
22 Senning A, *Sulphur in organic and inorganic chemistry* (Marcel Dekker, New York), Vol. 2 (1979) 239.
23 Chambers J Q, Moses P R, Shelton R N & Coffen D L, *J electroanal Chem*, 38 (1972) 245.

Indian Journal of chemistry
Vol. 31A, April 1992, pp. 243-250

Homogeneous catalytic hydrogenation of organic compounds using orthometallated schiff base complexes of palladium(II)

Deb K Mukherjee, Biman K Palit & Chitta R Saha*
Department of Chemistry, Indian Institute of Technology, Kharagpur 721 302

Received 21 August 1991; revised and accepted 3 December 1991

The dinuclear orthometallated schiff base complexes of palladium(II) are efficient catalysts for dihydrogen reduction of organic $-NO_2$, $>C=O$, $>C=C<$, $>C=N-$, $-N=N-$ and $-C\equiv N$ groups under normal or high pressure conditions. The dependence of the catalytic activity on the nature of the bridging group and the schiff base ligands has been established. The experimental conditions control the nature and number of the reduction products in case of nitroaromatics. Reduction mechanism has been proposed on the basis of the nature of intermediate and final reduction products, change of physico-chemical properties of the catalyst solutions, polarographic data of the ligands and the complexes and the kinetic data.

Numerous methods have been developed for the catalytic reduction of organic nitrocompounds[1-7], alkenes[8-12] and alkynes[8,13,14] in homogeneous phase, but relatively few investigations have been made on the reduction of nitriles[15-17] and aliphatic nitrocompounds[18-22]. The importance of the reduction lies in the use of the products for the manufacture of dyes, drugs, pharmaceuticals etc. The elucidation of unambiguous reaction mechanism for the reductions was difficult due to several limitations[20,22]. We have investigated the catalytic activities of various dinuclear orthopalladated complexes with differently C,N-substituted schiff base ligands in order to find out the influence of electron density and steric environment at different points of the complex on their catalytic efficiencies. This may help in the modification of the catalyst system. The present paper reports the results of such investigations.

Materials and Methods

Pure and recrystallised solid reagents, predistilled solvents and pure, dry and deoxygenated hydrogen and nitrogen gases were used for all the experiments. Dimethylformamide (DMF) was dried by storing it over CaH_2 under N_2 for 24 h followed by distillation under reduced pressure. H_2 and N_2 gases were deoxygenated and dried by passing them successively through alkaline pyrogallol, liquid N_2 trap and silica gel tower before introduction into the reaction system.

The complexes used in the present investigation were prepared according to the literature methods[23] and purified by recrystallization from dichloromethane/*n*-hexane and their purities were checked by physico-chemical means before use as catalysts.

Analyses of the product mixture were done on a Varian 3700 gas chromatograph equipped with a flame ionization detector using a S.S. column packed with 25% SE-30 on Chromosorb W mesh. Temperature programming was done in the range 180° to 300°C with the increase of temperature at the rate of 17°C/min. Vibrational, electronic and PMR spectra were recorded in Perkin-Elmer-883, Shimadzu MPC-3100, and Varian EM-390, 90 MHz spectrometers respectively. Molecular weights of the complexes in C_6H_6 and DMF were determined in a Knauer Dampdruck osmometer.

Preparation of the catalysts

The schiff base ligands were prepared by refluxing equimolar quantities of the appropriate aldehyde or ketone and amine in benzene or xylene[24,25]. The sterically hindered schiff bases required extended reflux period (2-3 days) in xylene. The preparation of benzophenoneanil using appropriate reagents required the presence of $POCl_3$ in the medium[26]. Reaction of the schiff base ligand and Pd(II) acetate in refluxing acetic acid resulted in the precipitation of the corresponding complex which was further purified by repeated crystallization from solvent mixture[23]. The purities of the complexes were checked by TLC, IR and electronic spectral data. The metathetical reaction of acetato-bridged complexes with NaCl or NaBr in acetone yielded the corresponding chloro- and bromo-analogues[23].

Another series of orthopalladated complexes was

prepared using the secondary amine LH_3. The latter were obtained by the dihydrogen reduction of the corresponding schiff base ligand, LH in the presence of the presently investigated catalysts or otherwise[27]. Reaction of $Pd(OAc)_2$ with LH_3 in refluxing AcOH produced $Pd_2(LH_2)_2(OAc)_2$. The corresponding chloro- and bromo-analogues were prepared by metathetical reactions. The catalytic activities of the orthometallated complexes, $Pd_2(LH_2)_2X_2$ (Fig. 1a) towards the reduction processes were found to be comparable to those of $Pd_2L_2X_2$ (Fig. 1b).

Reduction procedure

The procedures for normal and high pressure reductions were mentioned in our earlier papers[8,17]. In case of normal pressure reduction, the yellow DMF solution of the catalyst turned deep greenish brown within 10 min on stirring under hydrogen at 20°C. The substrate addition at this stage slightly faded the solution colour and hydrogen absorption started at a maximum rate which was measured using a graduated gas reservoir. The intermediate samples (0.20 ml) were withdrawn from the reaction mixture at an interval of 10 min and analysed immediately by GLC. In the case of high pressure reductions, the final reaction mixture was quenched and the components were estimated by GLC using appropriate columns. The intermediate sample analysis in this case was made at an interval of 30 min only.

Results and Discussion

The compounds have low solubilities in non-polar solvents like benzene, cyclohexane, etc., and moderate solubilities in mild coordinating solvents like DMF, DMSO, etc. The reduction rate of a given substrate was highest in DMF medium and hence most of the reactions were carried out in this medium. Detailed investigations were made with the acetato-bridged complexes due to their better solubilities and higher catalytic activities (Table 1).

Reduction of nitroaromatics, alkenes, alkynes and other organic substrates

The catalytic hydrogenation of nitroaromatics leads to the formation of the corresponding anilines in almost all cases except nitrophenol and *m*-dinitrobenzene where the final products were only the corresponding hydroxylamines (Table 2). Analysis of the intermediate reacton samples indicated the primary formation of hydroxylamines in the case of substrates which are finally reduced to the corresponding anilines. The formation of coupled products such as azo- or azoxybenzene was not ob-

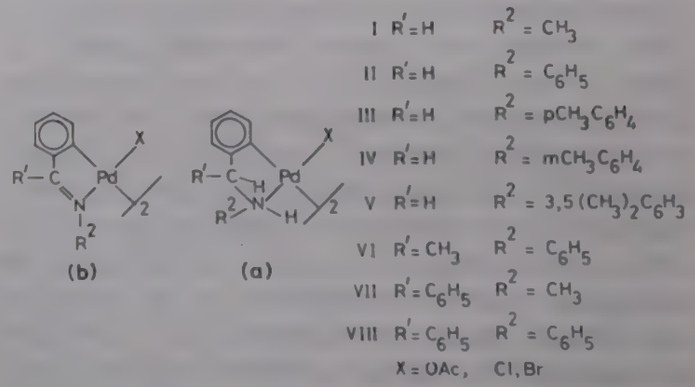

Fig. 1—Structure of (a) $Pd_2(LH_2)_2X_2$ and (b) $Pd_2L_2X_2$.

Table 1—Relative catalytic activity of Pd(II) schiff base complexes in DMF medium at 25°C

Catalyst	Nitrobenzene			Styrene		
	Cat. Conc. (mol. lit^{-1} × 10^{-4})	Sub. Conc. (mol. lit^{-1})	Initial rate of H_2 abs. (ml.min^{-1})	Cat. Conc. (mol. lit^{-1} × 10^{-4})	Sub. Conc. (mol. lit^{-1})	Initial rate of H_2 abs. (ml.min^{-1})
$Pd_2(mbi)_2(OAc)_2$	4.8	0.32	7.90	2.4	0.86	12.90
$Pd_2(BAN)_2(OAc)_2$	4.8	0.32	6.30	2.4	0.86	11.95
$Pd_2(pTBAN)_2(OAc)_2$	4.8	0.32	6.05	2.4	0.86	11.70
$Pd_2(mTBAN)_2(OAc)_2$	4.8	0.32	5.85	2.4	0.86	11.55
$Pd_2(dmBAN)_2(OAc)_2$	4.8	0.32	5.80	2.4	0.86	10.30
$Pd_2(apkt)_2(OAc)_2$	4.8	0.32	5.65	2.4	0.86	07.10
$Pd_2(mbpkt)_2(OAc)_2$	4.8	0.32	3.20	2.4	0.86	04.55
$Pd_2(bpkt)_2(OAc)_2$	4.8	0.32	—	2.4	0.86	01.10

mbi = N-methylbenzaldimine; BAN = N-phenylbenzaldimine; pTBAN = (N-(*p*-tolyl)benzaldimine); mTBAN = (N-(*m*-tolyl)benzaldimine); dmBAN = (N-(3,5-dimethyl)benzaldimine); apkt = N-phenylacetophenoneketimine; bpkt = N-phenylbenzophenoneketimine; mbpkt = N-methylbenzophenoneketimine.

Table 2—Optimum conditions and yields of main products at 1 atm pressure of Hydrogen and 25°C using (a) = $Pd_2(mbi)_2(OAc)_2$, (b) = $Pd_2(pTBAN)_2(OAc)_2$, (c) = $Pd_2(apkt)_2(OAc)_2$ as catalysts

Substrate		Catalyst (mol $lit^{-1} \times 10^{-4}$)	Initial rate of H_2-abs. ($ml.min^{-1}$)	Initial turnover number (min^{-1})	Product %				
1 Nitrobenzene	a	4.8	7.90	14.60	Aniline	98	(a)		
	b	4.6	5.50	10.60		94	(b)		
	c	4.6	5.20	08.80		96	(c)		
2 *o*-Chloronitro-benzene	a	4.8	2.70	05.00	*o*-Chloroaniline	93	(a)		
	b	4.6	2.40	04.60		88	(b)		
	c	4.6	2.15	04.40		88	(c)		
3 *p*-Chloronitro-benzene	a	4.8	3.40	06.30	*p*-Chloroaniline	90	(a)		
	b	4.6	2.70	05.20		86	(b)		
	c	4.2	2.20	04.65		83	(c)		
4 *m*-Dinitrobenzene	a	4.8	7.82	12.40	*m*-Phenylenehydroxyl-amine	94	(a)		
	b	4.6	6.30	09.80		83	(b)		
	c	4.2	5.70	07.65		80	(c)		
5 *o*-Nitrotoluene	a	4.8	2.82	05.20	*o*-Toluidine	96	(a)		
	b	4.6	2.35	04.50		90	(b)		
	c	4.2	2.20	04.05		92	(c)		
6 Pent-1-ene	a	4.2	5.40	31.40	Pentane	66	(a)	Pent-2-ene	30 (a)
	b	5.6	4.15	18.80		66	(b)		30 (b)
	c	5.2	3.15	15.30		58	(c)		40 (c)
7 Hex-1-ene	a	4.2	5.05	28.60	Hexane	64	(a)	Hex-2-ene	28 (a)
	b	5.6	3.70	15.80		60	(b)		30 (b)
	c	5.2	2.70	12.80		66	(c)		30 (c)
8 Cyclohexene	a	4.2	3.15	19.30	Cyclohexane	88	(a)		
	b	5.6	3.30	14.70		80	(b)		
	c	5.2	2.40	09.80		80	(c)		
9 Benzaldehyde	a	5.7	2.70	14.20	Benzylalcohol	96	(a)		
	b	4.8	1.15	13.10		90	(b)		
	c	4.8	1.00	04.55		90	(c)		
10 Benzylidine aniline	a	5.9	2.55	13.80	N-Phenylbenzylamine	96	(a)		
	b	4.8	1.00	07.80		90	(b)		
	c	4.8	0.70	02.60		93	(c)		

served in any case (Figs 2a and 2b). Addition of bases like Py or $(CH_3)_2NH$ (Fig. 3) in the reaction mixture increased the proportion of hydroxylamine at intermediate and final stages and it was possible to reduce the aromatic nitrocompounds only to the corresponding hydroxylamines by controlling the concentration of the base. The presence of oximes was not detected at any stage though aromatic oximes and hydroxylamines were reduced to the corresponding anilines by the present catalytic system. *p*-OHC_6H_4NHOH and *m*-$C_6H_4(NHOH)_2$ are probably not strong enough ligands to coordinate to the metal atom by displacement of DMF from (A) (vide infra) and hence they could not be reduced further. The same situation arises in the case of other aromatic hydroxylamines in the presence of Py or $(CH_3)_2NH$ in the reaction medium.

The presence of alkali in low concentration (0.01 *M*) does not affect the reduction rates or the nature and yields of final products but its presence in high concentration decomposes most of the catalytic species. The addition of acid as expected from the equilibrium reaction (2) (vide infra) decreases the reduction rate and stops hydrogenation if the acid concentration exceeds 0.5 *M*.

Reduction of alkenes

Alk-1-enes undergo simultaneous reduction and isomerization. The initial rates of reduction of styrene, acrylonitrile or isoprene where the double bond is a part of delocalized system are much higher than those of alk-1-enes or penta-1,4-diene where the double bond is either single or non-conjugated.

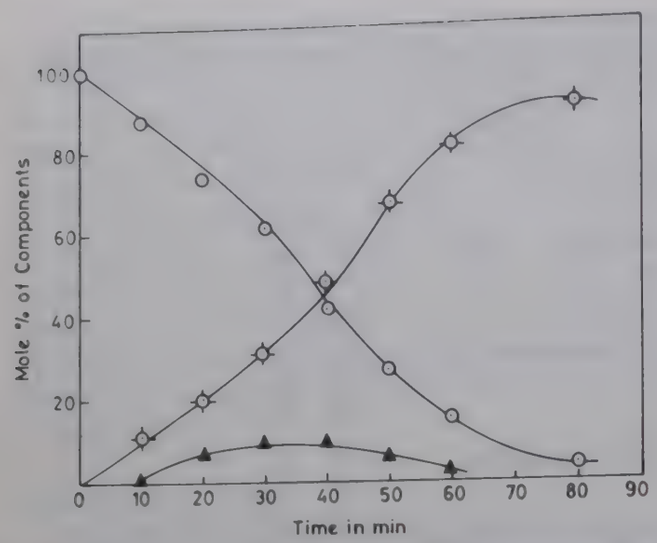

Fig. 2a—Reduction of nitrobenzene with $Pd_2(mbi)_2(OAc)_2$ in DMF at 25°C and under 1 atm. of hydrogen. $Pd_2(mbi)_2(OAc)_2 = 4.82 \times 10^{-4}$ mol dm^{-3}, [nitrobenzene] = 0.32 mol dm^{-3}. ⊙ = nitrobenzene; ◈ = aniline; ▲ = phenylhydroxylamine.

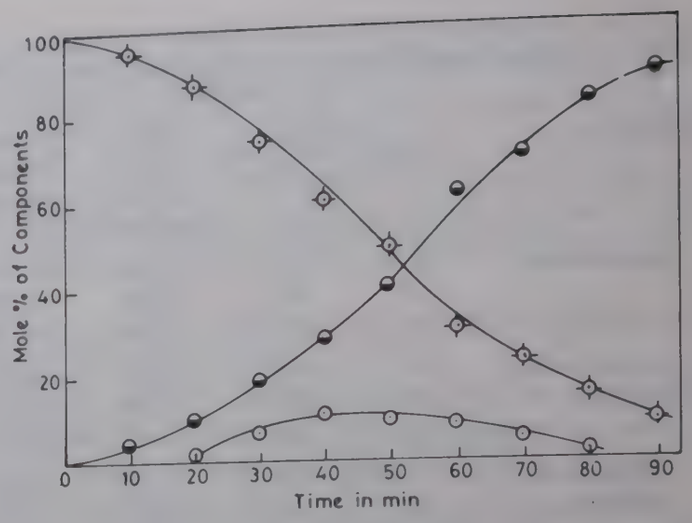

Fig. 2b—Reduction of nitrobenzene with $Pd_2(apkt)_2(OAc)_2$ in DMF at 25°C and under 1 atm. of hydrogen. $Pd_2(apkt)_2(OAc)_2 = 4.82 \times 10^{-4}$ mol dm^{-3}, [nitrobenzene] = 0.32 mol dm^{-3}; ◈ = nitrobenzene; ◒ = aniline; ⊙ = phenylhydroxylamine.

Table 3—Yields of main products of the reduction of nitroalkanes, benzophenone and benzonitrile using (a) $Pd_2(mbi)_2(OAc)_2$; (b) $Pd_2(apkt)_2(OAc)_2$ as catalysts under high pressure and high temperature conditions

[Substrate]		[Catalyst] (mol.$dm^{-3} \times 10^{-4}$)	Hydrogen pressure (KNm^{-2})	Temp. °C	Reaction time (hr)	Products	(%)
1 Nitromethane	a	5.7	11.3×10^3	70	6.00	Methylamine	(93)
(0.25 *M*)	b	5.2	11.7×10^3	85	6.00		(90)
2 Nitroethane	a	5.7	11.3×10^3	70	6.00	Ethylamine	(92)
(0.25 *M*)	b	5.2	11.7×10^3	90	6.50		(92)
3 1-Nitropropane	a	5.7	11.3×10^3	75	5.50	1-Aminopropane	(90)
(0.25 *M*)	b	5.2	11.7×10^3	80	7.00		(84)
4 2-Nitropropane	a	5.7	11.3×10^3	75	5.70	2-Aminopropane	(88)
(0.25 *M*)	b	5.0	11.7×10^3	80	7.00		(80)
5 Benzophenone	a	5.6	11.7×10^3	75	6.50	Diphenylmethanol	(90)
(0.30 *M*)	b	4.8	11.7×10^3	80	7.00		(88)
6 Benzonitrile	a	5.6	11.7×10^3	80	7.00	Dibenzylamine	(80)
(0.30 *M*)	b	4.8	11.7×10^3	90	8.00		(64)

Reduction of nitroalkanes, benzonitrile and benzophenone

The reduction of these substrates is possible only under high pressure and high temperature conditions. The reduction rate decreases with increasing molecular weight of the nitroalkanes and increases with increasing branching at the α-carbon atom (Table 3). Relatively higher hydrogen pressure and higher temperature are necessary for the reduction of benzophenone and benzonitrile. The former produced the corresponding alcohol while the latter was reduced to a mixture of benzylamine (15-20%) and dibenzylamine (80-85%).

The DRS and solution spectra of any complex catalyst in benzene solution are almost identical but differ appreciably from those taken in DMF or DMSO. The molecular weight measurements of the complexes in dilute DMF solution indicated nearly 100% dissociation. These facts together with the bridge cleavage of the dinuclear complexes by PPh_3, Py etc.[23,28] suggest them to undergo the following reaction in DMF solution.

$$Pd_2L_2X_2 \overset{DMF}{\rightleftharpoons} 2\,Pd.L.X.DMF \qquad \ldots(1)$$

HL = schiff base ligand
X = OAc, Cl, Br

The passage of H_2 through the yellow DMF solution of the catalyst changed the solution colour to greenish brown. The visible electronic spectra of the greenish brown solution and that of the final solution after catalytic run were identical for any catalyst in both normal and high pressure conditions indicating the formation of the same catalytic species in both the cases. The actual catalytic species could not be isolated from the final solutions as they decompose to Pd^0 at the final stage of concentration. It was, however, possible to isolate the secondary amine (LH_3) corresponding to reduced schiff base ligand from the decomposed solution. The ^1H NMR spectra of the concentrated solution exhibit a signal at τ 21-22 ppm indicating the presence of metal hydride complexes in them. The liberation of HX during hydrogen activation was inferred from the increase in conductance and decrease in *p*H of the solution and the liberation of CO_2 from $NaHCO_3$. The

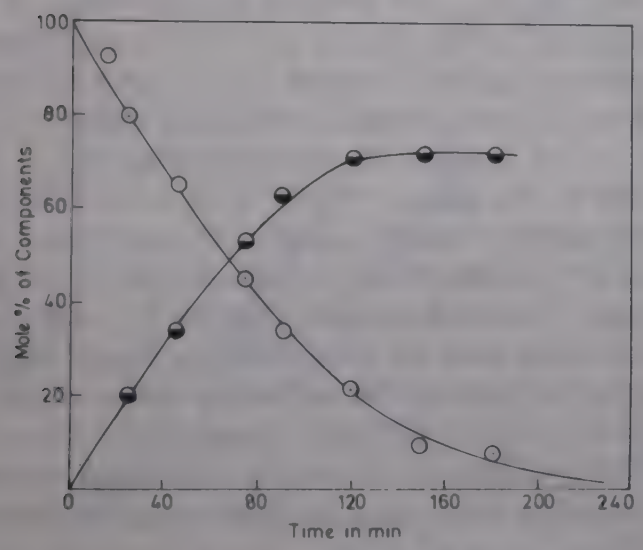

Fig. 3—Reduction of nitrobenzene with $Pd_2(apkt)_2(OAc)_2$ in DMF at 25°C, under 1 atm. of hydrogen and in presence of pyridine as additive. ⊙ = nitrobenzene; ◒ = phenylhydroxylamine.

DMF solution spectra of palladium(II) complexes with schiff bases, their H_2 activated species and the amines corresponding to schiff bases are presented in Table 4. The spectra of hydrogen activated solutions derived from $Pd_2L_2(OAc)_2$ or $Pd_2(LH_2)_2(OAc)_2$ are almost identical indicating the formation of same catalytic species in both cases. The actual catalytic species, suggested to be $Pd(LH_2)(H)DMF$ may be formed as follows:

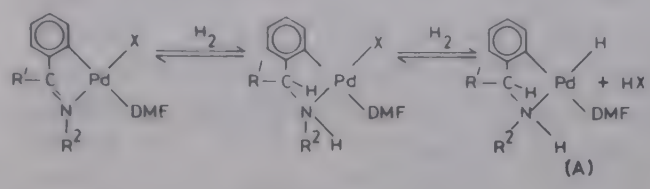

(2)

The equilibrium concentration of (A) should depend on the nature of HX as the weaker is the acid HX, the higher will be the concentration of (A). This is in accordance with the observed dependence of the activity of the complex on the nature of the bridging group: OAc > Br > Cl. The higher catalytic activities of the acetato-bridged complexes are due to their greater percentage of conversion to the actual catalytic species (A) during substrate reduction.

The reduction could be carried out only in DMF or DMSO and no reductions occurred in non-coordinating solvents like C_6H_6, $C_6H_5CH_3$ or in moderate coordinating solvents like CH_3CN or PhCN. In alcohol, the decomposition of the complex to Pd^0 occurs during hydrogen treatment. The reduction is inhibited in the presence of PPh_3, Py, acacH or Dipy. The strong coordinating agents (reaction medium or added ligands) probably occupy the vacant coordination site and thus prevent substrate coordination to the metal. In alcohol the corresponding catalytic species $PdLH_2(H)C_2H_5OH$ is probably too unstable to withstand the reaction conditions. The activities

Table 4—Electronic spectral data of the simple and H_2-activated DMF solution of the complexes

Compounds	ν_1 (cm^{-1})	ν_2 (cm^{-1})	ν_3 (cm^{-1})
1 $Pd_2L_2(OAc)_2$	24,400	33,800	
2 $Pd_2(LH_2)_2(OAc)_2$	22,700	32,200	
3 $Pd_2L_2(OAc)_2 + H_2$	22,650	27,700 (sh)	31,200 (sh)
4 $Pd_2(LH_2)_2(OAc)_2 + H_2$	22,700	27,700 (sh)	31,160 (sh)
5 $Pd_2L'_2(OAc)_2$	23,800	32,600	
6 $Pd_2(L'H_2)_2(OAc)_2$	24,700	29,400	33,330
7 $Pd_2L'_2(OAc)_2 + H_2$	25,900	29,700	32,800 (sh)
8 $Pd_2(L'H_2)_2(OAc)_2 + H_2$	25,580	29,680	32,600 (sh)

$LH = C_6H_5CH=N-C_6H_5$ $L'H = C_6H_5CH=NC_6H_4CH_3$ (p)

$LH_3 = C_6H_5CH_2-NH-C_6H_5$ $L'H_3 = C_6H_5CH_2-NH-C_6H_4CH_3$ (p)

of the complexes decrease in the presence of low concentration of added HX (X = bridging group) and are lost completely if the concentration exceeds 0.1 *M*. All these results support the existence of equilibrium (Eq. 2) in the reaction medium.

The complex $Pd_2L_2(OAc)_2$ ($LH = C_6H_5CH = NH$) could not be synthesized and hence its catalytic activities could not be studied. The catalytic activities of $Pd_2L_2(OAc)_2$ and their corresponding $Pd_2(LH_2)_2(OAc)_2$ are almost identical and their yellow DMF solutions undergo the same type of transformations during hydrogen activation and substrate reduction. The complexes $Pd_2L_2(OAc)_2$ (Fig. 1b) with varying L can be arranged in the following order according to their catalytic activities:

$$I > II \sim III \sim IV \sim V > VI \sim VII > VIII$$

The complex with N-methylbenzaldimine (complex-I) required low induction period and showed highest catalytic activity both under normal and high pressure conditions. The activities of (II to V) though considerably less than that of I, are almost equal. The solutions derived from ketimine complexes (complex VI to VIII) are highly sensitive to air and decompose to Pd^0 in the presence of traces of air. The complexes may be divided into four groups depending on their activities. The first group (compound-I) having only alkyl substituent on N-atom of the $>C=N-$ group has the highest activity while the second group (compound II-V) having only aryl substituents on the N atom is far less reactive. The activities, however, do not change appreciably with the number of alkyl substituents on the phenyl ring. The third group (compound VI and VII) with alkyl and aryl substituents on C and N atom respectively or vice-versa have far less activities while the fourth group (compound VIII) having aryl substituents on both the atoms of the azomethine group is least reactive.

The above results show that the substituents on either C or N atoms of $>C=N-$ group decrease the catalytic activities of the complexes and that the aryl substituents are far more effective in this respect. The structures of the complexes $Pd_2L_2X_2$ suggest planarity of the chelate ring with the consequent electron delocalization on it. Any change in electron density caused by the nature of the substituent at the C or N atom of the $>C=N-$ group will be partially distributed in the chelate ring. The effect of substitutions on the electron density and steric crowding around the metal atom appears inappreciable and only its involvement in the rate determining step should not influence the catalytic activities of the complexes to such a great extent as observed experimentally. This is, however, possible if the $>C=N-$ group itself is directly involved in the rate determining step. The substitutions on C and N atoms will stabilize the $>C=N-$ group by sterically hindering the attack of H_2 on it and the aryl substituents will further stabilize the azomethine group by delocalizing the latter's π-electron density on their own rings. Thus the complex catalysts containing more stable $>C=N-$ group are expected to be less efficient as found experimentally.

The polarographic reductions of the schiff base ligands LH, the corresponding secondary amines LH_3, and their corresponding orthopalladated complexes were studied in DMF solution in the range of -0.1 V to -1.7 V. The studies were made using tetraethyl ammonium iodide as the supporting electrolyte and the potentials are referred to the usual saturated colomel electrode. Each of the schiff base ligands and its corresponding complex showed two well defined reduction steps each involving one electron. The linearity of the plot of E_i versus $\log(i/(i_d - i))$ in each case indicated the reversibility of the process. The $E_{1/2}$ and n values and the shape of the polarograms of the ligand and the corresponding complex are almost identical. $(E_{1/2})_1$ value of the ligands and the complexes lie within the range -0.49 V to -0.54 V while the corresponding $(E_{1/2})_2$ values fall in the range -0.715 V to -0.73 V. The corresponding reduced ligands LH_3 and their complexes do not exhibit any reduction wave in the given range. The results suggest that the $E_{1/2}$ and n values obtained both for the schiff base ligand and its complex are actually the reduction values of the ligands only. The schiff base ligand in the complex, therefore, undergoes an overall 2-electron reversible reduction which may be represented as follows (Eq. 3):

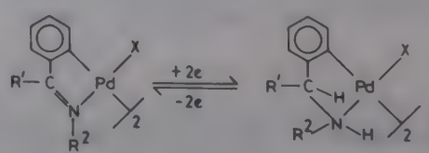

(3)

Kinetic studies and mechanism

Kinetic studies using the two most active complexes as catalytic system and nitrobenzene and styrene as substrates have been made under normal pressure at 25°C. Studies under high pressure conditions were carried out using the same two catalytic systems and CH_3NO_2 as substrate at 110°C. The rate was determined by analysis of the product composition at different time intervals and the initial rates were determined from graphical extrapolation of the rate curve to zero time.

Variation of catalyst concentration

Kinetic studies revealed that the initial rates of hydrogenation of nitrobenzene and styrene were first order dependent on [catalyst].

Variation of hydrogen pressure

The initial rate of reduction of nitrobenzene and styrene was found to be second order dependent on the hydrogen pressure in the range of 200-1000 mm of Hg (Fig. 4). A first order rate dependence on the hydrogen pressure was observed for the reduction of nitromethane. Variation of substrate concentrations was found to have no appreciable effect on the reduction rate in the range of 0.5 to 3.5 M (Fig. 5).

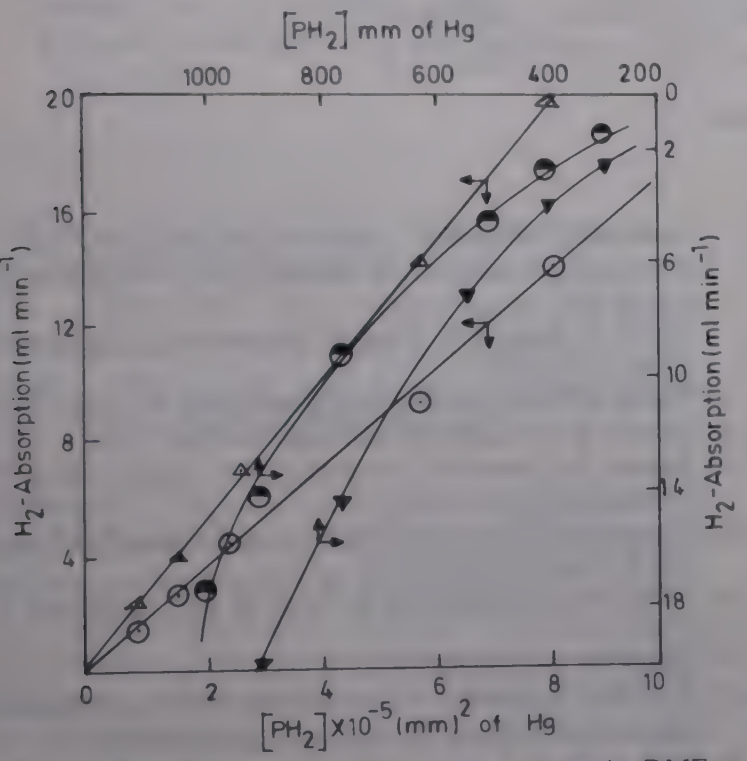

Fig. 4—Rate dependence on hydrogen pressure in DMF at 25°C. $Pd_2(BAN)_2(OAc)_2 = 4.12 \times 10^{-4}$ mol dm^{-3}. [nitrobenzene] = 0.32 mol dm^{-3} (⊙, ◒) [styrene] = 0.86 mol dm^{-3} (△, ▲).

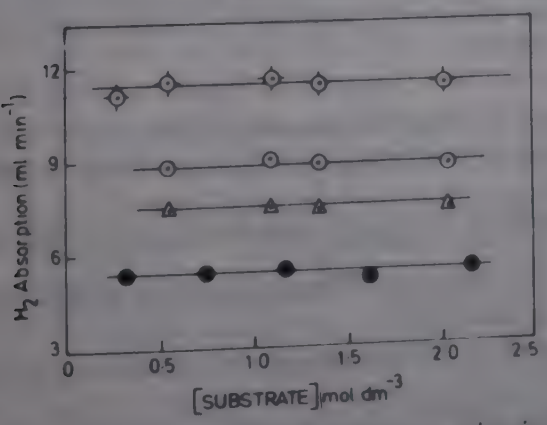

Fig. 5—Rate dependence on substrate concentration in DMF at 25°C. Substrate = nitrobenzene (⊙); styrene (◈) using $Pd_2(mbi)_2(OAc)$ as catalyst and (△, ●) = nitrobenzene, styrene using $Pd_2(apkt)_2(OAc)_2$ as catalyst.

The average initial rate of nitrobenzene reduction during the first 10 min, as determined from the volume of H_2 absorption and the G.C. analysis, lies in the range 1.93×10^{-5} to 2.02×10^{-5} mol dm^{-3} s^{-1} and the corresponding value of k_4 lies in the range 9.9×10^4 to 11.5×10^4 dm^6 mol^{-2} s^{-1}. The above mechanism supports the comparable catalytic activities of $Pd_2L_2X_2$ and $Pd_2(LH_2)_2X_2$. The actual catalytic species is suggested to be (A) formed as per Eq. 2. Simultaneous hydrogenation and isomerization of alk-1-enes require the presence of monohydride species[29] like (A) and supports the formation of similar monohydride species like (B), (D) and (F) during $\geq C-NO_2$ reduction (Scheme 1). The influence of C, N substituents on the catalytic activities of the complexes suggest step (V) (Scheme 1) to be the rate determining step. Polarographic studies indicate the reversibility of the process Pd L X DMF $\overset{H_2}{\rightleftarrows}$ $Pd(LH_2)X$ DMF, and thereby indirectly supports the above reaction mechanism. The conversion of C to D is in accordance to β-hydrogen transfer[30] ($R'-\overset{\beta}{C}-H$) to the metal atom.

According to Scheme 1

$$\text{Rate} = k_4[E][H_2]^2$$

$$[Cat]_T = [A] + [B] + [C] + [D] + [E] + [F]$$

Considering the steady state equilibrium of E and D and substituting the concentration of the species, we get:

$$[Cat]_T = \frac{K_4[E][H_2]^2}{[PhNO_2]} + \frac{K_5[E][H_2]^2}{[DMF]} + K_6[E][H_2]^2 + \frac{E(K_7 + K_8[H_2]^2)}{[DMF]} + [E] + \frac{K_9[E][H_2]^2[PhNHOH]}{[PhNO_2]}$$

where

$$K_4 = \frac{k_4}{k_1K_1K_2},\ K_5 = \frac{k_4}{k_1K_2},\ K_6 = \frac{k_4}{k_1},\ K_7 = \frac{k_2}{K_3}$$

$$K_8 = \frac{k_4}{k_3},\ K_9 = \frac{K_3k_4}{k_1K_1K_2}$$

$$[Cat]_1 = \{[E]\{K_4[H_2]^2[DMF] + K_5[H_2]^2 \times [PhNO_2] + K_6[H_2]^2[DMF][PhNO_2] + K_7[PhNO_2] + [DMF][PhNO_2] + K_8[H_2]^2[PhNO_2] + K_9[H_2]^2 \times [PhNHOH][DMF]\}\}/[DMF][PhNO_2]$$

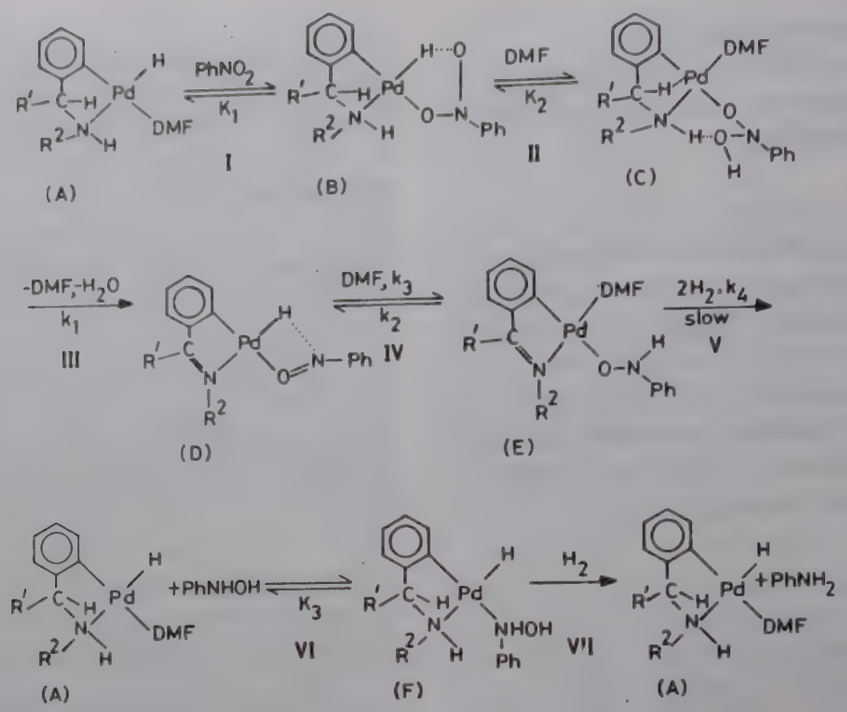

Scheme 1

$$[E]=\frac{[Cat]_T[DMF][PhNO_2]}{\left\{K_7[PhNO_2]+[DMF][PhNO_2]+[H_2]^2\{K_4[DMF]+K_5[PhNO_2]+K_6[DMF][PhNO_2]+K_8[PhNO_2]+K_9[PhNHOH][DMF]\}\right\}}$$

$$[E]=\frac{[Cat]_T[DMF][PhNO_2]}{K_7[PhNO_2]+[DMF][PhNO_2]}=\frac{[Cat]_T[DMF]}{K_7+[DMF]}$$

as $[H_2]^2$ is negligibly small; $\sim 10^{-5}$ mol lit^{-1} (ref. 31)

Now

$$\text{Rate}=\frac{k_4[Cat]_T[DMF][H_2]^2}{K_7+[DMF]}=K[Cat]_T[H_2]^2$$

where $K=\dfrac{k_4[DMF]}{K_7+[DMF]}$ as [DMF] is constant.

References

1 Abley P & McQuilin F J, *Discuss Faraday Soc*, 46 (1968) 31.
2 Knifton J F, *J org chem*, 41 (1976) 1200.
3 Chepalkin E G & Khiedekel M L, *J mol Catal*, 4 (1978) 103.
4 Bhattacharya S, Santra P K & Saha C R, *Indian J Chem*, 23A (1984) 724.
5 Li Nai Hong & Frechet J M J, *J chem Soc Chem Commun*, (1985) 1100.
6 Saha C R & Bhattacharya S, *J chem Tech Biotechnol*, 37 (1987) 233.
7 Bose Ashis & Saha C R, *Indian J Chem*, 29A (1990) 461.
8 Card R J, Liesner C E & Neckers D C, *J org Chem*, 44 (1979) 1095.
9 Chem B, Feng Z & Chin R, *Fundum Res Organometal Chem*, (1982) 613.
10 Saurez T, Fontal B & Garcia D, *J mol Catal*, 34 (1986) 163.
11 Santra P K & Saha C R, *J mol Catal*, 39 (1987) 279.
12 Bartani R, Carturan G & Scrivanti A, *Angew-chem*, 95 (1983) 241.
13 Teresawa M, Yamamoto H, Kaneda K, Imanaka T & Teranishi S, *J Catal*, 57 (1979) 315.
14 Albers M O, Singleton E & Viney M M, *J mol Catal*, 30 (1985) 213.
15 Holy N L, *J org Chem*, 44 (1979) 239.
16 Ram S & Ehrenkaufer E, *Tetrahedron Lett*, 25 (1984) 3415.
17 Bose Ashis & Saha C R, *J mol Catal*, 49 (1989) 271.
18 Knifton J F, *J org Chem*, 38 (1973) 3296.
19 Knifton J F, *J org Chem*, 40 (1975) 519.
20 Kwiatek J, *Catal Rev*, 1 (1967) 37.
21 German (East) patent, *Chem Abstr*, 102 (1985) p 184710k.
22 Hungarian patent, *Chem Abstr*, 104 (1986) p 226705m.
23 Onoue Hiroshi & Moritani I, *J organometal Chem*, 43 (1972) 431.
24 Fieser & Fieser, *Reagents for Organic synthesis*, 3,291.
25 Smith F Wendell, *Tetrahedron*, 19 (1963) 445.
26 Weston A W & Michaels R J, *J Am Chem Soc*, 73 (1951) 1381.
27 Baranyai A, Ungvary F & Marko L, *J mol Catal*, 32 (1985) 343.
28 Crociani B, Boschi T, Pietropaolo R & Belluco U, *J chem Soc A*, (1970) 531.
29 Cotton F A & Wilkinson G, *Advanced inorganic chemistry* (1988) 1249.
30 Johnstone R A *et al.*, *Chemical Rev*, 85 (1985) 129.
31 International Critical Tables, Vol. III, 242.

Indian Journal of chemistry
Vol. 31A, April 1992, pp. 251-255

Studies on the coordination of Cu(II) with *o*-hydroxyacetophenone-phenylhydrazones

S G Kulkarni, D V Jahagirdar* & D D Khanolkar
Department of Chemistry, Marathwada University, Aurangabad 431 004

Received 24 July 1991; revised and accepted 23 December 1991

Complexes of *o*-hydroxyacetophenone-phenylhydrazone (OHAPH) and its methyl and chloro derivatives with Cu(II) ion have been isolated. The complexes have been characterised on the basis of magnetic susceptibility and IR and ESR spectral measurements. ESR spectra reveal superhyperfine splitting, characteristic of the coordinated nitrogen of C = N bond. The bonding parameters α and β, though approximate, indicate in-plane and out-of-plane π-bonding which stabilises the square-planar stereochemistry of the complexes. The solution stability constants of the metal chelates obtained from the potentiometric study provide supporting evidence for (i) intermolecular H-bonding between the phenolic oxygen and the nitrogen of the secondary amino group, and (ii) back donation from metal to ligand through π-bonding.

Schiff bases constitute a very important group of N,O donor chelating ligands[1-4]. Another group of ligands containing the azomethine grouping (−C=N) found in schiff bases is constituted by hydrazones which have also been used as ligands though they are not as widely studied[5-9] as the schiff bases.

A study of Cu(II) chelates of phenylhydrazones of ring substituted methyl and chloro derivatives of 2-hydroxyacetophenone is presented in this paper. The complexes have been studied in solid state as well as solution phase using potentiometry and EPR techniques in addition to the other physical methods in order to provide a detailed interpretation of the structures of the complexes.

Materials and Methods

All the reagents such as copper perchlorate, sodium perchlorate, sodium hydroxide, etc., were of AR grade. Dioxane was purified by the method described by Vogel[10].

Magnetic susceptibility measurements were carried out using a Gouy type of apparatus. Electronic absorption spectra were recorded on a Unicam SP 500 spectrophotometer. The diffused reflectance spectra were measured using an SP 540 attachment. Solution conductivities of metal complexes were measured by a precision conductivity meter (Elico, Hyderabad, India). A cell with platinised platinum electrode and a cell constant of 0.5888 was used. Infrared spectra of the ligands and their metal complexes were recorded in KBr on a Perkin-Elmer infrared spectrophotometer model 337. The EPR spectra of the samples at room and liquid nitrogen temperatures were recorded on an X-band Varian instrument consisting of Varian (V-4500-40) X-band microwave bridge, a Varian klystron power supply (V-4500-20) and a Klystron control unit (V-4500-10).

Preparation of phenylhydrazones

2-Hydroxyacetophenone and its substituted derivatives, which are the starting substances for the preparation of the phenylhydrazones, were prepared by the Fries-migration reaction. Acetylated phenol (1.0 mol) was treated with anhydrous $AlCl_3$ (1.0 mol) with or without solvent and heated in an oil bath at 120°C for an hour and then at 140°C for 30 min. After the completion of the reaction, the aluminium complex was decomposed with ice and dil HCl. 2-Hydroxyacetophenone, which was isolated by steam distillation, was collected and then converted into its phenylhydrazone by treatment with phenylhydrazine hydrochloride.

Preparation of metal complexes

Copper(II) was used in the form of its nitrate because of its high solubility in water. The metal to ligand ratio was maintained at 1:2 with ligand slightly in excess. An ethanolic solution (100 ml) of 5 g of copper nitrate was slowly added from a burette to an ethanolic solution of the ligand, the concentration of which was so maintained as to get 1:2 (metal:ligand) ratio. The mixture was stirred while addi-

Table 1—Analytical data of copper(II) complexes

Metal complexes	Copper %		Carbon %		Hydrogen %		M.P./decomp. temp. (°C)
	Calc.	Found	Calc.	Found	Calc.	Found	
Cu(II)-OHAPH $Cu(C_{14}H_{13}ON_2)_2$	12.36	12.30	65.42	66.24	5.06	5.17	1.90
Cu(II)-3-methyl-OHAPH $Cu(C_{15}H_{15}ON_2)_2$	11.70	11.77	66.47	66.76	5.91	5.51	200
Cu(II)-4-methyl-OHAPH $Cu(C_{15}H_{15}ON_2)_2$	11.70	11.21	66.47	66.79	5.91	5.56	200
Cu(II)-5-methyl-OHAPH $Cu(C_{15}H_{15}ON_2)_2$	11.70	11.10	66.47	65.40	5.91	5.55	205
Cu(II)-3-chloro-OHAPH $Cu(C_{14}H_{12}ON_2Cl)_2$	10.90	10.70	57.67	58.80	4.12	4.42	210
Cu(II)-4-chloro-OHAPH $Cu(C_{14}H_{12}ON_2Cl)_2$	10.90	10.60	57.67	58.30	4.12	4.30	195
Cu(II)-5-chloro-OHAPH $Cu(C_{14}H_{12}ON_2Cl)_2$	10.90	10.50	57.67	57.40	4.12	4.17	198

tion was continued drop by drop. The *p*H of the resulting solution was maintained in the range 5-6 by addition of ethanolic ammonia to obtain a precipitate of the copper complex. The solution containing the precipitate was digested on a water-bath at 70°C for half an hour. The precipitate was filtered and dried *in vacuo* over calcium chloride. It was stored in a well stoppered glass container. The copper(II) complexes were analysed for carbon, hydrogen and metal contents. The metal contents were determined by complexometric method using a standard EDTA solution[11].

Potentiometric measurements

A Beckman *p*H meter model H-2 was used for the measurement of *p*H. It was calibrated by buffer solutions of *p*H 4.01 and 9.11 (30°C). The temperature of the solutions in the titration vessel was maintained at 30° ± 0.02°C with a thermostat. The details regarding Irving-Rossotti titration[12] are given in an earlier paper[13]. Thermodynamic *pK* and log *K* values were obtained for dioxane-water medium by applying the correlations as indicated by Van Uitert and Hass[14].

Results and Discussion

Solid complexes

The elemental analyses of copper complexes indicated that they have 1:2 (metal:ligand) stoichiometry (Table 1). The molar conductivities in DMSO showed that these are non-electrolytes. The complexes are insoluble in water and sparingly soluble in ethanol, methanol, dioxane, chloroform and benzene. The magnetic moment (μ_{eff}) values of Cu(II)-phenylhydrazone complexes are in the range 1.75-1.92 B.M. These values are within the range expected for square-planar or tetragonally distorted octahedral complexes of Cu(II)[15].

The diffuse reflectance spectra of Cu(II) complexes of hydrazones show (Table 2) two or three prominent shoulders in the range 13.00-24.40 kK. In dioxane solution the complexes exhibit a strong band around 15.00 kK, which may be assigned to the $^2B_{1g} \rightarrow {}^2B_{2g}$ transition. Two other bands observed at 31.25-35.70 kK and 26.30-29.40 kK have high extinction coefficient and correspond to bands observed in the solution spectra of the ligands at 32.70-33.90 kK and 28.60-29.40 kK respectively. These are, therefore, ascribed to intra-ligand π-π^* and n-π^* transitions. The third band observed in the range 38.40-41.60 kK in all copper(II) complexes appears to be a charge-transfer band. The observed solid reflectance and the solution spectra of present Cu(II) complexes support square-planar or tetragonally distorted octahedral stereochemistry for Cu(II) in the light of literature data for various other reported copper complexes[15-19].

The EPR spectra of Cu(II) complexes of OHAPH and its 4-methyl-, 3-chloro and 4-methyl-5-chloro derivatives were taken at room temperature and liquid nitrogen temperature in polycrystalline state and in solution. The spectra were analysed by Kheubuhl's method[20]. $g_\perp$ (300 K), $g_\perp$ (80 K) and $g_\parallel$ (80 K) values for the four copper complexes were found to be almost identical, the values being 2.04, 2.04, and 2.21 respectively. Similarly g_{iso}, A_{Cu} and A_N at 300 K are 2.10, 82 and 12 respectively while g_1 (g_x), g_2 (g_y), g_3 (g_z) at 80 K are 2.05, 2.18 and 2.2 respectively.

Table 2—Solid reflectance and solution electronic absorption spectra of Cu(II) complexes of hydrazones (ε_{max} in parenthesis for solution in dioxane)

Copper(II) complex of	Absorption maxima (kK)	
	Reflectance	Solution
OHAPH	24.40, 21.74, 16.95, 14.28	39.20 (2500), 31.25 (1000), 26.30 (320), 15.60 (354), 14.70 (380)
3-CH_3OHAPH	24.40, 16.40, 15.15, 13.90 Sh	39.20 (21,000), 34.50 (10,500), 29.80 (11,400), 14.30 (300)
4-CH_3OHAPH	24.40, 22.70, 16.60, 15.15, 11.35	41.60 (24,500), 33.30 (20,400), 29.40 (28,600), 14.30 (290)
5-CH_3OHAPH	16.15, 14.70, 10.50	40.00 (22,500), 34.50 (9,400), 28.50 (11,300), 15.60 (340)
3-Cl OHAPH	16.65 Sh, 14.90, 13.00 Sh	41.60 (22,200), 35.70 (14,900), 29.40 (12,800), 15.90 (360), 13.70 (350)
4-Cl OHAPH	24.40, 16.40, 14.30 Sh	40.80 (25,800), 33.30 (15,800), 29.40 (28,400), 15.60 (280)
5-Cl OHAPH	24.40 Sh, 18.50, 16.65, 15.00, 12.50	40.00 (6,040), 33.30 (4,290), 29.40 (5,440), 15.60 (380)
4-CH_3-5-Cl OHAPH	24.40, 16.65, 14.70	38.50 (21,400), 34.50 (18,100), 29.40 (10,300), 14.30 (300)

The spectra of Cu(II) complexes in the polycrystalline state were similar both at room temperature as well as at liquid nitrogen temperature and were characteristic of tetragonal distortion. The solution spectra at room temperature gave a four line pattern due to copper hyperfine interactions. The pattern is typical of Cu(II) in a planar environment.

The superhyperfine splitting due to the interaction of the electron in Cu(II) with two equivalent ^{14}N nuclei of the ligand molecule giving five components was also observed in the high field region of the spectrum. In general, these spectra resemble those reported for Cu(II) porphyrins[21] and copper pthalocyanine[22,23,24] which are known to possess square planar symmetry. The superhyperfine splitting is an indication of delocalisation of the unpaired electron from Cu(II) over the ligand atom and resultant metal-ligand covalent bonding.

The approximate values of in-plane σ-bonding parameter, α^2, were derived from the expression[25],

$$\alpha^2 = \frac{A}{PK} + \frac{g - 2.0023}{K}$$

where P is the free ion dipole which is assigned a value of 0.036 cm^{-1} and K is the fermi contact term which is usually assigned a value of 0.43.

To obtain in-plane and out-of-plane bonding parameters β and γ, respectively, the following simplified expressions were used assuming tetragonal D_{4h} symmetry for Cu(II) in these complexes.

$$g_{\parallel} = 2.0023 - \frac{8 \times 828 \times \alpha^2\beta^2}{(E_{xy} - E_{x^2-y^2})}$$

$$g_{\perp} = 2.0023 - \frac{2 \times 828 \times \alpha^2\gamma^2}{(E_{yz,\,zx} - E_{x^2-y^2})}$$

The observed transition energies[26] for $E_{xy} \leftarrow E_{x^2-y^2}$ and $E_{yz,\,zx} \leftarrow E_{x^2-y^2}$ indicate the presence of unpaired electron in the ground state $d_{x^2-y^2}$.

The magnitudes of α^2, β^2 and γ^2 for chelates of OHAPH and its -4-CH_3, -3-Cl and -4-CH_3-3-Cl derivatives are listed below in that order.

$\alpha^2 = (0.75, 0.78, 0.78, 0.74)$

$\beta^2 = (0.64, 0.64, 0.60, 0.64)$

$\gamma^2 = (0.58, 0.59, 0.56, 0.61)$

The bonding parameters α is a measure of the covalency of the in-plane σ-bonding. A value of $\alpha^2 = 1$ indicates complete ionic character while $\alpha^2 = 0.5$ indicates essentially 100% covalent bonding. The β and γ parameters are a measure of covalency in the in-plane and out-of-plane π-bonding respectively. β^2 or $\gamma^2 = 1$ indicates no covalent bond and β^2 or $\gamma^2 = 0.5$ correspond to total covalent character.

The observed values of α,β and γ parameters in the present copper(II) complexes are indicative of strong in-plane σ and π-covalent bonding and out-of-plane π-bonding in the complexes.

Infrared absorption frequencies

The N—H stretching frequency of the ligand molecules (3310-3355 cm^{-1}) is lowered by about 70-175 cm^{-1} in all the complexes. The N—H stretching band which is a single sharp band in the ligand spectra, splits into two closely spaced bands or shoulders probably due to lowering of the symmetry in the complexes. The negative shift of the N—H stretching frequency is attributed to the intramolecular hydrogen bonding[27] in copper complexes as shown in structure I.

There is an overlapping of the C=N frequency with the aromatic νC=C mode in both the ligands and the metal complexes. The νC=N occurs at lower positions in the chelates compared to the positions

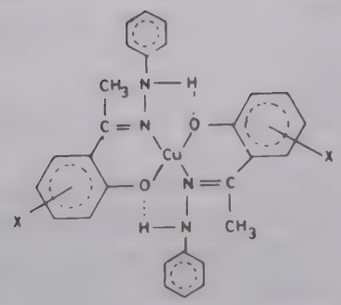

I

in the corresponding ligands. N−O stretching frequency which is observed in the ligands at 990-995 cm^{-1} is shifted to 1020-1035 cm^{-1} and appears as a sharp, medium sharp or weak band in the copper(II) complexes of hydrazones. The fairly strong C−O stretching band observed around 1300 cm^{-1} in the ligands is observed in the region 1305-1330 cm^{-1} in the copper(II) complexes, with significant change in the intensity.

In copper(II) complexes of phenyl hydrazones M−N and M−O stretching vibrations are found respectively in the regions 405-455 cm^{-1} and 505-555 cm^{-1}. These bands of weak or moderate intensity were not present in the spectra of ligand molecules. Lever and co-workers[28] have empirically observed that for octahedral complexes νM−N occurs below 400 cm^{-1} and for square-planar complexes it occurs in the range 400-500 cm^{-1}.

Potentiometric measurements

The *pK* values of the ligands and the stability constants of the corresponding copper(II) chelates were calculated by the method of Irving and Rossotti[29]. The log *K* values were computed by half-integral method, successive approximation method and the method of least squares. The values obtained by the method of least squares are given in Table 2.

The salient points arising from the observed data are as follows:

(i) The difference between $\log K_1$ and $\log K_2$ is around 1 log unit. This shows that 1:2 complexation commences before the complete formation of 1:1 complexes. Formation of 1:2 complex is more favourable than that of the 1:1 complex because in the former case the two ligands are symmetrically situated. Further, formation of 1:2 complex is also statistically favoured over that of 1:1 complex. The additional stability of the present 1:2 chelates is also due to the intramolecular H-bonding anticipated in the solid phase. This observation also explains the formation of only 1:2 complexes in the solid phase.

(ii) Burger *et al.*[30] have correlated C=N band frequency with stability constants of a number of metal complexes of 5-methylsalicylaldoxime. The νC=N values and stability constants of Cu(II) complexes of hydrazones are presented in Table 3. νC=N is expected to decrease on coordination. It is very well known and almost all schiff base complexes show this trend. This is attributable to decrease in C=N bond order on coordination through N. The experimental data of Burger *et al.*[30] on methylsalicylaldoxime complexes showing increase in νC=N with increasing stability of the metal complexes are in broad agreement with present data on Cu(II) hydrazones[31].

(iii) The frequency of the secondary amino group, which is involved in an intramolecular H-bonding with phenolic oxygen of another ligand molecule in the Cu(II) complex can also be correlated with stability. The electron withdrawing chloro group, which lowers the stability constant of the chloro substituted phenylhydrazone compared to that for unsubstituted ligand, weakens the hydrogen bridge by reducing the electron density on phenolic oxygen whereas the electron donating methyl group strengthens the hydrogen bond. In the former case a relatively higher N−H group frequency is obtained in comparison with that in the latter.

Table 3—Thermodynamic *pK* values of OHAPH and its substituted derivatives and thermodynamic log*K* values of their Cu(II) chelates

{t = 30°C; I = 0.1 *M*; medium, 50% v/v dioxane-water}

Ligand	*pK*	$\log K_1$	$\log K_2$
OHAPH	12.95	9.78	8.60
3-CH_3OHAPH	12.84	9.63	8.63
4-CH_3OHAPH	12.55	9.49	8.42
5-CH_3OHAPH	12.87	9.70	8.70
3-Cl OHAPH	12.42	9.23	8.11
4-Cl OHAPH	12.06	9.16	8.38
5-Cl OHAPH	12.61	9.50	8.45
4-CH_3-5-Cl OHAPH	12.24	9.30	8.46

Error limits of *pK* and log*K* values are +0.02 and ±0.02 - ±0.03 respectively

Table 4—Correlation of potentiometric data with IR data of solid complexes of Cu(II) with OHAPH and its derivatives

Complex of	log β	C=N (cm^{-1})	N−H (cm^{-1})
OHAPH	18.38	1600	3180
3-CH_3OHAPH	18.26	1620	3220
4-CH_3OHAPH	17.91	1620	3240
5-CH_3OHAPH	18.40	1620	3245
3-Cl OHAPH	17.34	1590	3265
4-Cl OHAPH	17.54	1590	3240
5-ClOHAPH	17.95	1600	—

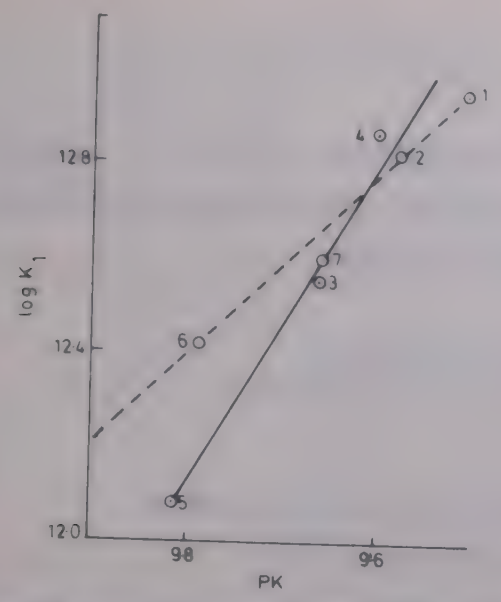

Fig. 1—Plot of log$K$ vs pK for Cu(II) chelates of OHAPH [OHAPH (1), 3-CH_3(2), 4-CH_3(3), 5-CH_3(4), 3-Cl(5), 4-Cl(6), 5-Cl(7)

A similar correlation is observed between metal-ligand stability constants and hydrogen bonded N – H group frequencies (Table 4).

Potentiometric data thus provide additional proof of the existence of intramolecular hydrogen bonding in metal complexes, involving secondary amino group.

(iv) The earlier observation regarding π-bonding through back donation was checked through the plots of log$K$ vs pK. If the partial molar energies of the metal-ligand and proton-ligand complexes exactly compensate each other, then log$K$ vs pK values should give a straight line with unit slope passing through the parent unsubstituted compound[32-35].

It was observed (Fig. 1) that only points corresponding to 3-CH_3 and 3-Cl substituted complexes were falling on this line. All the remaining points exhibited minor deviation[33] showing thereby an 'extra stabilisation' in these chelates because of the d_π-p_π interaction. Substituents like methyl and chloro at the *ortho* position to the –OH group of OHAPH are expected to offer steric hindrance to the incoming metal ion. The steric hindrance should have resulted in a major deviation[33] of these points from the straight line plot. The contrary observation in the present case can be explained if it is assumed that the destabilisation due to the steric factor has probably been compensated to a certain extent by the extrastabilisation due to the d_π-p_π interaction in this case.

References

1 Cotton F A, *Modern coordination chemistry* (Wiley Interscience) 1960, 301.
2 Hatfield W E & Whyman R, *Transition metal chemistry* (Marcel Dekker, New York), 1969, 95.
3 Holm R H & O'Connor M J, *Progr inorg Chem*, 14 (1971) 338.
4 Sacconi L, *Transition metal chemistry* (Marcel Dekker, New York), 1968, 199.
5 Taylor T W J & Callow N H, *J chem Soc*, (1939) 257.
6 Fabriken F & Bayer A G, *Brit Abstr*, 726 (1956) 187.
7 Sacconi L, *Z anorg allg Chem*, 275 (1954) 249.
8 Ray H L, Garg B S & Singh R P, *Curr Sci*, 42 (24) (1973) 852.
9 Ohtak H, *Bull chem Soc Japan*, 33 (1960) 202.
10 Vogel A I, *A text book of quantitative inorganic analysis* (ELBS, London) 1956, 177.
11 Schwarzenbach G, *Complexometric titrations* (Interscience, NY) 1957.
12 Martell A E, *Chemistry of the metal chelate compounds* (Prentice Hall, London) 1962, 158.
13 Jahagirdar D V & Khanolkar D D, *J inorg nucl Chem*, 55 (1973) 921.
14 Van Uitert L G & Hass C G, *J Am chem Soc*, 75 (1953) 451.
15 Earnshaw A, *Introduction to magnetochemistry* (Academic Press, N.Y.), 1968, 104.
16 Sacconi L & Ciampolini M, *J chem Soc*, (1964) 276.
17 Calvin M & Barkelew C H, *J Am chem Soc*, 68 (1946) 2267.
18 Narin G, *J inorg nucl Chem*, 28 (1966) 2441.
19 Sone K, *J Am chem Soc*, 75 (1953) 5207.
20 Kheybuhl F K, *J chem Phys*, 33 (1960) 1074.
21 Manoharan P T & Roger M T, *Electron spin resonance of complexes* (1969) edited by T F Yen (Plenum Press, New York) 143.
22 Assour J M, *J chem Phys*, 43 (1965) 2477.
23 Harrizon S E & Assour J M, *Paramagnetic resonance*, Vol 2 edited by W Low (Academic Press, N.Y.) 1963, 855.
24 Bonnett J E & Ingram D E, *Nature*, 175 (1955) 130.
25 Martell A E, *Coordination chemistry* (Von Nostrand Reinhold Co, New York) 1971, 258.
26 Proctor I M, Hathway B J & Nicholl S P, *J chem Soc* (*A*), 1968, 1678.
27 Pannu B S, Chopra S L & Parmar S S, *Indian J Chem*, 2 (1971) 1396.
28 Lever A B P & Mantovani E, *Can J Chem*, 51 (1973) 1567.
29 Irving H & Rossotti H, *J chem Soc*, (1954) 2904.
30 Burger K, *Coordination chemistry experimental methods* (Butterworths, London) 1973, 67.
31 Percy G C & Thornton D A, *J inorg nucl Chem*, 34 (1972) 3369.
32 Bruehlman R J & Verhoek F H, *J Am chem Soc*, 70 (1948) 1401.
33 Irving H & Rossotti H, *Acta chem scand*, 10 (1956) 72.
34 Ernst Z L & Menashi J, *Trans Faraday Soc*, 59 (1963) 2838.
35 Jahagirdar D V & Khanolkar D D, *J inorg nucl Chem*, 38 (1976) 1673.

Indian Journal of chemistry
Vol. 31A, April 1992, pp. 256-259

Studies on biologically relevant ternary metal complexes: Part VI—Stability of ternary Co(II), Ni(II), Cu(II) and Zn(II) complexes involving aminopolycarboxylic acids and amino acids

A Koteswar Rao, G Narender Kumar & M Srinivas Mohan*
Department of Chemistry, Osmania University, Hyderabad 500 007
and
Y Lakshmi Kumari
Department of Chemistry, Sarojini Naidu Vanitha Mahavidyalaya, Hyderabad 500 001

Received 16 April 1991; revised and accepted 21 December 1991

Ternary metal complexes of the type MLA, where M = Co(II), Ni(II), Cu(II) and Zn(II); L = iminodiacetic acid (IMDA) or nitrilotriacetic acid (NTA) and A = glycine, alanine, valine, leucine, norleucine, phenylalanine, tryptophan, serine, threonine, methionine, aspartic acid, ethylenediamine or pyrocatechol have been investigated potentiometrically at 35°C and $\mu = 0.2\ M\ (KNO_3)$. The stabilities of the ternary complexes have been quantitatively compared with the stabilities of the corresponding binary metal complexes (MA) determined under identical experimental conditions. Ternary complexes containing IMDA are found to be more stable than the corresponding complexes containing NTA. With respect to ligand L, the stability of ternary complexes increases in the order: pyrocatechol ($^-O - O^-$ donor) < bidentate amino acid ($N - O^-$ donor) < ethylenediamine ($N - N$ donor). Cu(II) ternary complexes are found to be less stable than the corresponding Co(II), Ni(II) or Zn(II) complexes. Ternary Cu(II) complexes containing bis(imidazol-2-yl)methane are more stable than the corresponding complexes containing IMDA or NTA. Various factors leading to differences in the relative stabilities of the ternary complexes are discussed.

In our earlier studies of ternary metal complexes the effect of imidazole and its derivatives such as bis-(imidazol-2-yl)methane (BIM) and bis(imidazol-2-yl)nitromethane (NBIM) on the stability of various ternary complexes was investigated[1-5]. In the present investigation the formation and stability of ternary Co(II), Ni(II), Cu(II) and Zn(II) complexes (MLA) involving the aminopolycarboxylic acids (L), i.e., iminodiacetic acid (IMDA) or nitrilotriacetic acid (NTA) and various ligands (A) containing $N - O^-$, $^-O - O^-$ or $N - N$ donor atoms have been investigated by *p*H-metric methods at 35°C and $\mu = 0.2M\ (KNO_3)$. The stabilities of these ternary complexes have been quantitatively compared with those of the corresponding binary metal complexes determined by us earlier under identical experimental conditions[5,8,9]. The relative ability of the imidazole derivative (BIM) and the aminopolycarboxylic acids in influencing the stability of the ternary Cu(II) metal complexes has been compared.

Materials and Methods

The amino acids glycine (Gly), DL-alanine (Ala), valine (Val), leucine (Leu), phenylalanine (Phe), tryptophan (Trypt), methionine (Met), serine (Ser), threonine (Thr), aspartic acid (Asp), ethylenediamine dihydrochloride (En) and pyrocatechol (Pyr) were obtained from Sigma Chemical Co., USA. Iminodiacetic acid (IMDA), nitrilotriacetic acid (NTA), ethylenediaminetetraacetic acid (EDTA), potassium hydrogen pthalate, potassium nitrate, metal nitrates and sodium hydroxide were BDH reagents of Analar grade. Stock solutions (0.02 *M*) of Co(II), Cu(II), Ni(II) and Zn(II) were prepared and standardised by complexometric titration with EDTA[6]. Carbonate-free NaOH was prepared and standardized by titrating with potassium hydrogen pthalate.

Formation constants of ternary complexes were determined by potentiometric titration of solutions containing a 1:1:1 molar ratio of ligand L, metal ion and ligand A, with standard carbonate-free NaOH. IMDA, bidentate amino acids, En and Pyr were used in diprotonated form while NTA and Asp were used in triprotonated form. The potentiometric titrations were carried out in a double walled titration cell maintained at 35°C ± 0.2. The ionic strength was maintained effectively constant at 0.2 by suitable addition of reagent grade KNO_3. Further details of the experimental procedure are given in our earlier papers[3,8,9].

Formation constants of ternary complexes

Stability constants for ternary complexes formed according to equilibrium (1)

$$ML + A \overset{K^{ML}_{MLA}}{\rightleftharpoons} MLA \quad \ldots (1)$$

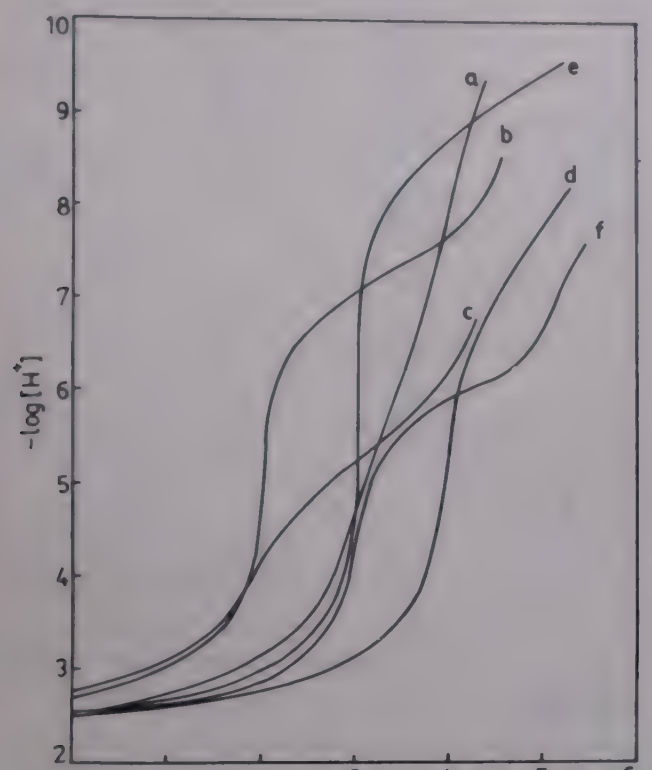

Fig. 1—Potentiometric titration curves for ternary systems containing IMDA or NTA(L), Cu(II) [M] and Ala/Trypt/Pyr/En in a 1:1:1 molar ratio [Curve a = IMDA-Cu(II)-Trypt; b = IMDA-Cu(II)-Pyr; c = IMDA-Cu(II)-En; d = NTA-Cu(II)-Ala; e = NTA-Cu(II)-Pyr; and f = NTA-Cu(II)-En. $T_L = T_M = T_A = 1.00 \times 10^{-3}$ *M*, t = 35°C; $\mu = 0.2$ *M* (KNO_3), m = mol of base added per mole of metal ion]

where

$$K^{ML}_{MLA} = \frac{[MLA]}{[ML][A]} \quad \ldots (2)$$

were calculated from the *p*H-metric data using the appropriate mass balance equations given in our earlier papers[8,9]. The ternary constants were further refined with the computer program SCOGS[10].

Results and Discussion

Representative potentiometric titration curves for ternary systems containing IMDA or NTA, Cu(II) and Ala/Trypt/Pyr/En in a 1:1:1 molar ratio are shown in Fig. 1. Formation constants (Eq. 2) were calculated from the potentiometric data and are listed in Tables 1 and 2. The stabilities of the various ternary complexes have been quantitatively compared with the stabilities of the corresponding binary complexes (determined by us earlier, under identical experimental conditions[8,9]) in terms of the parameter $\Delta\log K$, given by the expression

$$\Delta\log K = \log K^{ML}_{MLA} - \log K^{M}_{MA} \quad \ldots (3)$$

These values are also listed in Tables 1 and 2. The parameter $\Delta\log K$ is a quantitative measure of the extent to which the two ligands (L and A) in coordination sphere of the metal ion mutually influence each other. The statistical ratio for the coordination of a bidentate ligand with an octahedral [M(II)-IMDA] binary complex [M = Co, Ni or Zn] relative to the octahedrtal aquo metal ion is 3/12; hence $\Delta\log K = -0.6$.

The data in Table 1 show that the $\Delta\log K$ values for ternary Co(II), Ni(II) and Zn(II) complexes in-

Table 1—Stability constants* of ternary complexes of Co(II), Ni(II) and Zn(II) containing iminodiacetic acid {Temp. = 35°C; $\mu = 0.2$ *M*(KNO_3)}

Ligand (A)	Co(II)			Ni(II)			Zn(II)		
	$\log K^{ML}_{MLA}$	$\log K^{M}_{MA}$	$\Delta\log K$	$\log K^{ML}_{MLA}$	$\log K^{M}_{MA}$	$\Delta\log K$	$\log K^{ML}_{MLA}$	$\log K^{M}_{MA}$	$\Delta\log K$
Glycine	3.84	4.62	−0.78	5.01	5.90	−0.89	4.02	4.86	−0.84
Alanine	3.48	4.35	−0.87	4.65	5.60	−0.95	3.93	4.80	−0.87
Valine	3.31	4.24	−0.93	4.90	5.70	−0.80	3.91	4.70	−0.79
Leucine	3.51	4.27	−0.76	4.56	5.47	−0.91	3.90	4.69	−0.79
Phenylalanine	3.05	3.90	−0.85	4.12	5.13	−1.01	3-73	4.61	−0.88
Tryptophan	3.19	4.10	−0.91	4.32	5.25	−0.93	3.57	4.59	−1.02
Serine	3.25	4.19	−0.94	4.53	5.42	−0.89	3.73	4.66	−0.93
Threonine	3.32	4.13	−0.81	4.64	5.52	−0.88	3.93	4.69	−0.76
Methionine	3.09	3.98	−0.89	4.35	5.32	−0.97	3.56	4.37	−0.81
Aspartic acid	4.49	5.78	−1.29	5.84	7.17	−1.33	3.80	5.23	−1.43
Ethylenediamine	5.18	5.81	−0.63	6.80	7.46	−0.66	5.57	6.25	−0.68
Pyrocatechol	6.55	7.69	−1.14	6.52	7.60	−1.08	6.92	8.11	−1.19

*Constants accurate to ±0.02. Binary constants K^{M}_{MA} are taken from ref. 5.

Table 2—Stability constants* of ternary Cu(II) complexes containing IMDA, NTA or BIM {Temp. = 35.0°C; $\mu = 0.2\ M(KNO_3)$}

		IMDA		NTA		BIM†	
Ligand (A)	$\log K^{M}_{MA}$	$\log K^{MI}_{MLA}$	$\Delta\log K$	$\log K^{MI}_{MLA}$	$\Delta\log K$	$\log K^{MI}_{MLA}$	$\Delta\log K$
Glycine	8.00	6.14	−1.86	5.35	−2.65	7.25	−0.75
Alanine	7.94	5.95	−1.99	4.96	−2.98	7.29	−0.65
Valine	8.08	6.30	−1.78	5.24	−2.84	7.39	−0.69
Leucine	8.04	6.09	−1.95	5.40	−2.64	7.29	−0.75
Phenylalanine	7.64	5.84	−1.80	5.05	−2.59	7.45	−0.19
Tryptophan	7.96	6.25	−1.71	5.28	−2.68	8.15	+0.19
Serine	7.80	5.84	−1.96	5.10	−2.70		
Threonine	7.90	5.89	−2.01	5.34	−2.56		
Methionine	7.70	5.81	−1.89	5.05	−2.65	7.10	−0.60
Aspartic acid	8.38	5.79	−2.59	5.20	−3.18		
Ethylenediamine	10.32	9.32	−1.00	8.25	−2.07	9.35	−0.97
Pyrocatechol	13.64	11.28	−2.36	10.64	−3.00	13.35	−0.29

*Constants accurate to ±0.02. Binary constants K^{M}_{MA} are taken from refs 8 & 9.
†Values from ref. 4.

volving IMDA and bidentate amino acids Gly, Ala, Val, Leu, Phe, Trypt, Ser, Thr or Met are slightly more negative than expected on statistical grounds alone. The extra destabilization results from electrostatic repulsion between the negative charges on IMDA and the amino acid anion. Electrostatic repulsion between IMDA and Pyr (both of which bear two negative charges each) result in further destabilization of ternary complexes containing these two ligands. The $\Delta\log K$ values for ternary systems containing Asp are more negative than those observed for all other systems. Asp is tridentate and dinegative and hence both statistical and electrostatic effects lead to loss of stability. Since En is a neutral molecule, the $\Delta\log K$ values are of the statistically expected magnitiude. *p*H-Metal complex species distribution profiles for (IMDA-Ni-Ala), (IMDA-Ni-Pyr) and (IMDA-Ni-En) ternary systems were computed from the protonation and stability constant data using the computer programme Complex[11]. Typical curves are given in Fig. 2 for the IMDA-Ni(II)-En system. These plots showed that the pecentage of the ternary complex (MLA) was 88, 60 and 28, respectively, for the ligands, En, Ala and Pyr. Similar trends were observed for ternary systems containing Co(II) and Zn(II). Hence, with respect to the nature of the donor atoms on ligand A, the stability of the ternary complexes containing IMDA increase in the order: $^{-}O-O^{-} < N-O^{-} < N-N$.

The $\Delta\log K$ values in Tables 1 and 2 show that the stabilities of ternary Cu(II) complexes containing IMDA are lower than those of the corresponding

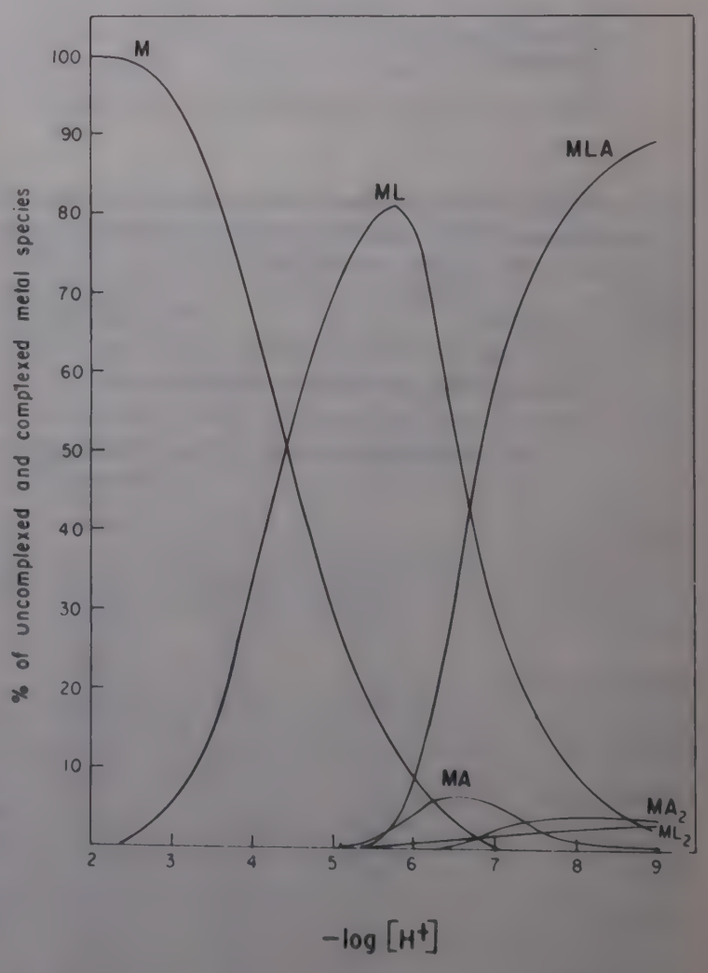

Fig. 2—*p*H-species distribution profile for the ternary 1:1:1 IMDA-Ni(II)-En system. Ordinate represents the percentage of a given metal complex species as a function of the total metal concentration {M = Ni, L = IMDA, A = ethylenediamine; [M] = [L] = [A] = 0.001 *M* each, temp. = 35°C, $\mu = 0.2\ M(KNO_3)$}

Co(II) or Zn(II) complexes. The greater destabilization could result from the fact that Cu(II) is tetragonally distorted with only four strong equitorial binding sites and two weak axial sites. It is worthwhile to compare the relative stabilities of ternary Cu(II) complexes containing IMDA, NTA and BIM. The $\Delta\log K$ values (Table 2) for ternary complexes involving BIM and amino acids without an aromatic side chain (Gly, Ala, Val, Leu, Ser, Thr and Met) are more positive relative to the corresponding complexes containing IMDA or NTA. The greater stability of BIM containing complexes may be attributed to (a) favourable statistical factor for binding the second ligand, since BIM occupies only two sites on the metal ion, whereas IMDA and NTA bind to 3 or 4 sites respectively, (b) favourable electrostatic interaction between the positively charged $(Cu\text{-}BIM)^{2+}$ complex and the mononegative amino acid anion (similar stabilization does not occur with neutral (Cu-IMDA) or negative $(Cu\text{-}NTA)^{-}$ complexes), and (c) metal-ligand back-bonding in binary $(Cu\text{-}BIM)^{2+}$ complexes causing the metal centre to become more positive and hence favouring the interaction with anionic amino acids and Pyr. In binary (Cu-IMDA) and $(Cu\text{-}NTA)^{-}$ complexes the absence of such back-bonding effects allows electron density to build up on the metal centre and interaction with ligand A is not favoured.

Ternary Cu(II) complexes containing BIM and the amino acids Phe and Trypt (which possess aromatric side chains) are considerably stabilised due to intramolecular metal ion mediated stacking interactions between the aromatic moieties of the two ligands. Due to the aliphatic nature of IMDA or NTA, such stabilizing stacking interactions do not occur. In ternary complexes containing En the stability of the complexes with respect to ligand L increases in the order NTA < IMDA < BIM. Since En is a neutral ligand the above order may primarily be consequence of a favourable statistical factor resulting from the increasing number of binding sites on the binary ML complexes. The present investigation emphasizes the important role of statistical, electrostatic, metal-ligand back-bonding and metal ion mediated stacking interactions in stabilizing ternary complexes.

Acknowledgement

A K R and G N R thank the CSIR, New Delhi for providing research fellowships.

References

1 Srinivas Mohan M, Bancroft D & Abbott E H, *Inorg Chem*, 18 (1979) 1527.
2 Prasad K, Venkataiah P & Srinivas Mohan M, *Indian J Chem*, 28A (1989) 325.
3 Srinivas Mohan M, *Indian J Chem*, 20A (1981) 252.
4 Prasad K, Bathina H B & Srinivas Mohan M, *J coord Chem*, 17 (1988) 63.
5 Koteswar Rao A, Venkataiah P, Bathina H B & Srinivas Mohan M, *J coord Chem*, 20 (1989) 69.
6 Flashka H A, *EDTA titrations* (Pergamon Press, Oxford) 1964.
7 Schwarzenbach G & Biederman R, *Helv chim Acta*, 31 (1948) 337.
8 Prasad K & Srinivas Mohan M, *J coord Chem*, 16 (1987) 1.
9 Prasad K, Koteswar Rao A & Srinivas Mohan M, *J coord Chem*, 16 (1987) 251.
10 Sayce I G, *Talanta*, 15 (1968) 1397.
11 Ginsburg G, *Talanta*, 23 (1976) 149.

Indian Journal of chemistry
Vol. 31A, April 1992, pp. 260-264

Studies on the complexes of 3-(*o*-carboxyphenyl)-1-phenyltriazene 1-oxide: Part II—Nickel(II) complex and its reaction products with some neutral N-donors

Sailesh C Saha*, Piyush K Chakraborty, Nirmalendu Roychaudhuri† & Subrata Maji
Department of Chemistry, Jadavpur University, Calcutta 700 032

Received 11 July 1990; revised 5 August 1991; accepted 13 January 1992

3-(*o*-Carboxyphenyl)-1-phenyltriazene 1-oxide (LH_2) reacts with aqueous solutions of nickel(II) salts to form a polymeric paramagnetic complex $[NiL(H_2O)_2]$ of octahedral geometry which on treatment with N-donors (X) transforms to polymeric diamagnetic square-planar [NiLX] (X = NH_3, MA, EA, DMA, *i*-PA, *n*-BA, *i*-BA, py, α, β, γ-pic, quin and morp) and polymeric paramagnetic octahedral $[NiLX_3]$ (X = DMA, *i*-BA, py, β & γ-pic and morp) complexes. $[NiL(H_2O)_2]$ and all [NiLX] complexes undergo pyrolytic change to an isolable paramagnetic intermediate [NiL], suggested to have a polymeric distorted tetrahedral geometry. The [NiL] species are, however, not isomorphous. The ligand with coordinating centres NH, NO and COOH (C = O, OH) shows different structural modes. In $[NiL(H_2O)_2]$ and [NiL] it is tetradentate (O^-, N^-, O_2) but in [NiLX] and $[NiLX_3]$ it is tridentate (O^-, N^-, O) due to flexible nature of carboxy group acting as bridging bidentate in the former and monodentate in the latter. The triazene is highly prone to produce mixed complexes of flexible stereochemistry in presence of nucleophiles.

In an earlier paper[1] we observed that 3-(*o*-carboxyphenyl)-1-phenyltriazene 1-oxide (LH_2) shows a tendency to form mixed complexes. The reported complexes were not well characterised and the triazene 1-oxide was shown to behave only as a dibasic tridentate ligand. But in a later communication[2], we showed that the said triazene acts as a dibasic tetradentate ligand forming various mixed complexes of different geometries with zinc(II) in presence of neutral monodentate N-donors. Besides, the ligand forms complexes of analytical importance[3-5] with a variety of transition and non-transition metals.

In the present paper, we describe the results of our studies on the complexes of Ni(II) with LH_2 and other reaction products obtained in presence of neutral N-donors.

Materials and Methods

The ligand (LH_2) was prepared following our earlier method[1]. The N-bases were distilled before use. All other chemicals were of AR grade.

Elemental analyses (C, H and N) were carried out using a Perkin Elmer 240C elemental analyser and Cary 17 D spectrophotometer was used for recording electronic spectra. IR spectra were recorded in KBr disk with the help of a Beckmann IR 20A or in nujol on a Perkin Elmer 297 or 337 model spectrophotometer. Magnetic susceptibilities were determined at room temperature by the Gouy technique using $Hg[Co(CNS)_4]$ as standard. X-ray powder patterns were taken using a Philips diffractometer and CuK_α radiation.

Preparation of the complexes

$[NiL(H_2O)_2]$

Hot solutions of aquated NiX_2 (X = Cl^-, CH_3COO^- and $1/2SO_4^{2-}$) (2 mmol in water) and the ligand (LH_2) (2 mmol in hot ethanol) were mixed together with stirring and *p*H of the mixture was maintained at 6-7. The parrot-green granular precipitate formed immediately was filtered, washed with hot ethanol and dried in air. The complex was also obtained by boiling [NiL] with aqueous ethanol.

The complex was insoluble in methanol, ethanol, chloroform and benzene but was soluble in DMSO.

[NiLX] (X = NH_3, MA, EA, DMA, i-PA, n-BA, i-BA, py, α-, β- & γ-pic, quin and morp)

Complexes [NiLX] (X = NH_3, MA, EA, DMA, *i*-PA, *n*-BA, *i*-BA, α-pic, quin and morp) were prepared by slowly adding the base to a hot ethanolic suspension of $[NiL(H_2O)_2]$ or [NiL] until it just dissolved. On slow cooling, red or reddish-brown crystals separated almost immediately and these were washed thoroughly with ethanol and dried in air.

The complexes [NiLX] (X = py, β- and γ-pic) were prepared by the following method:

†Department of Chemistry, IACS, Calcutta 700 032.

Hot solutions of the ligand (2 mmol in ethanol) and $NiCl_2.6H_2O$ (2 mmol in water) were mixed together and then a measured amount of pyridine base (2 mmol in ethanol) was added with constant stirring. The mixture was then diluted with water and the clear solution was kept overnight. Brown or reddish-brown crystals formed were filtered off, washed with ethanol and dried in air.

[NiLX] with X = NH_3, β-pic and quin were insoluble in common organic solvents but were soluble in DMSO. On the other hand, other [NiLX] complexes were more or less soluble in common organic solvents like chloroform, benzene, ethanol, etc.

[$NiLX_3$](X= DMA, i-BA, py, β- &γ-pic and morp)

On addition of excess base either to the suspension of [$NiL(H_2O)_2$] in hot ethanol or to the corresponding monobase mixed complex, at first a green solution was obtained which yielded green crystals on standing overnight. The crystals were filtered off, washed with ethanol and dried in air. [NiL] was also transformed to [$NiLX_3$] by a similar manner. The complexes were soluble in common organic solvents like benzene, chloroform, etc.

It is interesting to note that [$NiL(\alpha\text{-pic})_3$] could not be prepared following the method described above; on dissolving [$NiL(\alpha$-pic)] in α-picoline, the same reappeared from the solution. Similar behaviour was also observed with [NiLquin]. On the other hand, when excess amine base (NH_3, MA, EA, *i*-PA or *n*-BA) was added to the ethanolic suspension of the respective brown [NiLX] complex, an unstable shining green complex (probably [$NiLX_3$]) was formed which reverted to the original brown [NiLX] form on drying.

[NiL]

This interesting moiety was obtained from [$NiL(H_2O)_2$ and also from all [NiLX] by heating for ~ 1h at 170°-200°C in an air oven. It was highly insoluble in common organic solvents except DMSO.

Results and Discussion

[$NiL(H_2O)_2$]

The identity of parrot-green paramagnetic complex [$NiL(H_2O)_2$], formed by the reaction of Ni(II) with LH_2 at *p*H ~ 6.0, was confirmed* by the analytical, thermal, magnetic and spectral data. Treatment of [NiL] with aqueous ethanol also yielded [$NiL(H_2O)_2$]. The complex is almost insoluble in water and in non-coordinating organic solvents. A very poor molar conductance (1.6×10^{-4} ohm^{-1} cm^2 mol^{-1}) in DMSO indicates the non-electrolytic nature of the complex.

The IR bands due to νNH (at 3240 cm^{-1}) and νOH of COOH group (at 3020 and 2570 cm^{-1}) of the ligand (LH_2) are found to be absent in the spectrum of [$NiL(H_2O)_2$]. This clearly indicates deprotonation of NH and OH and bonding of the ligand through N^-, O^- to Ni(II)[1,2]. The νNO band observed at 1275 cm^{-1} in LH_2 gets shifted to 1210 cm^{-1} in the complex, which shows the coordination of NO group through O-atom[1,2]. The ν_{as}COO (1510 cm^{-1}) and ν_sCOO (1375 cm^{-1}) bands of carboxylate ion of the present ligand (L^{2-} in Na-salt) are shifted to 1498 cm^{-1} (with a shoulder at 1510 cm^{-1}) and 1388 cm^{-1}, respectively, in its [$NiL(H_2O)_2$] complex. Here only a little change in $\Delta\nu$COO (from 135 to 110 cm^{-1}), proves the bridging bidentate nature of the carboxylate group of the ligand in its complex[2,6-8]. A band at 528 cm^{-1} is tentatively assigned to νMN while bands at 460, 420, 370 and 335 cm^{-1} are assigned to νMO modes[2,9]. Thus, from the IR studies it is suggested that the triazene 1-oxide is tetradentate (O^-, N^-, O_2) in nature in the Ni(II) complex. The presence of water in the complex was confirmed by the occurrence of a broad band at 3400 cm^{-1} due to νOH and a shoulder at 1640 cm^{-1} due to δHOH in IR spectra of the complex. Thermal analysis (obtained on a DT 30 Shimadzu Thermal Analyser, heating rate of 5°C/min) showed that the removal of H_2O at 160°-200°C is very slow and not complete even at the decomposition point (at 200°C) of the complex. But on prolonged heating at 180°C for 1h [$NiL(H_2O)_2$] loses two H_2O molecules to form [NiL]. This provides enough evidence to conclude that the two H_2O molecules are directly coordinated to Ni(II).

Thus, the tetradentate behaviour of the ligand (O^-, N^-, O_2) and coordination of two H_2O molecules clearly indicate the octahedral nature of the complex [$NiL(H_2O)_2$]. The observed magnetic moment of 3.09 B.M. at room temperature is also in good agreement with that geometry. In the reflectance spectra of the complex, two broad bands at 600 and 455 nm were observed which can be assigned[10] to $^3A_{2g} \rightarrow {}^3T_{1g}(F)$ and $^3A_{2g} \rightarrow {}^3T_{1g}(P)$ transitions of octahedral Ni(II). We could not observe the weak ν_1 band expected around 1000 nm. Due to its insolubility in the non-coordinating solvents, the solution spectrum of the complex could be recorded in DMSO only which shows two broad bands at 870 nm (ε = 12) and 590 nm (ε = 68) and one strong charge transfer band at 415 nm (ε = 30, 465). These also support the octahedral structure of [$NiL(H_2O)_2$].

*Repeated analysis showed the complex to conform to the composition [$NiL(H_2O)_2$] and not [$NiLH_2O$] reported earlier (Ref. 1).

An almost strain free octahedral polymeric structure of the complex as shown in structure Ia or Ib, where the ligand carboxy group bridges the two metal ions, can be made by the stick-ball model [Minit molecular building system (Ref. No. 7.10) manufactured by Cochranes of Oxford Ltd., Leafield, Oxford, England] in which the entire triazene 1-oxide molecule does not remain in the same plane as the nickel atom but the coordinating atoms of the ligands (O^-, N^-, O_2) and nickel atom exist in the same plane. The structure (Ia) is preferred to structure (Ib) since (Ia) can be transformed to polymeric [NiLX] (II) (vide infra) but not (Ib), on treatment of $[NiL(H_2O)_2]$ with the X-ligands.

Further, the X-ray powder diffraction patterns of $[NiL(H_2O)_2]$ are identical with those of octahedral polymeric $[ZnL(H_2O)_2]$[2] as shown by their list of *d*-lines.

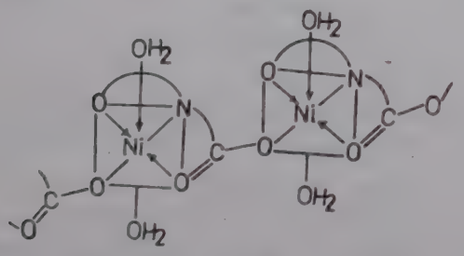

Ia

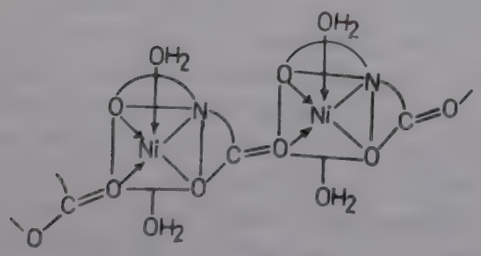

Ib

[NiLX]

Treatment of alcoholic suspension of $[NiL(H_2O)_2]$ or a mixture of alcoholic LH_2 and Ni(II) salts with the hot N-bases afforded [NiLX]. [NiL] also transformed to [NiLX] in hot ethanolic solution of N-bases (X). All the complexes were formed with a remarkable change in colour of the solution. The complexes are either red or reddish-brown, diamagnetic and non-electrolytes (molar conductance in DMSO, $0.01\text{-}2.14 \times 10^{-4}$ ohm^{-1} cm^2 mol^{-1}). $[NiLNH_3]$, [NiL(β-pic)] and [NiLquin] were highly insoluble in non-coordinating organic solvents but others were slightly soluble in benzene or in chloroform.

Elemental analysis of the complexes and their weight loss on heating corresponded to the composition [NiLX]. Their IR spectra show that the binding sites of the triazene 1-oxide with Ni(II) are not exactly the same as in the case of aqua complex. As in the aqua complex, absence of bands due to νOH (COOH) and νNH of LH_2 indicate their deprotonation and bonding through O^- and N^- to Ni(II) in these complexes also. Sufficient lowering of νNO band with respect to that of the free ligand confirmed the coordination of NO through O-atom[2]. The ν_{as}COO appreciably shifted to higher frequency region in all the complexes. Similarly, ν_sCOO shifted to higher frequency in most cases; in a few cases it moved slightly to lower region. These shifts of COO group frequencies result in considerable increase in $\Delta\nu$COO (~ 170 cm^{-1}) in the complexes compared to that of the free L^{2-}. This clearly supports the monodentate nature[6-8] of the carboxylate group of the triazene 1-oxide in [NiLX]. LH_2 may, therefore, be considered as tridentate (O^-, N^-, O) in [NiLX]. The bands appearing in the range 3350-3150 cm^{-1} (νNH$_2$/NH) and 3100-2800 cm^{-1} (CH stretching indicate the presence of N-bases in the complexes and their coordination to the metal ions is evident from the sufficient lowering of νNH$_2$/NH bands.

The complexes are diamagnetic and exhibit an absorption band at ~ 570 nm (ε 70-188) along with a very strong charge transfer band at ~ 410 nm. All these support square-planar geometry[11] of the complexes. Of the four coordination sites, one is held by unidentate N-donor and the rest three are occupied by the triazene 1-oxide ligand. Thus, COO group of the ligand is definitely unidentate. The complexes are not sufficiently soluble in non-coordinating solvents, which indicates the polymeric nature of the square-planar complexes [NiLX] (II).

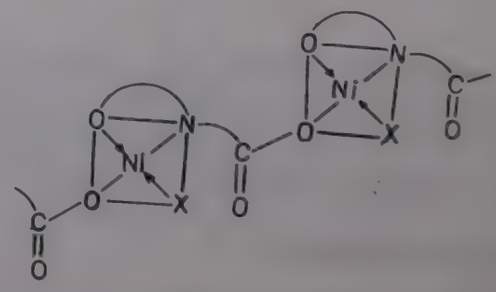

II

[NiLX$_3$]

The treatment of $[NiL(H_2O)_2]$, [NiLX] or [NiL] with hot ethanolic solution of excess N-bases affords green $[NiLX_3]$ complexes. These complexes are slightly more soluble than others in non-coordinating solvents like benzene, chloroform etc. All are non-electrolytes and their analytical data correspond to $[NiLX_3]$. IR data show that the mode of bonding of the triazene 1-oxide with Ni(II) in these

Table 1—Analytical, magnetic and electronic spectral data of the nickel(II) complexes

Complex[a]	Found (Calc.), %				μ_{eff} (B.M.)	λ^{b}_{max} (nm) (ε_{max})
	Ni	C	H	N		
$[NiL(H_2O)_2]$	17.0 (16.8)	44.5 (44.6)	3.8 (3.7)	11.8 (12.0)	3.09	600, 455[f]; 590[g] (68), 870 (12)
$[NiLNH_3]$	17.6 (17.7)	47.0 (47.1)	3.5 (3.6)	16.8 (16.9)	Diamagnetic	560[c]
[NiLMA]	17.0 (17.0)	46.0 (46.3)	3.7 (3.9)	16.0 (16.2)	"	570[d] (160)
[NiLEA]	16.4 (16.4)	47.6 (47.7)	4.3 (4.3)	15.6 (15.6)	"	560[d] (178)
[NiLDMA]	16.5 (16.4)	50.0 (50.1)	4.5 (4.5)	15.4 (15.6)	"	570[e] (97)
[NiL(*i*-PA)]	15.6 (15.7)	51.4 (51.5)	4.9 (4.9)	15.0 (15.0)	"	570[d] (188)
[NiL(*n*-BA)]	15.0 (15.2)	52.8 (52.7)	5.3 (5.2)	14.6 (14.5)	"	560[e] (82)
[NiL(*i*-BA)]	15.0 (15.2)	52.6 (52.7)	5.3 (5.2)	14.4 (14.5)	"	570[d] (70)
[NiLpy]	14.9 (14.9)	55.0 (54.9)	3.5 (3.6)	14.1 (14.3)	"	470[d] (87)
[NiL(α-pic)]	14.6 (14.8)	56.1 (56.0)	3.8 (4.0)	13.6 (13.8)	"	580[d] (161)
[NiL(β-pic)]	14.7 (14.8)	56.0 (56.0)	3.9 (4.0)	13.5 (13.8)	"	580[c]
[NiL(γ-pic)]	14.7 (14.8)	56.1 (56.0)	3.9 (4.0)	13.6 (13.8)	"	570[d] (136)
[NiLquin]	13.5 (13.3)	60.1 (59.6)	3.6 (3.7)	12.8 (12.6)	"	580[c]
[NiLmorp]	14.7 (14.7)	50.8 (50.9)	4.5 (4.5)	13.7 (14.0)	"	560[d] (174)
$[NiL(DMA)_3]$	13.0 (13.1)	50.6 (50.7)	6.7 (6.7)	18.6 (18.7)	3.21	570[e] (92), 890 (15), 1300 (16)
$[NiL(i\text{-}BA)_3]$	11.0 (11.0)	56.2 (56.2)	8.0 (7.9)	15.6 (15.8)	2.94	570[d] (100), 840 (20), 1130 (14)
$[NiL(py)_3]$	10.5 (10.7)	60.8 (60.9)	4.3 (4.4)	15.0 (15.2)	2.99	580[e] (225), 840 (13), 1120 (6)
$[NiL(\beta\text{-pic})_3]$	9.8 (9.9)	62.6 (62.7)	5.1 (5.1)	13.7 (14.1)	3.06	580[e] (225), 840 (12), 1120 (5)
$[NiL(\gamma\text{-pic})_3]$	9.8 (9.9)	62.6 (62.7)	5.1 (5.1)	14.0 (14.1)	3.00	580[e] (190), 840 (16), 1100 (10)
$[NiL(morp)_3]$	10.3 (10.2)	52.1 (52.2)	6.3 (6.3)	14.6 (14.6)	3.31	570[d] (217), 840 (28), 1115 (5)
[NiL] (1)	18.6 (18.7)	49.5 (49.7)	2.9 (2.9)	13.2 (13.4)	3.26	418[f]
[NiL] (2)	18.7 (18.7)	49.5 (49.7)	3.0 (2.9)	13.2 (13.4)	2.96	410[f]

[a]$[NiL(H_2O)_2]$ is parrot-green, [NiL] (1) and [NiL] (2) are dirty green and brownish-yellow, respectively, all $[NiLX_3]$ are deep-green and all [NiLX]'s are red or brown in colour. [b]All the complexes exhibit the charge-transfer band at 440-400 nm of high ε_{max} value. [c]In nujol. [d]In chloroform, [e]In benzene, [f]Bands obtained in reflectance spectra, [g]In DMSO.

complexes is the same (O^-, N^-, O) as that in [NiLX]. Presence of N-bases and their coordination through N-atom is clear, like that in [NiLX], from the IR spectra. The magnetic moments of the complexes at room temperature are ~3.0 B.M. which indicates octahedral structure of the complexes. Three well-defined electronic spectral bands at ~1120, 840 and 570 nm (Table 1) are in good agreement with octahedral geometry of $[NiLX_3]$ complexes[10]. Due to the low solubility in non-coordinating solvents a polymeric structure (III) is suggested for the complexes. Mode of transformation of $[NiL(H_2O)_2]$ to $[NiLX_3]$ is clear in the presence of excess X-ligands.

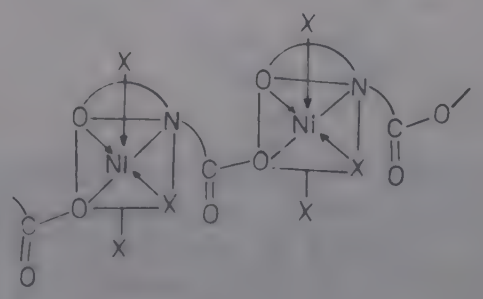

III

[NiL]

It was obtained by continuous heating of $[NiL(H_2O)_2]$ or [NiLX] for ~1h at 170°-200°C. It is interesting to note that if [NiL] is treated with aqueous ethanol, it is transformed to $[NiL(H_2O)_2]$ and if heated with other nucleophiles (X) in ethanol it is converted to [NiLX] or $[NiLX_3]$ depending on the amount of N-base used. The dirty-green [NiL] (1) derived from $[NiL(H_2O)_2]$ is not the same in properties as brownish-yellow [NiL] (2) obtained from $[NiLNH_3]$. The former decomposes at 200°C whereas the latter is stable upto 230°C. The magnetic value of [NiL] derived from paramagnetic $[NiL(H_2O)_2]$ (μ_{eff} = 3.09 B.M.) is 3.26 B.M. and that of [NiL] obtained from diamagnetic $[NiLNH_3]$ is 2.96 B.M. at room temperature. The remarkable differences in magnetic moment and colour of NiL obtained from two different parent compounds indicate a definite change of structure.

The ν_{as}COO and ν_sCOO bands in both the forms are found at 1490 and 1380 cm^{-1}, respectively, along with a weak broad band at 1550 cm^{-1} which may also be assigned to ν_{as}COO. The IR spectra of the two complexes differ due to the presence of a strong band at 1430 cm^{-1}, assumed as ν_sCOO, for [NiL] (dirty-green) which is absent in [NiL] (brownish-yellow). $\Delta\nu$COO in both the forms is 110 cm^{-1} which suggests the bidentate bridging character of COO group of the ligand as in aqua-complex. Absence of νOH (COOH), νNH, lowering of νNO band and $\Delta\nu$COO value of the triazene 1-oxide in [NiL] suggest that the mode of bonding of the ligand with Ni(II) in both the forms is the same (O^-, N^-, O_2) as in [NiL(H_2O)$_2$]. A minor difference in IR bands due to νMN/MO in the two forms is observed which could not be explained.

Both the [NiL] species are highly insoluble and reflectance spectra of the two varieties are not well resolved. Only a strong band due to charge transfer is observed at ~ 410 nm. For this reason we could not assign an exact geometry to [NiL] complex. The magnetic moment of the four-coordinated Ni(II) in [NiL] (Table 1) suggests tetrahedral structure of [NiL]. But this value is comparatively lower than that required for the regular tetrahedral Ni(II). Literature reports show[12] that tetrahedral Ni(II) of low magnetic value is due to distortion of the regular form, for which distorted polymeric tetrahedral structure is suggested for the two [NiL] species (IV).

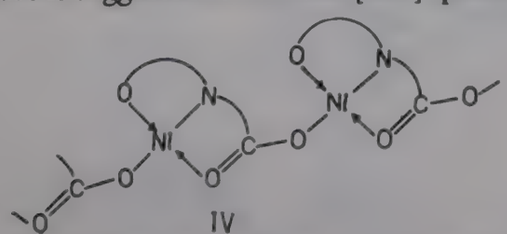

IV

In the species [NiL] all the four-coordination sites of Ni(II) are occupied by the triazene 1-oxide ligand anion (L^{2-}). Without the two axial H_2O molecules, the metal ion can no longer maintain the planarity and acquires a distorted tetrahedral geometry (greenish form). But in the brownish species after the removal of X-molecule from one of the planar positions, the complex has to make up the coordination through free >C=O. These different situations probably make the nature of the distortion different leading to different properties of the two isomers. Further, the X-ray diffraction patterns of the two isomers are different which points out that the two are non-isomorphous.

In the formation of various substituted complexes, the nucleophiles (X) behave differently towards [NiL(H_2O)$_2$]. Ammonia and alkylamines have strong tendency to form stable red or reddish brown square-planar complexes even in presence of excess of the nucleophiles. Although, green crystalline unstable adducts appear after treatment with huge excess of the base nucleophiles, probably, due to attainment of octahedral geometry, they revert to the planar forms losing the extra bases, while drying. Only with dimethyl and isobutyl amines, both the mono and tris-base complexes could be obtained in stable forms using controlled amount and excess of the base, respectively. On the other hand, the pyridine bases are highly prone to form the tris-base octahedral complexes even when present in slight excess. The brown planar pyridine base complexes could only be prepared by the careful addition of calculated amount of pyridine bases to the aqueous suspension of [NiL(H_2O)$_2$]. The green tris-morpholine complex obtained after prolong heating of red planar [NiLmorp] with excess of the base, gradually turned to original square-planar form on keeping for a few days showing a strain in the tris-base complex due to the presence of two bulky base molecules.

The ligand shows different structural modes in the formation of Ni(II) complexes in presence of N-donors due to the flexible behaviour of the carboxy group. In the absence or presence of weak O-donors (H_2O), COO of the triazene 1-oxide acts as a bidentate bridging group and in presence of strong N-donors it acts as a monodentate one. Thus, presence of groups like COOH, NH and NO in the triazene makes it a highly versatile ligand capable of forming mixed complexes and further flexibility in the stereochemistry of the complexes is introduced by the presence or absence of nucleophiles.

References

1 Majumdar A K & Saha S C, *J Indian chem Soc*, 53 (1976) 226.
2 Saha S C & Maji Subrata, *Indian J Chem*, 29A (1990) 573.
3 Majumdar A K & Saha S C, *Anal chim Acta*, 40 (1968) 299; 44 (1969) 85.
4 Saha S C, Chakraborti D & Chakraborty P, *Indian J Chem*, 15A (1977) 816.
5 Saha S C, Ghosh Keya, Bhattacharya B & Chaudhury B, *Proceedings of the international seminar on base metal technology*, Jamshedpur-India (1989) 239.
6 Sandhu S S, Manhas B S, Mittal M R & Parmar S S, *Indian J Chem*, 7 (1969) 286.
7 Manhas B S & Trikha A K, *J Indian chem Soc*, 59 (1982) 315.
8 Nandi M M & Debnath P, *Indian J Chem*, 26A (1987) 498.
9 Purohit D N, *Spectrochim Acta*, 41A (1985) 873.
10 Zacharias P S & Chakravorty A, *Inorg Chem*, 10 (1971) 1961; Zacharias P S & Johnson K E, *J inorg nucl Chem*, 38 (1976) 1957.
11 Zacharias P S & Chakravorty A, *Inorg chim Acta*, 6 (1972) 623.
12 Cotton F A & Wilkinson G, *Advanced inorganic chemistry* (Wiley Eastern Reprint, New Delhi) 1976, 896.

Indian Journal of chemistry
Vol. 31A, April 1992, pp. 265-269

Liquid-liquid extraction of molybdenum(VI) from ascorbate solution with high molecular weight amines

(Ms) M A Karve & S M Khopkar*
Department of Chemistry, Indian Institute of Technology, Bombay 400 076

Received 24 October 1991; revised 5 December 1991; accepted 1 January 1992

Molybdenum(VI) is quantitatively extracted at *p*H 4.0 from 5×10^{-3} *M* ascorbic acid with 1×10^{-1} *M* Aliquat 336S in xylene. It is stripped with 1 *M* nitric acid and determined spectrophotometrically at 390 nm as its complex with tiron. Mo(VI) has been separated from iron, chromium, nickel, zirconium, hafnium, titanium and vanadium which are generally associated with it in minerals. Molybdenum in stainless steel and soil samples has been analysed.

Amberlite La-1[1], triisooctylamine[2,3] and trioctylmethylammonium chloride[4] have been used for the solvent extraction of molybdenum(VI) from mineral acid media. Mo(VI) has also been extracted from thiocyanate solution with tribenzylamine[5,6] or Aliquat 336S[7]. Trioctylamine[8] and Amberlite La-2[9] have been used to extract molybdenum as its oxalato and malonato complexes respectively but no extraction has been carried out with the ascorbate complex. Therefore, these studies were taken up by us and the results are reported in this paper.

Materials and Methods

A digital *p*H meter, Type 822 (ECIL, India) with combined glass electrode; ECIL GS866C spectrophotometer with matched 10 cm corex glass cuvettes; a wrist-action flask shaker (Toshnival and Co.) were used in the present studies.

The stock solution of molybdenum(VI) was prepared by dissolving 2.30 g of ammonium molybdate tetrahydrate (BDH, AR) in 250 ml of distilled water. This solution was standardised with quinol-8-olate[10]; it contained 5 mg/ml of molybdenum. A 100 μg/ml solution of molybdenum(VI) was prepared by appropriate dilution.

Aliquat 336S (General Mills Ltd.), Amberlite LA-1, Amberlite LA-2, Primene JMT (Rohn and Hass Co., Ltd.), trioctylamine (Riedel de Haen) were used in ascorbate form without further purification[11,12]. A 2% aqueous solution of tiron was used for colorimetry.

Procedure

To an aliquot containing 100 μg molybdenum, 5 ml of 5×10^{-3} *M* ascorbic acid solution was added. The *p*H of solution was adjusted to 4.0 with dilute ascorbic acid or ammonia. The solution was made upto 10 ml with distilled water; and was transferred into a separatory funnel. Then 10 ml of 1×10^{-1} *M* Aliquat 336S in xylene was added. It was shaken for 5 min on a wrist-action flask shaker. The two phases were allowed to settle and separate. Molybdenum from the organic phase was stripped with 10 ml of 1 *M* nitric acid. After dry ashing, it was determined spectrophotometrically at 390 nm as its complex with tiron[13].

Results and Discussion

Extraction as the function of pH

When molybdenum(VI) was extracted between *p*H 1.0 and 8.0, it was noticed that the extraction was quantitative with Aliquat 336S (*p*H 2.5-6.5), Amberlite LA-1 (*p*H 1-4), Amberlite LA-2 (*p*H 0.5-4.0), trioctylamine (*p*H 3.0). But Primene JMT was a poor extractant. Aliquat 336S was preferred as the extractant, as not only it permitted extraction over a broad *p*H range but it also provided better phase separations. As a rule, quaternary amines offer better separations and Aliquat 336S is not an exception to this rule.

Extraction as the function of Aliquat 336S concentration

When molybdenum(VI) was extracted from $1\text{-}100 \times 10^{-3}$ *M* Aliquat 336S, the extraction was quantitative with $7 \times 10^{-2}\text{-}10 \times 10^{-1}$ *M* Aliquat 336S. The concentration 1×10^{-1} *M* was preferred as it allowed quantitative extraction of the whole amount of molybdenum ascorbate complex. In case of high molybdenum loading, higher concentration of Aliquat 336S would be needed. However, it is not

Table 1—Separation of binary mixtures

[[Mo(VI)] = 100 μg; pH = 4.0; [Aliquat 336S] = 1×10^{-1} M; [Ascorbic acid] = 5×10^{-3} M]

Foreign ion	Tolerance limit (mg)	Ratio of Foreign ion/ Mo(VI)	Foreign ion	Tolerance limit (mg)	Ratio of (Foreign ion/ Mo(VI)
Li^+	4.5	45.0	Cr^{3+}	1.5	15.0
Na^+	4.5	45.0	U^{6+}	0.18	1.8
K^+	4.5	45.0	Mn^{2+}	1.0	10.0
Ca^{2+}	4.0	40.0	Fe^{2+}	1.2	12.0
Sr^{2+}	4.5	45.0	Co^{2+}	0.8	8.0
Ba^{2+}	4.5	45.0	Ni^{2+}	1.0	10.0
Al^{3+}	1.0	10.0	Cu^{2+}	1.5	15.0
Ga^{3+}	0.4	4.0	Zn^{2+}	0.9	9.0
In^{3+}	0.45	4.5	Cl^-	1.0	10.0
Tl^+	2.0	20.0	NO_3^-	1.5	15.0
Pb^{2+}	2.5	25.0	NO_2^-	2.0	20.0
Sc^{3+}	0.35	3.5	PO_4^{3-}	1.0	10.0
Ti^{4+}	0.30	3.0	SO_4^{2-}	1.5	15.0
Zr^{4+}	0.20	2.0	SCN^-	0.9	9.0
Hf^{4+}	0.20	2.0	Cit^{3-}	2.0	20.0
V^{4+}	0.35	3.5	Mal^{2-}	2.0	20.0
Th^{4+}	0.25	2.5	$Tart^{3-}$	1.2	12.0

advisable to use high concentration of Aliquat 336S as there is possibility of third phase formation and emulsification.

Extraction as the function of ascorbic acid concentration

The extraction of molybdenum(VI) was carried out from 5×10^{-4} to 1×10^{-2} *M* ascorbic acid. The extraction was quantitative from 5×10^{-3} to 1×10^{-2} *M* ascorbic acid; 5×10^{-3} *M* ascorbic acid concentration was employed in all further work. It is not worthwhile to use high concentration of ascorbic acid as excess of anion will set up competitive equilibria with anionic ascorbate complex during extraction thereby decreasing the extent of extraction.

Effect of diluents

Various inert solvents such as benzene, toluene, xylene, chloroform, carbontetrachloride, cyclohexane, amylalcohol and cyclohexanol were used as the diluents. The phase volume ratio was maintained as 1:1. Benzene, toluene and xylene were effective while remaining solvents proved to be poor diluents. The extractions involving ion pair formation with nonpolar diluents results in extensive ion association of extracted species leading to quantitative extraction. Xylene was preferred as it is nontoxic, offers better phase separation and eliminates the problem of emulsion formation.

Nature of extracted species

The nature of the extracted species was ascertained by plotting log D vs log of [Aliquat 336S] at fixed ascorbic acid concentration and log D versus log [ascorbic acid] at fixed Aliquat 336S concentration. The slopes were 1.5 and 1.6 respectively. The extracted species had the Mo(VI): Aliquat 336S: ascorbic acid ratio 1:2:2 with the formula as $[(RNH_4)_2MoO_2(ascorb)_2]$[8,9].

Effect of stripping agents

When mineral acids such as hydrochloric, nitric, and perchloric acids and ammonium acetate and ammonium nitrate were used as the stripping agents, 0.5-8 *M* nitric and 2-7 *M* perchloric acids were found to be better stripping agents. Maximum back extraction with hydrochloric and sulphuric acids was 45.0 and 36.0% respectively. The reason for this anomaly being these acids form negatively charged complexes with molybdenum which were re-extracted by the liquid anion exchanger in the organic phase. The back extraction was between 65.0-89.0% with 2 *M* of ammonium acetate or ammonium nitrate. Therefore, 1 *M* nitric acid was preferred as the stripping agent as it permitted stripping over a broad range of acid viz. 1-7 *M*.

Separation from binary mixtures

Molybdenum was extracted in the presence of several ions. The tolerance limit was set as the

Table 2—Separation from multicomponent mixtures

Element	Amount taken (μg)	Amount found (μg)	Stripping agent	Recovery (%)	Chromogenic ligand/ Anal method	λ_{max} (nm)
Sc	100	99.0	HCl (6*M*)	99.0	Arsenazo III	670
Mo(VI)	100	99.6	HNO_3 (1*M*)	99.6	Tiron	390
Ca	250	249.0	Unextracted	99.0	At. emission spect.	423
Zr(IV)	100	99.1	HCl (3*M*)	99.1	Arsenazo III	660
Mo(VI)	65	64.5	HNO_3 (1*M*)	99.5	Tiron	390
Fe(II)	200	199.2	Unextracted	99.6	1,10-Phenanthroline	540
Hf(IV)	100	99.6	HCl (6*M*)	99.6	Xylenol orange	540
Mo(VI)	100	99.6	HNO_3 (1*M*)	99.6	Tiron	390
Pb(II)	250	248.5	Unextracted	99.5	Dithiozone	570
Th(IV)	100	99.6	HCl (6*M*)	99.6	Arsenazo III	650
Mo(VI)	65	64.5	HNO_3 (1*M*)	99.5	Tiron	390
Cr(III)	250	199.2	Unextracted	99.6	Sym diphenyl carbazide	540
Ti(IV)	150	149.4	H_2SO_4 (0.5*M*)	99.6	Tiron	380
Mo(VI)	100	99.1	HNO_3 (1*M*)	99.1	Tiron	390
Fe(II)	250	248.5	Unextracted	99.6	1,10-Phenanthroline	540
Mo(VI)	100	99.6	HNO_3 (5*M*)	99.6	Tiron	390
U(VI)	100	99.0	NaOH (0.5*M*)	99.0	Arsenazo III	650
Tl(I)	200	198.0	Unextracted	99.0	Crystal violet	610
Ti(IV)	100	99.0	H_2SO_4 (0.5*M*)	99.0	Tiron	380
Zr(IV)	100	198.0	HCl (3*M*)	99.0	Arsenazo III	660
Mo(VI)	100	99.6	HNO_3 (1*M*)	99.6	Tiron	390
Fe(II)	250	245.0	Unextracted	99.0	1,10-Phenanthroline	540

amount of foreign ion required to cause ± 2% error in the recovery of molybdenum.

The separation of molybdenum(VI) from other ions in binary mixtures is based upon exploitation of the difference in the stabilities of the respective ascorbate complexes. Elements like alkali and alkaline earths, aluminium, thallium, lead, chromium, manganese, cobalt, nickel, copper and zinc do not form negatively charged complex and are therefore not extracted. The extracted molybdenum(VI) was stripped with 1 *M* nitric acid.

Some elements like scandium, titanium, zirconium, hafnium, thorium, vanadium, gallium and indium form strong ascorbate complexes; these were coextracted along with molybdenum. In such cases, molybdenum was first stripped by 1 *M* nitric acid followed by stripping of all other ions with 3 *M* hydrochloric acid. It was possible to separate molybdenum from these ions in ratios ranging from 1:50 to 1:5 (Table 1).

Separation from multicomponent mixtures

The basis of separation of coextracted metals is the breaking of ascorbate complex with simultaneous formation of anionic complexes and reextraction of anionic complexes with mineral acids, e.g., when 6 *M* hydrochloric acid was used for stripping scandium, zirconium, hafnium and thorium, metals like molybdenum, uranium formed anionic chloro complexes and were reextracted. Similarly, when 0.5 *M* sulphuric acid was used for stripping of titanium, zirconium and molybdenum formed anionic sulphato complexes and were reextracted with Aliquat 336S. Finally, when 5 *M* nitric acid was used for stripping of molybdenum, uranium formed anionic nitrato complex and was reextracted. Since these metals did not form anionic complexes at lower acidity, they were stripped with dilute acids. Various separations based upon this principle are described in Table 2.

Table 3—Analysis of steel and soil samples

Metal	Extractant	Solvent	Acidity/*p*H	Amount present (%)	Amount found (%)
		Steel sample			
Mo	Aliquat 336S	Xylene	4.0	2.21	2.18
Fe	Diethylether	—	8 *M* HCl	70.0	69.0
Cr	Symm-diphenylcarbazide	$CHCl_3$	0.2 *M* H_2SO_4	17.6	17.1
Mn	8-Hydroxyquinoline	$CHCl_3$	12.5	0.66	0.61
Ni	Dimethylglyoxime	$CHCl_3$	7.0	8.68	8.50
		Soil sample			
Mo	Aliquat 336S	Xylene	4.0	11.0	10.0
Fe	Diethylether	—	8 *M* HCl	55.0	53.0
Cr	Symm-diphenylcarbazide	$CHCl_3$	0.2 *M* H_2SO_4	71.4	71.0
Ni	Dimethylglyoxime	$CHCl_3$	7.0	86.0	81.0

Scandium(III), molybdenum(VI) and calcium were separated by stripping scandium(III) with 6 *M* hydrochloric acid and molybdenum(VI) with 1 *M* nitric acid when calcium was not extracted.

Zirconium(IV), molybdenum(VI) and iron(II) were separated by stripping zirconium(IV) with 3 *M* hydrochloric acid, molybdenum(VI) with 1 *M* nitric acid when iron(II) was not extracted.

Hafnium(IV), molybdenum(VI) and lead(II) were separated by stripping hafnium(IV) with 6 *M* hydrochloric acid, and molybdenum(VI) with 1 *M* nitric acid when lead(II) was not extracted.

Thorium(IV), molybdenum(VI) and chromium(III) were separated by stripping thorium(IV) with 6 *M* hydrochloric acid and molybdenum(VI) with 1 *M* nitric acid when chromium(III) was not extracted.

Titanium(IV), molybdenum(VI) and iron(II) were separated by stripping titanium(IV) with 0.5 *M* sulphuric acid, and molybdenum(VI) with 1 *M* nitric acid when iron(II) was not extracted.

Molybdenum(VI), uranium(VI) and thallium(I) were separated by stripping molybdenum(VI) with 5 *M* nitric acid and uranium(VI) with 0.5 *M* sodium hydroxide when thallium(I) was not extracted.

Titanium(IV), zirconium(IV), molybdenum(VI) and iron(II) were separated by stripping titanium(IV) with 0.5 *M* sulphuric acid, zirconium with 3 *M* hydrochloric acid and molybdenum(VI) with 1 *M* nitric acid when iron(II) was not extracted.

In all the above separations, the metals after stripping were determined spectrophotometrically using appropriate chromogenic ligands (Table 2).

Analysis of stainless steel

The method was extended for analysis of a steel sample (BC5 No. 466). A sample (0.5 g) was dissolved in a mixture of hydrochloric, nitric and hydrofluoric acids (4:2:1) taken in a teflon container. The solution was evaporated almost to dryness, the residue was dissolved in 2 ml of conc. hydrochloric acid and the resulting solution was diluted to 50 ml with distilled water. This step of evaporation was necessary as excess of acid (~ 3 *M*) in stock solution would need large volumeof ammonia for neutralization during adjustment of *p*H and the presence of oxidising agent used, nitric acid, would hinder the formation of the anionic ascorbate complex of molybdenum. An aliquot (2 ml) of solution was extracted as per the procedure. The organic phase contained molybdenum, but chromium, iron, nickel and manganese were not extracted. Molybdenum(VI) from the organic phase was stripped with 1 *M* nitric acid while the unextracted metals were individually separated by the process of selective extraction followed by spectrophotometric determination[13] with chromogenic ligands (Table 3).

The method was also extended to the analysis of soil. A finely powdered sample (5.0 g) of soil was digested and brought into solution[14] (10 ml). Molybdenum(VI) was first extracted and stripped as usual. Iron, chromium, nickel and manganese were extracted and determined later by selective extraction and spectrophotometry (Table 3).

The proposed method is simple, rapid and selective. It permits separation of molybdenum from iron, chromium and lead which are associated with it in minerals or from titanium, zirconium, thorium and uranium, generally found in fission products.

The total time required for extraction and determination is less than one hour. The method is reproducible with the relative standard deviation of ± 1.2%.

Acknowledgement

One of us (MAK) is thankful to the CSIR, New Delhi for the award of a senior research fellowship.

References

1 Kamiya S, Tokutami M & Matsuda Y, *Bull chem Soc Japan*, 40 (1967) 407.
2 Vieux A S, Rutagenwa N & Noki V, *Inorg Chem*, 15 (1976) 22.
3 Ki Kuchi S & Hatsutori H, *Proc Symp Sol Ext*, Hamamatsu, Japan, (1982) 113; *Chem Abstr*, 99 (1982) 182413.
4 Mironova E A, *Zh neorg Khim*, 33 (1988) 172.
5 Khosla M M & Rao S P, *Anal Chim Acta*, 57 (1971) 323.
6 Yatirajam V & Ram J, *Anal Chim Acta*, 59 (1972) 381.
7 Kim C H, Alexander P W & Symthe L E, *Talanta*, 23 (1976) 229.
8 Takabe K & Minami S, *Chem Soc Japan*, 7 (1983) 51.
9 Rao R R & Khopkar S M, *Analyst*, 108 (1983) 316.
10 Vogel A I, *A text book of quantitative inorganic analysis*, (Longmans Green, London), 1968, 509.
11 Karve M A & Khopkar S M, *Bull chem Soc Jpn*, 64 (1961) 655.
12 Karve M A & Khopkar S M, *Anal Sci*, 8 (1992).
13 Snell F D, *Photometric and fluorometric methods of analysis*, (John Wiley and Sons, New York), 1978, Parts I and II.
14 Kim C H, Owens C M & Smythe L E, *Talanta*, 21 (1974) 445.

Indian Journal of chemistry
Vol. 31A. April 1992, pp. 270-272

Notes

Effect of processing parameters on Bi-Sr-Ca-Cu-O system

D Venkataraman, N S Raman & B Viswanathan*
Department of Chemistry, Indian Institute of Technology, Madras 600 036, India
and
R Pragasam & V R K Murthy
Department of Physics, Indian Institute of Technology, Madras 600 036, India

Received 25 October 1991; revised and accepted 24 December 1991

The effect of calcium content on the formation of the superconducting phases in the Bi-Sr-Ca-Cu-O systems has been examined. The influence of sintering temperature and the duration of sintering time has been studied.

There are atleast two prominent phases[1] in the Bi-Sr-Ca-Cu-O system. These are having compositions $Bi_2Sr_2Ca_1Cu_2O_y$ (2212) and $Bi_2Sr_2Ca_2Cu_3O_y$ (2223), with transition temperatures (T_c) at 80K and 110K respectively.

One of the major problems associated with this system is that it always appears as a multiphasic compound. Though it is somewhat easier to prepare single phase of 2212 compound, the preparation of the single phase of 2223 is still a difficult proposition.

In this note, the effect of the variation of calcium content, sintering time and temperature on the formation of 2223 phase has been reported.

Experimental

The samples were prepared from appropriate compositions of AR grade Bi_2O_3, CuO, $CaCO_3$ and $SrCO_3$ powders. The thoroughly mixed powders were heated at 1093 K for about 20h, then reground and pelletized with disks of 12 mm diameter and 2 mm thickness at a pressure of 5.86×10^6 Pascals, the pellets thus obtained were sintered at various temperatures in air for various lengths of time. The samples were removed at specified intervals of time for X-ray analysis and transition temperature measurements.

The X-ray diffractogram of the various oxide samples were obtained with a Philips diffractometer (Philips Generator, Holland, Model PW 1410 provided with an on-line recorder and a dot-matrix printer, teletype, USA), with Ni filtered CuK_α radiation. The lattice parameters were computed by least square fitting of the higher angle lines.

Pressure contact four probe dc electrical resistivity (ρ) measurements were carried out using an automatic measurement setup with a nanovoltmeter (Keithley, USA, Model 181)[2]. The valence states of copper in the superconducting oxides have been identified by cyclic voltammetry and oxygen evolution method[3]. In the cyclic voltammetry, the peak due to the reduction of Cu^{3+} was monitored ($E^0_{Cu^{3+}/Cu^{2+}} = -150$ mV versus Ag/Ag^+) in formamide medium. A known amount of the sample was taken and introduced into a graduated burette containing 10% HNO_3 and the volume of oxygen evolved was recorded.

Results and discussion

The starting composition for the preparation of the Bi-based high T_c oxides was taken to be $Bi_1Sr_1Ca_{1+x}Cu_2O_y$ ($x = 0$, 0.25, 0.50, 0.75, 1.00). The 1112 composition was taken, as it had yielded higher content of superconducting fraction when Maeda *et al.*[1] synthesized the first bismuth based superconductor. The sintering temperature for all the samples was fixed at 1148K since the sample melted at 1153K. It was observed that as the calcium content was increased the sintering of the samples occurred.

After 20h of sintering, the X-ray analysis showed the formation of 2212, $CaCuO_2$, CuO and 2201 phases. The 2223 phase was present in small amounts. It was found that the content of the 2212 phase was maximum when the starting composition was in the molar ratio 1.0:1.0:1.5:2.0 (Bi:Sr:Ca:Cu) (Fig. 1). The amount of $CaCuO_2$ increased with increasing content of calcium (Fig. 1) which was in accordance with the observations of Tsuchiya *et al.*[4]. There was no marked change in the amount of 2201 phase with increasing calcium content (except for $x = 0.25$, where 2201 phase was found in trace amounts) (Fig. 1). It was also observed that with increasing content of calcium, melting occurred which could be due to calcium oxide acting as a flux.

The content of the 2223 phase increased with increasing calcium content, though marginally (Fig. 1). The sample with starting composition 1.0:1.0:1.25:2.0 was rich in 2223 as there was negligible amounts of 2201 phase in the sample, which was present in all other samples of the order of 20%. The forma-

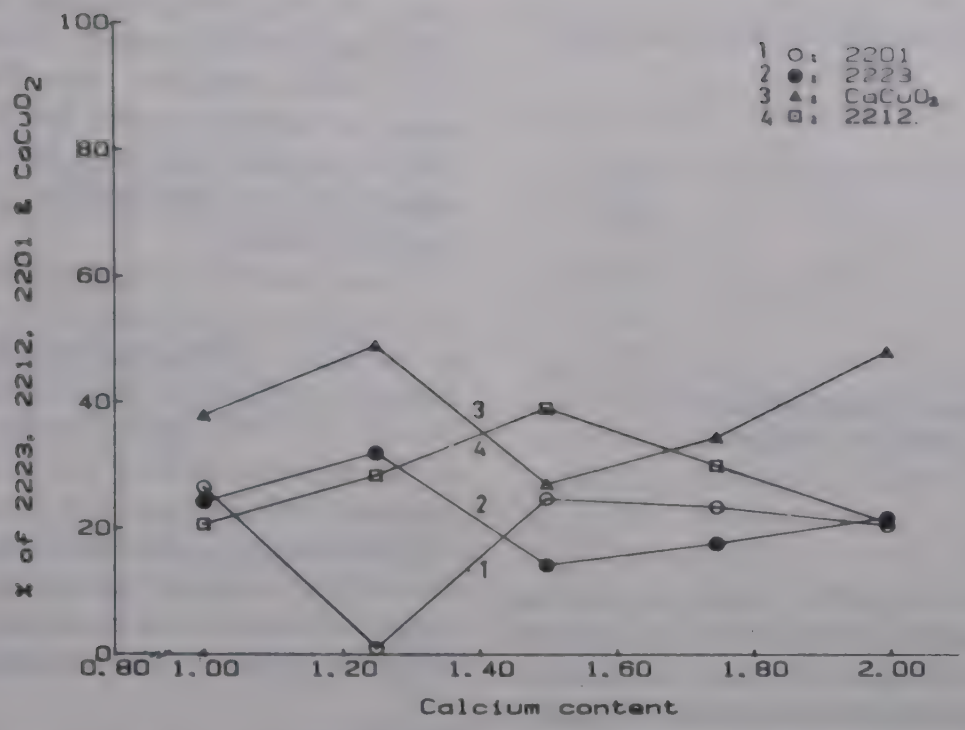

Fig. 1—Variation of percentage of 2223, 2212, 2201 and $CaCuO_2$ as a function of calcium content.

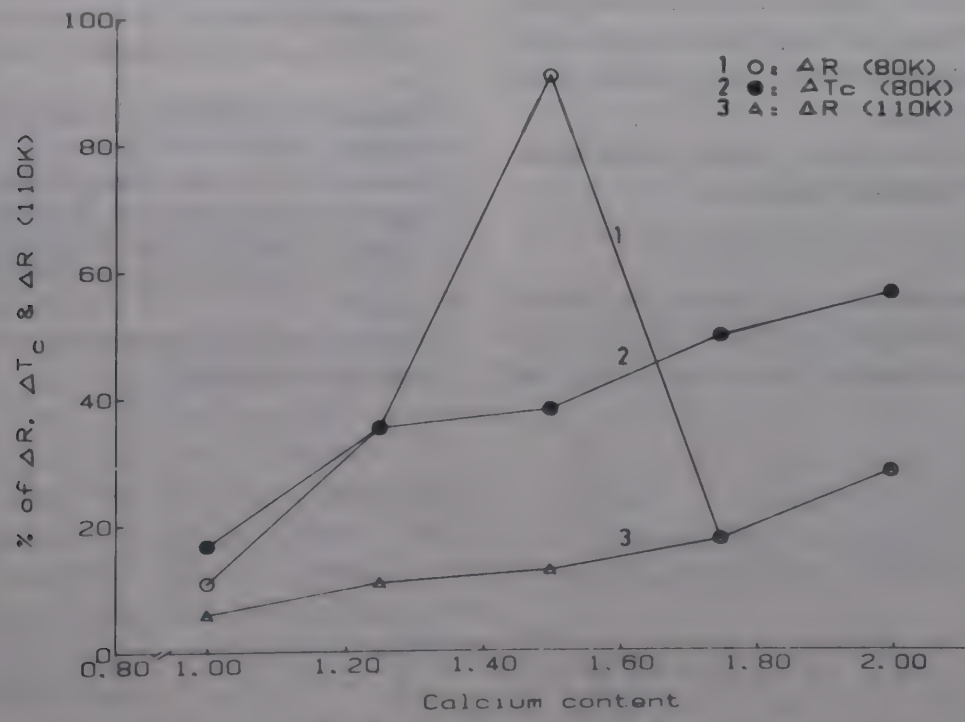

Fig. 2—Variation of percentage of ΔR (80K), T_c (80K) and ΔR (110K) as a function of calcium content in the starting material.

tion of the 2223 phase without the 2201 phase indicates that there was no disproportionation of the 2212 phase to give rise to 2223 phase. The superconducting transition temperature (T_c) measurements indicated that there was a large drop in the resistance around 80K when $x = 0.5$, this sample was rich in 2212 phase (Fig. 2).

On increasing the calcium content, it was found that the T_c (T_c^{onset}-T_c^{zero}) increased, pointing to the fact that the sample had become increasingly multiphasic (Fig. 2). Sharp drop in resistance was observed in all the samples around 110K and 80K. The resistance drop (ΔR) around 110K increased with increase in the calcium content (Fig. 2). However, in certain samples a drop was observed around 180K. Zero resistance was not attained in these samples as they were always multiphasic. The resistance drop at 180K was reproducible only for some compositions measured later, but not always.

The resistance drop around 110K became more predominant with increasing calcium content due to increase in the proportion of the 2223 phase.

The content of the 2223 phase in the sample initially decreased and then increased with sintering

Table 1—Variation of 2223 and 2212 phases with $CaCuO_2$ content

Molar ratio of $CaCuO_2$	% of 2223 phase*	% of 2212 phase†
0.66	13.5	38.9
0.72	17.1	29.7
0.78	23.7	24.0
0.80	21.3	20.5
0.85	31.7	19.2

*as deduced from the intensity of the 0012 line.
†as deduced from the intensity of the 105 line.

time. The increase in the 2223 phase with increase in sintering time can be accounted for by the fact that the rate of the formation of the 2223 phase is rather slow. The initial decrease in the percentage of the 2223 phase could be due to increased formation of 2212 or $CaCuO_2$ phases.

Huang *et al.*[5] reported that sintering the sample at 1173K for about 5 min and then sintering the sample at lower temperatures led to an increase in the content of the 2223 phase.

The formation of the 2212 phase could be accounted for by the following reaction:

$$Bi_2Sr_2CuO_6 + CaCuO_2 \rightarrow Bi_2Sr_2CaCu_2O_8$$

The maximum amount of 2212 phase is formed when the molar ratio of $CaCuO_2$ is 0.5 (ref. 6). The evidence for this mechanism comes from the fact that with increasing sintering time the amount of 2201 and $CaCuO_2$ phases decreases while that of 2212 phase increases. Also the amount of 2212 phase is maximum when the starting composition was in the molar ratio of 1.0:1.0:1.5:2.0. The molar ratio of $CaCuO_2$ was found to be 0.66 closer the value of 0.5 (Table 1).

It was found that with increase in the calcium content, the peak current (cathodic peak at ≈ 0.150 mV) in the cyclic voltammogram also increased. This could be attributed to the increase in the concentration of Cu^{3+}. This indicates that there is a increase in the superconducting fraction which was in accordance with the results of X-ray analysis.

By the oxygen evolution method, it was observed that the Cu^{3+} concentration was about 2.64% in the sample taken. However individual contributions from the phases need to be worked out.

References

1 Maeda H, Tanaka Y, Fukutomi M & Asano T, *Japan J appl Phys*, 27 (1988) L209.
2 Pragasam R, Murthy V R K, Viswanathan B & Natarajan T S, *IEEE Trans on Instrumentation and Measurement*, 39 (1990) 792.
3 Raman N S, Ph.D. Thesis, Indian Institute of Technology, Madras, 1991.
4 Tsuchiya J, Endo H, Kijima N, Sumiyama A, Mizuno M & Oguri Y, *Japan J appl Phys*, 28 (1989) L1918.
5 Huang H S, Mao S N, Yao Z T, Liu M L, Ren X D, Zhang K S, Wu Z Y, Zhao X & Liu Y Z, *IEEE Trans Mag*, 25 (1989) 2017.
6 Pekker S, Sasavari J, Hutiray G Y & Mihaly L, *J less comm Metals*, 156 (1989) 277.

Indian Journal of chemistry
Vol. 31A, April 1992, pp. 273-275

Studies on electrochemical characterization of reinforced cholesterol membrane

A K Tiwari

Department of Chemistry, Gorakhpur University, Gorakhpur 273 001

Received 28 June 1991; revised and accepted 9 December 1991

A reinforced cholesterol membrane has been prepared by impregnation with the object of determination of its ion selective nature using membrane potential and conductance measurements. This membrane when tested using sodium chloride solutions exhibits anion selectivity which varies with concentration and *p*H as inferred from the estimation of its permselectivity and fixed charge density. For the estimation of fixed charge density, a mathematical expression has been derived.

In a previous publication we reported electrochemical characterization of a cellulose acetate supported cholesterol liquid membrane on the basis of membrane potential studies[1]. The present investigation deals with a reinforced cholesterol membrane formed by impregnation[2]. Variation of membrane potential with concentration and *p*H has been studied to derive ionic transport numbers using sodium chloride solutions. These studies show that the cholesterol membrane behaves as if it is endowed with anion selectivity within the range of investigation. Estimation of permselectivity and fixed charge density, and their variation with concentration and *p*H have also been studied. The dimensional characterization of the membrane was carried out by its conductance measurements[3].

Experimental

A solution of cholesterol of known composition was prepared in *n*-hexane. Cholesterol was procured from the Patel Chest Institute, New Delhi and used as such without any purification. A macroporous Whatman filter paper was used for cholesterol impregnation.

A piece of suitable size of this filter was attached to a glass tube having internal cross-sectional area 1.56 cm^2 using araldite cement. Cholesterol solution in *n*-hexane was placed on the Whatman paper and left undisturbed to undergo drying at about 35°C. Incorporation of cholesterol in the voids of the supporting paper produced the reinforced membrane which was used throughout the present investigations.

Membrane potential and conductance measurements

The experimental set-up and method of measurement of potential difference across the membrane were the same as reported earlier[1].

For the determination of membrane conductance, known potential differences in steps were applied in either direction, and the resulting currents were measured. Salt bridges positioned near the membrane faces were connected to saturated calomel electrodes for the application of potential difference; for current measurements, silver-silver chloride electrodes were used.

Results and discussion

Cholesterol as such does not possess any ionogenic character. The present investigation, however, shows that the reinforced cholesterol membranes is endowed with some selectivity. There are reports which indicate that cholesterol when used as a diaphragm exhibits electrokinetic activity[4]. Thus, cholesterol in contact with electrolyte solution seems to acquire electric charge perhaps as a result of ionic adsorption. The electrified nature of the cholesterol-solution interface in a dense membrane may impart it some ionic selectivity.

When a membrane separates aqueous electrolyte solutions of unequal concentrations, it may be shown using thermodynamic principles that the so called liquid junction potential[6] is given by,

$$[(\Delta\phi)_{I=0}]_I = (2t_- - 1)\frac{RT}{F}\ln\frac{a_2}{a_1} \qquad \ldots (1)$$

where a_2 and a_1 denote the activities of the sodium chloride solutions, and t_- denotes the transport

Table 1—Membrane potential data keeping $C_1 = 0.1$ *M* NaCl, activity coefficient $f_1 = 0.6948$

C_2 (mol dm^{-3})	f_2	$(\Delta\phi)_{I=0}$ (mV)	$[(\Delta\phi)_{I=0}]_I$ (mV)	$[(\Delta\phi)_{I=0}]_{max}$ (mV)
0.01	0.8912	41.0	12.18	53.5
0.02	0.8497	27.5	11.9	36.6
0.04	0.7943	12.0	4.6	20.3
0.06	0.7542	5.6	2.5	11.1
0.08	0.7220	3.0	1.1	4.8

Table 2—Membrane potential at different mean concentrations keeping ΔC constant

C_1 (mol dm^{-3})	C_2 (mol dm^{-3})	f_1	f_2	$(\Delta\phi)_{I=0}$ (mV)	$[(\Delta\phi)_{I=0}]_L$ (mV)	$[(\Delta\phi)_{I=0}]_{max}$ (mV)
0.06	0.02	0.7542	0.8497	18.0	8.51	25.2
0.08	0.04	0.7220	0.7943	9.3	3.34	18.1
0.10	0.06	0.6948	0.7542	4.9	2.39	10.5
0.12	0.08	0.6712	0.7220	3.5	1.86	8.7

Table 3—Transport numbers permselectivities and fixed charge densities at different mean concentration keeping ΔC constant

$\bar{C}$ (mol dm^{-3})	t_-	$\bar{t}_-$	P_s	$\phi\bar{X}$ (mol dm^{-3})
0.04	0.6058	0.8070	0.4624	0.0417
0.06	0.6057	0.7942	0.4305	0.0672
0.08	0.6056	0.7163	0.2436	0.0401
0.10	0.6055	0.6985	0.2030	0.0414

t_- values were taken from reference 6.

Table 4—Transport numbers, permselectivities and fixed charge densities at different pH, using $C_1 = 0.01$ mol dm^{-3}, $C_2 = 0.09$ mol dm^{-3}, and $f_1 = 0.8912$; $f_2 = 0.7089$

pH	$(\Delta\phi)_{I=0}$ (mV)	t_-	$\bar{t}_-$	P_s	$\phi\bar{X}$ (mol dm^{-3})
7.0	31.3	0.612	0.8105	0.4611	0.0519
6.0	24.9	0.612	0.7470	0.3055	0.0318
5.0	22.5	0.612	0.7232	0.2471	0.0255
4.0	19.5	0.612	0.6756	0.1380	0.0139

number of the anion. If on the other hand the membrane is idealy selective,

$$(\Delta\phi)_{I=0} = \frac{RT}{F} \ln \frac{a_2}{a_1} \quad \ldots (2)$$

Experimentally measured values of the membrane potential $(\Delta\phi)_{I=0}$ are compared with the values derived using Eqs (1) and (2) in Tables 1 and 2. Membrane potential data given in Table 1 were obtained keeping sodium chloride solution concentration on one side of the membrane fixed at 0.1 mol dm^{-3}. Ion selectivity of membrane may vary with concentration. In order to obviate this possibility, data presented in Table 2 were obtained keeping mean concentration constant. Mean activity coefficients needed for the purpose of computation of activities were obtained using ionic activity coefficients included in these Tables.

The experimentally determined membrane potentials are significantly different from the calculated values, and this clearly indicates that the cholesterol impregnated membrane is endowed with some selectivity. The potential on the dilute solution side is negative with respect to the concentrated solution side taken as positive. Furthermore, $(\Delta\phi)_{I=0}$ is always greater than $[(\Delta\phi)_{I=0}]_L$. This is possible only if the anion is accelerated, since $t_- > t_+$ in the case of sodium chloride. For a partially anion selective membrane, using TMS approach, the membrane potential in the present case may be expressed as[5,6],

$$(\Delta\phi)_{I=0} = (2\bar{t}_- - 1) \frac{RT}{F} \ln \frac{a_2}{a_1} \quad \ldots (3)$$

For the estimation of transport numbers in the membrane phase, it follows from Eqs (1) and (3) that

$$\bar{t}_- = \frac{(\Delta\phi)_{I=0}}{[(\Delta\phi)_{I=0}]_L} (1 - 2t_-) + 0.5 \quad \ldots (4)$$

The $\bar{t}_-$ values derived using Eq. (4) are presented in Table 3. An ion selective membrane is endowed with permselectivity[7-9], P_s, defined as

$$P_s = \frac{\bar{t}_- - t_-}{t_- - (2t_- - 1)\bar{t}_-} \quad \ldots (5)$$

Fixed charge density $\phi\bar{X}$ may be expressed in the following manner[10,11],

$$\phi\bar{X} = \frac{(t_+ \cdot \bar{t}_- - t_- \cdot \bar{t}_+) C_s}{\sqrt{(t_+ \cdot t_-)(\bar{t}_+ \cdot \bar{t}_-)}} \quad \ldots (6)$$

where C_s denotes mean concentration.

Permselectivity, P_s, is a measure of the extent to which counter-ion migration is facilitated by an ion selective membrane. It may be noted that the permselectivity decreases with increase in concentration although fixed charge density remains practically unchanged. Membrane potential data as well as derived parameters, i.e., transport numbers, permselectivity and fixed charge density under different experimental conditions are shown in Tables 3 and 4. Both permselectivity and fixed charge density rapidly decrease with lowering of pH.

Table 5—Membrane conductance at different mean concentrations keeping *p*H fixed at 7

Concentration (mol dm^{-3})	$(I/\Delta\phi) \times 10^5$ at $\Delta p = 0$ (ohm^{-1})	$k \times 10^5$ (ohm^{-1} cm^{-1})	A/l (cm)
0.04	3.7	6.61	0.55
0.06	7.0	7.24	0.96
0.08	10.0	7.80	1.28
0.10	—	9.09	—

An important membrane parameter relevant from the point of view of its electrochemical characterization is the so called membrane constant, A/l; A is the effective cross-sectional area of the membrane and l is the thickness. An estimation of A and l separately poses problems. A/l can, however, be easily estimated on the basis of conductance measurements and specific conductance k of the permeant. The membrane constant (Table 5) is seen to increase with increase in electrolyte concentration. This is the trend expected in the case of a membrane endowed with ion selectivity as observed earlier[3]. Thus, conductance behaviour of the reinforced cholesterol membrane is also consistent with its ion selective nature derived on the basis of membrane potential measurements.

Acknowledgement

The author is grateful to the Head, Department of Chemistry, for providing laboratory facilities and CSIR, New Delhi for financial assistance.

References

1 Singh K & Tiwari A K, *J memb Sci*, 34 (1987) 155.
2 Kesting R, *A structural perspective*, in *Synthetic polymeric membranes*, (Wiley-Interscience, New York) 1985, chapter 9.
3 Singh K & Tiwari A K, *J Colloid interface Sci*, 116 (1987) 42.
4 Srivastava R C & Jakhar R P S, *J phys Chem*, 85 (1981) 1957.
5 Lakshminarayanaiah N, *Membrane electrodes* (Academic Press, New York) 1976, 64.
6 Glasstone S, *An introduction to electrochemistry* (An East West Edition, New Delhi), 1974, 208.
7 Lakshminarayanaiah N, *J memb Biol*, 29 (1976) 243.
8 Lakshminarayanaiah N, *J memb Biol*, 21 (1975) 175.
9 Kobatke Y & Kamo N, *Prog polymer Sci, Japan*, 5 (1973) 257.
10 Fridrikhsberg D A, *A course in colloid chemistry* (Mir Publishers, Moscow), 1986.
11 Tasaka M, Aoki N, Kondo Y & Nagasawa M, *J phys Chem*, 79 (1975) 1307.

Indian Journal of chemistry
Vol. 31A, April 1992, pp. 276-278

Fluoridation of OH-apatite on interaction with sodium monofluoro phosphate

G C Maiti

Physical Research Wing, Projects & Development India Ltd.
Sindri 828 122, India

Received 8 July 1991; revised 15 October 1991;
rerevised and accepted 15 January 1992

OH-apatite when reacted with Na_2PO_3F in solid state transforms into a mixed apatite $Ca_5(OH)_{1-x}F_x(PO_4)_3$. The Ca-phosphate frame work of the apatite lattice remains unaffected during the fluoridation process. The evolved HF molecule on hydrolysis of Na_2PO_3F acts as fluoridating agent in the transformation of OH-apatite into F-apatite lattice.

The resistance of dental enamel which consists mainly of OH-apatite can be improved against caries lesion by surface fluoridation[1,2]. Several fluoridating agents have been considered for topical application[3-5]. Sodium monofluoro phosphate (Na_2PO_3F abbreviated MFP), has also been used as cariostic inhibitor[6,7].

In general, the formation of fluoro-apatite or mixed apatite is the desired goal of the fluoride enamel interaction. The nature of solid state interaction between $Ca_5(OH)(PO_4)_3$ and Na_2PO_3F during topical application is still disputed[8-10]. Obviously, the sluggishness of the fluoridation reaction at biologically relevant temperatures and the low depth penetration of the F^- into the dental enamel, which is virtually OH-apatite, represent serious obstacles to elucidating the nature of interaction. An alternative approach would be to speed up the reaction kinetically by using elevated or even rather high temperature and to bring it to near completion.

In the present communication we report the results of a study aimed at elucidating the nature of the fluoridation of OH-apatite by MFP using XRD and infrared (IR) absorption spectroscopy as main tools of investigation. IR spectroscopy is particularly suited because incipient fluoridation of the OH-apatite can readily be detected through $\nu O-H$ mode using the OH^- as a local probe which sensitively reacts to the presence of F^-. In OH-apatite structure, OH^- ions form one-dimensional chains parallel to the c-axis and they are replaceable by similar anionic species, specially by F^- ions[11,12].

Experimental

Apatite powder samples were prepared by solid state reaction between $Ca[HPO_4]\cdot 2H_2O$ and $Ca[CH_3COO]_2$ (Merck chemicals). The chemicals were thoroughly mixed as acetone slurries by mechanical stirring for 1 hr. The mixture was dried, peletised and heated in an open platinum crucible to 1000°C for 10 hr in a stream of decarbonated moist air ($P_{H_2O} = 4$ torr). The samples were cooled slowly, crushed and powdered in an agate ball mill. The heating and homogenisation cycles were repeated three times in moist air in order to complete the reaction. X-ray diffraction pattern indicated that the product consisted of a well-crystallized single phase of OH-apatite. The purity of the samples was also evident from the IR spectroscopic measurements.

Polycrystalline hydroxyapatite, $Ca_5OH(PO_4)_3$ powder was thoroughly mixed dry with 5 wt %, 10 wt % and 25 wt % Na_2PO_3F, corresponding to 15; 30 and 75 mol % respectively, in an agate ball mill for 1 hr. The samples were designated as A, B and C respectively. The Na_2PO_3F sample was supplied by M/s Deiersdorf Ag, Hamburg. The mechanical mixtures were heated separately in an open Pt crucible for 50 hr at different temperatures. After each heat treatment, the samples were analyzed by IR spectroscopic and X-ray diffraction methods.

Infrared and X-ray analysis

The IR spectra were recorded on a Perkin-Elmer 225 spectrophotometer for which samples (2 mg) were admixed with KBr (300 mg) in an agate mortar and pelletized in an evacuated 13 mm ϕ die. The apatite samples were dried for at least 10 hr at 110°C prior to preparing the KBr pellets. The crystal phase compositions of the samples and the reaction products were determined by taking X-ray diffraction photographs using a double-radius (229-2 mm) Guinier Camera and monochromatic $CuK_{\alpha 1}$ radiation and Ag as an internal standard. θ values were corrected by comparision with Ag diffraction lines. The unit cell parameters were determined by least squares refinement from corrected θ values using a suitable computer program.

Results and discussion

There are three spectral regions of interest: (i) the region of $O-H$ stretching vibration at 3500-3600 cm^{-1}, (ii) the region of $P-O$ and $P-F$ stretching vibrations at 900-1300 cm^{-1}, (iii) the region of $P-O$ and $P-F$ deformation modes at 400-800 cm^{-1} which also comprises the $O-H$ deformation vibration at 631 cm^{-1}. There is no IR-spectroscopic

indication of a solid state reaction at room temperature upon milling together of OH-apatite and MFP comparable to the reaction between OH-apatite and NH_4F, as spectral bands remain nearly unaffected upto 150°C (ref. 13). However, if the intimate mechanical mixture of OH-apatite and MFP is heated in dry air for an extended period of time, typically 50 hr at above 200°C, characteristic changes occur in the IR spectra.

Fig. 1 depicts the changes in the region of the O−H stretching vibration of sample B containing 10 wt %, corresponding to 30 mol % MFP. After heating to 250°C a small but distinct band appears at 3540 cm^{-1} which suggests incorporation of F^- ion in OH^- chain of apatite lattice along c-axis[12]. Upon further heating, this band increases in intensity while the sharp 3573 cm^{-1} band, indicative of pure OH-apatite, decreases. Eventually, at 800°C, the band predominates at about 3535 cm^{-1} with a small remainder of the 3573 cm^{-1} band. This is the typical IR spectrum of a partially fluorinated OH-apatite $Ca_{10}(OH_{1-x}F_x)_2(PO_4)_6$ with x-0.5[11,14,15]. Thus, the degree of fluoridation attained at 800°C, as detected by IR spectroscopy, seems to be quite high.

Fig. 2 shows the IR spectrum of sample B in the region of the P−O, P−F stretching and P−O, O−H deformation vibrations. The most instructive region lies between 600 and 800 cm^{-1}, because it is the range of O−H deformation mode of pure OH-apatite at 631 cm^{-1} which is clearly separated from the ν_4 modes of the PO_4 tetrahedra at 601 and 575 cm^{-1}. The OH deformation band decreases in intensity with increase in F^- ions substitution; at the same time, a new band at 745 cm^{-1} appears in infrared spectra[11,12]. Fig. 2 shows that the intensity of the IR band at 631 cm^{-1} is diminished markedly at 500°C, and it almost disappears at 800°C. A new band at 745 cm^{-1} becomes distinct above 500°C. The IR spectral change can be assigned to the partial fluoridation of OH-apatite lattice by the substitution of F^- ions in the OH-anionic chain along the c-axis. Unfortunately, the three medium strong bands of Na_2PO_3F at 715, 730 and 755 cm^{-1} (Fig. 2) fall in the same spectral region. However, as seen from Fig. 2 these bands rapidly disappear upon heating, which marks the breakdown of Na_2PO_3F molecules. Similar spectral changes have also been noticed in the case of sample C, where the original O−H deformation band at 631 cm^{-1} disappears completely at 600°C (Fig. 2). The results can be explained in terms of nearly complete fluoridation of OH-apatite lattice. The band at 745 cm^{-1} has been assigned to the presence of a few residual OH^- ions still present in the midst of F^- ions in the anion chain of apatite lattice, which are very difficult to replace further due to their strong hydrogen bonding with neighbouring F^- ions[11,12].

Further noteworthy features of Fig. 2 are the small bands or shoulders at 528 and 895 cm^{-1} which appear in the spectra of the samples heated between 250° and 600°C. They may be assigned to the ν_4 mode of a $(HPO_4)^{2-}$, thereby suggesting the

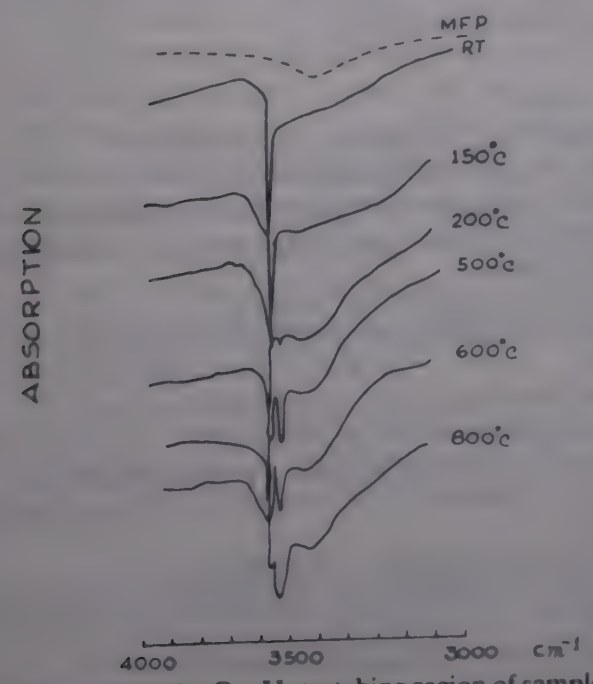

Fig. 1—IR spectra in the O−H stretching region of sample B (10 wt %) and MFP, heated to different temperatures.

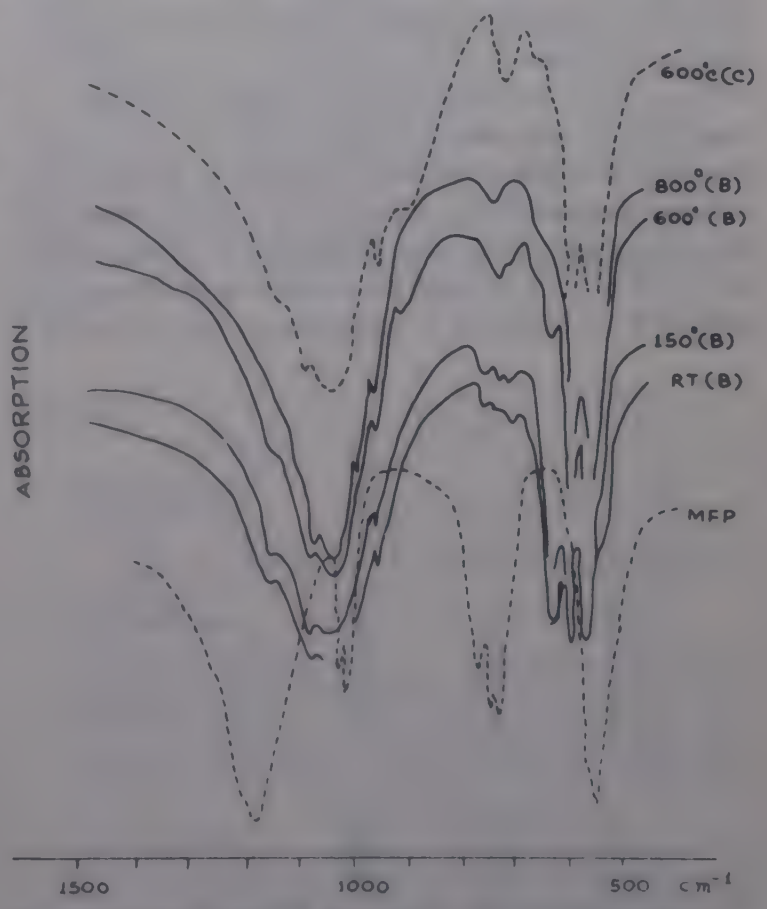

Fig. 2—Infrared spectra in the region of (P−O, P−F) stretching and OH deformation modes at different temperatures for sample B, sample C and MFP.

formation of an acid phosphate as an intermediate reaction product. In order to test this point, pure Na_2PO_3F was heated in moist air. Above 250°C, hydrolysis indeed occurred which was confirmed by XRD analysis. This is also confirmed by Fig. 2 showing the IR spectra of sample C containing 75 mol % of MFP. The formation of the acid phosphate is obviously enhanced compared to that in sample B. It also demonstrates that at 600°C no unreacted OH-apatite remains in the case of sample C.

The IR spectral changes can be explained, at least at the elevated temperatures used in this study, in terms of the formation of an acid phosphate as an intermediate during the reaction of MFP with OH-apatite. The hydrolysis of Na_2PO_3F under ambient condition via the interaction of adsorbed water molcules causes the evolution of MF molecules. The fluoridation of OH-apatite can be related to the interaction of evolved HF molecules.

$$Na_2PO_3F + H_2O \rightarrow Na_2HPO_4H_2O + HF$$

$$Ca_5(PO_4)_3OH + xHF \rightarrow Ca(PO_4)_3OH_{1-x}F_x + xH_2O$$

The evolved HF is reactive enough to cause replacement of OH^- ion by F^- ions in the anionic chain. Consequently, a mixed apatite lattice is built up. XRD results also indicate the formation of Na_2HPO_4 at the intermediate stage of heating of the mechanical mixture (Fig. 3). However, at and above 600°C, XRD patterns indicate that Na_2HPO_4 is transformed into more stable $Na_4P_2O_7$. However, the main residual product in the case of sample B is a mixed apatite (F, O−H apatite) and it is nearly a pure F-apatite in the case of sample C. The formation of mixed apatite and fluoroapatite in the case of sample B and sample C respectively has been confirmed by the measured lattice parameter values. The lattice parameter values in the case of the sample B are: $a_0 = 9.391$ Å (4); $c_0 = 6.878$ Å (3) whereas in the case of sample C $a_0 = 9.375$ Å (3); $c_0 = 6.876$ Å (2). The pure fluoroapatite lattice has lattice parameter values $a_0 = 9.368$ Å, $c_0 = 6.879$ Å, which are nearly similar to the measured values for the sample C. However, the fluoridation remains incomplete in the case of sample B, which is still lower in the case of sample A as the amount of Na_2PO_3F is insufficient. The results show that fluoridation of OH-apatite in bulk can occur only above 500°C. But as the hydrolysis of Na_2PO_3F is the first step in this solid state reaction liberating HF, the surface level fluoridation even at lower temperature may take place with the reactive HF molecules.

Another point worth mentioning is that the rigid framework of the apatite structure appears to be left unperturbed by the fluoridation reaction. This is in sharp contrast to the fluoridation reaction occurring between OH-apatite and NH_4F reported in our earlier communication[13] where Ca^{2+} ions are removed from the structure to form a CaF_2 overlayer.

According to XRD and infrared spectroscopic evidences, the interaction between Na_2PO_3F and $Ca_5(OH)(PO_4)_3$ does not occur favourably below 200°C as Na_2PO_3F is comparatively stable compared to other fluoridating agents. The direct substitution of PO_3F^{2-} into OH-apatite lattice in the place of HPO_4^{2-} seems to be unfavourable, as crystalline OH-apatite does not contain any noticeable amount of HPO_4^{2-} ions it its lattice. So the fluoridating can occur only via the hydrolysis of Na_2PO_3F, which seems to occur readily only above 200°C. Bulk fluoridation has been noticed above 500°C in the presence of excess Na_2PO_3F.

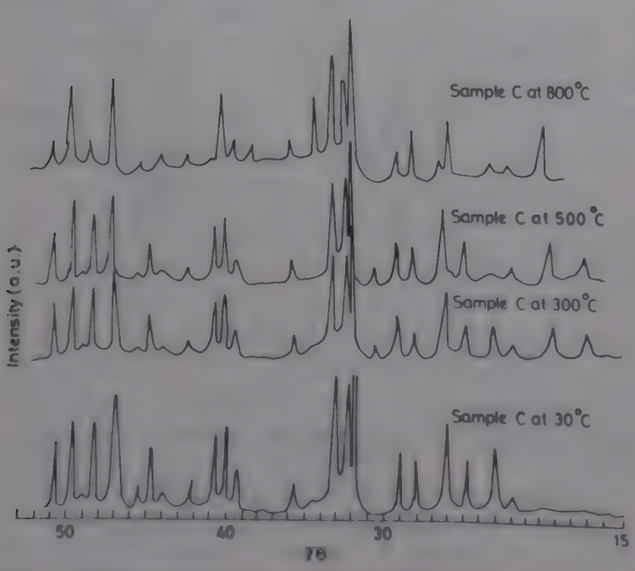

Fig. 3—XRD patterns of sample C at different temperatures.

References

1 Cheyne V D, *J Am dent Ass*, 29 (1942) 804.
2 Gron P, *Caries Res*, 11 (suppl 1) (1977) 172.
3 Wefel J S & Harless J D, *J dent Res*, 60 (1981) 1842.
4 Regolai B, Schait A & Mohlemann H R, *J dent Res*, 50 (1971) 764.
5 Wei S H Y, *J dent Res*, 43 (1974) 57.
6 Hawes R R, Sannes S & Brudevold F, *J dent Res*, 33 (1954) 661.
7 Finn S B & Jamson H C, *J dent Child*, 30 (1963) 17.
8 Eanes E D, *Caries Res*, 10 (1976) 59.
9 Wefel J S & Harless J D, *J dent Res*, 60 (1981) 1842.
10 Gron P, Brudevold F & Aasenden R, *Caries Res*, (1971) 502.
11 Fowler B O, *Inorg Chem*, 13 (1974) 194.
12 Freund F & Knobel R M, *J chem Soc (Dalton Trans)*, (1977) 1136.
13 Maiti G, *Indian J Chem*, 29A (1990) 402.
14 Fround F, *Inorg Nucl Chem Lett*, 13 (1977) 57.
15 Maiti G C & Freund F, *J chem Soc Dalton Trans*, (1977) 1136.

Indian Journal of chemistry
Vol. 31A, April 1992, pp. 279-280

A new method of synthesis of arsenic trithiophenoxide

S C Chaudhry*, R K Mahajan, S S Bhatt & Neeraj Sharma
Department of Chemistry, Himachal Pradesh University
Summer Hill, Shimla 171 005

Received 18 June 1991; revised 31 October 1991;
accepted 10 January 1992

Arsenic trithiophenoxide $As(C_6H_5S)_3$, has been synthesized by a novel method using arsenious oxide and thiophenol. The product has been characterized on the basis of IR and mass spectrometry.

As compared to the large work reported on synthesis and applications of alkyl and aryl esters of arsenic(III) and antimony(III)[1-7], only scattered references are available on the corresponding thioanalogues. Different routes have been used to synthesize trithiophenoxides of arsenic and antimony[8-12]. Although Brill and Campbell[10] have claimed that the method involving the use of sodium salt of aryl thiol and trichlorides of arsenic and antimony gives a purer product than even the ammonia method, the melting point of $As(C_6H_5S)_3$ isolated by this method significantly differs from that reported by Peach[13] and by Klement and Reuber[9]. This prompted us to isolate this compound by an alternative method using arsenious oxide and thiophenol.

Experimental

In the present method, a known amount of arsenious oxide (4.72 g) was allowed to react with thiophenol (20 ml) under reflux for 1h. The solution so obtained was filtered and the filtrate treated with pet ether and allowed to stand overnight when a pale yellow solid mass appeared. The solid was separated by filtration, washed repeatedly with pet ether and dried *in vacuo*. The compound was further recrystallised from solvent ether when fairly large colourless crystals were obtained. m.p. 95°C, yield 82%. The melting point coincided exactly with that reported by Klement and Reuber[9].

Analysis: [Found: As = 18.60; C = 53.78; H = 3.80; Calc. for $As(C_6H_5S)_3$, As = 18.64; H = 3.73; C = 53.74%].

Mass spectrum was taken on Varian MAT 711 mass spectrometer while infrared spectrum was scanned on Perkin Elmer IR spectrophotometer 337 and 621 in KBr.

Results and discussion

Arsenic trithiophenoxide can be considered to be formed by the following reaction:

$$As_2O_3 + 6C_6H_5SH \rightarrow 2As(SC_6H_5)_3 + 3H_2O$$

Arsenic trithiophenoxide is stable in air unlike other esters and thioesters of group Va elements which are known to be very sensitive to air. It can be stored without decomposition even for months. Like other thioanalogues, it is very bad smelling.

Although interpretation of IR spectra of thiophenolates for M—S bonds is normally difficult, the spectrum of the present compound in KBr on a Perkin Elmer spectrophotometer shows the principal bands at 492s, 400w and 372 vs cm^{-1} which have been assigned to ν(As—S) while those at 744 (vs) and 684 (vs) cm^{-1} have been assigned to ν(AsS—C) vibrations which are in agreement with the earlier reports[7].

In the mass spectra of $As(SC_6H_5)_3$, the molecular ion peak $[M]^+$ was observed at m/z 402. The other important fragments observed at m/z 293, 218, 184, 183 (base peak) and 109, can be explained in terms of the following Scheme 1.

The title compound does not seem to react with nitrogenous or oxygen bases. However, a preliminary investigation of this compound indicates that it reacts very easily with mercuric chloride dissolved in benzene resulting in the formation of a white solid. It also reacts with iodine dissolved in ethanol to form diphenyldisulphide as one of the products which has actually been isolated from the solution. The detailed investigations on these reactions are in progress.

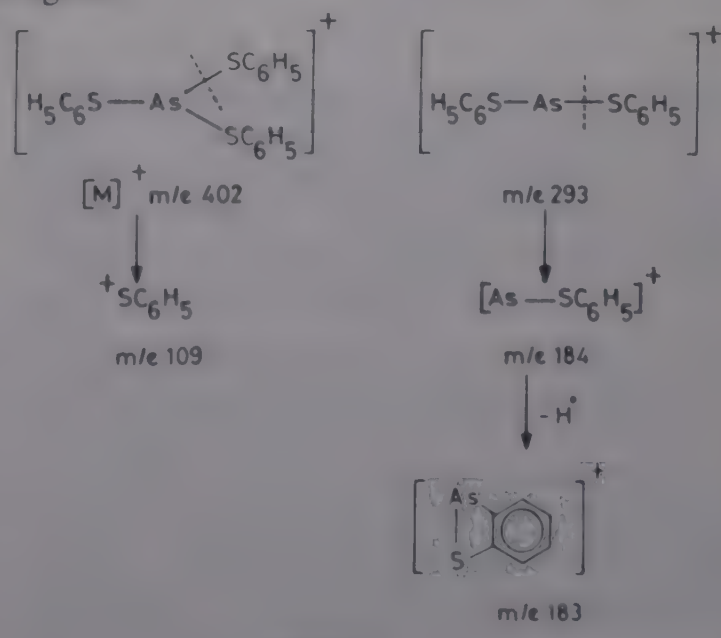

Scheme 1

Acknowledgement

The authors are thankful to Prof. (Dr) Dieter Kummer of Institut fur Anorganische Chemie der Universitat Karlsruhe for recording the mass spectrum of the sample. One of the authors (SSB) is also thankful to the UGC, New Delhi for the award of a junior research fellowship.

References

1 Herrmann W, *Methoden der organischen chemie*, Vol. 6, 4th Edn, edited by Houben Wey (G Thie e Verlag, Stuttgart) 1963, p 363.
2 Moedritzer K, *Inorg Synth*, 11 (1968) 181.
3 Mehrotra R C, Gupta V D & Chatterjee S, *Aust J Chem*, 21 (1968) 2929.
4 Anderson W P, Brill T B, Schoenberg A R & Stanger C W, *J organometal Chem*, 44 (1972) 161.
5 Brill T B, *J organometal Chem*, 40 (1972) 373.
6 Bertrand R D, Campton R D & Berkade J G, *J Am chem Soc*, 92 (1970) 2702
7 Dalton J, Paul I, Smith J G & Stone F G A, *J chem Soc*, (1968) 1195.
8 Vanderbroke A C, Hendricker D G, McCarley R E & Verkade J G, *Inorg Chem*, 7 (1968) 1825.
9 Klement K & Reuber R, *Ber*, 68 (1935) 1761.
10 Brill T B & Campbell N C, *Inorg Chem*, 12 (1973) 1884.
11 Howie R A, Grant D W & Wardell J L, *Inorg chim Acta*, 30 (1978) 233.
12 Vanion L & Mussgnug F, *Ber*, 50 (1917) 21.
13 Peach M E, *J inorg nucl Chem*, 41 (1979) 1390.

Indian Journal of chemistry
Vol. 31A, April 1992, pp. 281-284

Synthesis and characterization of N-alkyl-2-mercaptoacetamide complexes of antimony(III)

Ajay Kaushik, Yash Pal Singh & Audhesh K Rai*
Department of Chemistry, University of Rajasthan,
Jaipur 302 004
Received 22 March 1991; revised 30 August 1991;
accepted 19 December 1991

Reactions of antimony(III) isopropoxide with N-alkyl-2-mercaptoacetamides in 1:3 molar ratio in benzene yield complexes of the general formula $\{RNHC(O)CH_2S\}_3Sb$ where R = C_2H_5, *n*-C_3H_7, *i*-C_3H_7, *n*-C_4H_9, *sec*-C_4H_9 and CH = CH − CH_2. These complexes have been characterized by elemental analysis and spectral (IR, ^1H and ^{13}C NMR) studies. The complexes appear to exist in two isomeric forms in solution and the probable structures for both the isomers have been proposed.

N-Alkyl-2-mercaptoacetamides are known to behave as bidentate ligands and show linkage isomerism in their complexes[1-3]. These ligands also exist in two conformational isomeric forms.[4] The present note deals with the synthesis, characterization and structural elucidation of some antimony(III) complexes of N-alkyl-2-mercaptoacetamides.

Experimental

All the operations were carried out under strictly anhydrous conditions and chemicals used were of reagent grade. Antimony trichloride (Fluka) was distilled (80 /10 mm) before use.

Antimony isopropoxide was prepared by the literature method[5]. N-alkyl-2-mercaptoacetamides were synthesized by the condensation of thioglycolic acid and alkyl amines[6]. Sulphur, antimony and nitrogen were determined gravimetrically, iodometrically and by Kjeldahl's method, respectively[7].

The IR spectra were recorded on a Carl Zeiss Jena Specord M80 instrument in nujol mull and ^1H and ^{13}C NMR spectra on a JEOL FX-90Q spectrometer.

All the derivatives were synthesized by the reactions of $Sb(OPr^i)_3$ with the ligands in 1:3 molar ratio in benzene solution and preparation of only one representative complex is given below.

Preparation of $(n\text{-}C_3H_7NHC(O)CH_2S)_3Sb$

To a benzene solution of antimony isopropoxide (1.57g, 5.25 mmol), the ligand *n*-$C_3H_7NHC(O)CH_2SH$ (2.09g, 15.71 mmol) dissolved in benzene was added and the reaction mixture was refluxed under a fractionating column. The liberated isopropanol was fractionated off azeotropically in 4 hr. A white solid complex separated out from the solvent. After decanting off the supernatant liquid, the product was dried *in vacuo* at 60-70°C (yield 92%, m.p. 142°C). The azeotrope on analysis was found to have 0.98 g isopropanol (calculated 1.00 g for 3 mole). Analysis, [Found: Sb 23.31, N 7.93, S 18.19%; Calcd. for $Sb(n\text{-}C_3H_7NHC(O)CH_2S)_3$: Sb 23.51, N 8.12, S 18.56%].

Results and discussion

The ^1H NMR data of the antimony complexes are listed in Table 1.

The ^1H NMR spectra of ligands $RNHC(O)CH_2SH$ show a broad signal for − NH proton at ~ δ 6.8 ppm, a sharp singlet for − SH at ~ δ 3.5 ppm, alongwith other alkyl proton signals, at ambient temperature (20°C). At low temperature (0°C), the − NH proton signal splits into two which appear at ~ δ 7.6 and ~ δ 6.8 ppm, indicating the existence of the ligand in two isomeric forms (Ia and Ib) :

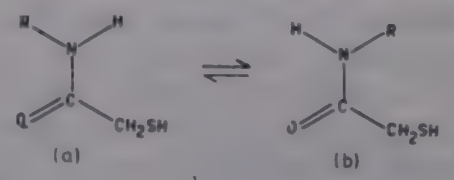

I

This has been further supported by the ^{13}C NMR spectra of the ligands, where two signals (at ~ δ 169.50 and 175.40 ppm) for carbonyl carbon (Table 2) have been observed. This difference of ~ 5-6 ppm in the position of carbonyl signals may be attributed to the steric and anisotropic effects of the alkyl group (R).

The appearance of two sets of signals for alkyl carbons further supports the existence of the ligand in two isomeric forms.

Reactions of antimony(III) isopropoxide with some N-alkyl-2-mercaptoacetamides have been carried out in 1:3 molar ratio in refluxing benzene solution.

$Sb(OPr^i)_3 + 3RNHC(O)CH_2SH \xrightarrow{\text{Benzene}} (RNHC(O)CH_2S)_3Sb + 3Pr^iOH \uparrow$

(where R = C_2H_5, *n*-C_3H_7, *i*-C_3H_7, *n*-C_4H_9, *sec*-C_4H_9 and $CH_2 = CH - CH_2-$)

Table 1—^{1}H NMR data of antimony(III) complexes of N-alkyl-2-mercaptoacetamides (δ ppm)

Sl.No.	Complex	$-CH_3$	$=CH_2$	$-CH=$	$-NH$	$-CH_2S-$
1.	$(CH_3CH_2NHC(O)CH_2S)_3Sb$	1.26t(0.82)	3.26q(2.99)	—	8.01br(7.65) 7.95br(6.80)	3.71s(3.22)
2.	$(CH_3\overset{a}{C}H_2\overset{b}{C}H_2NHC(O)CH_2S)_3Sb$	0.98t(0.67)	a 1.34-1.78m (1.07-1.43) b 2.81t(2.28)	—	8.00br(7.78) 7.86br(6.66)	3.71s(3.28)
3.	$(\overset{a}{C}H_3\text{-}CH(CH_3)\text{-}NHC(O)CH_2S)_3Sb$	a 1.11d(0.89) b 1.20d(1.16)	—	3.75-4.29st (3.35-3.89)	8.00br(7.64) 6.93br(6.92)	3.44s(3.31)
4.	$(\overset{a}{C}H_3\overset{b}{C}H_2\overset{c}{C}H_2CH_2NHC(O)CH_2S)_3Sb$	0.98t(0.77)	a,b 1.11-1.87m (1.11-1.75) c 2.97t(2.63)	—	8.44br(7.51) 8.40br(7.06)	3.75s(3.25)
5.	$(\overset{a}{C}H_3\overset{b}{C}H_2CH_3HNHC(O)CH_2S)_3Sb$	a 0.93t(0.89) b 1.20d(1.16)	1.51m(1.48)	3.93m(3.89)	8.10br(7.67) 6.92br(6.87)	3.48s(3.26)
6.	$(\overset{a}{C}H_2=\overset{b}{C}HCH_2NHC(O)CH_2S)_3Sb$	—	a 1.79d(1.74) b 3.17t(2.59)	5.00-6.03m (4.91-6.25)	8.71br(7.64) 8.44br(7.00)	3.62s(3.17)

Values in parentheses indicate values for the ligands

The resulting derivatives are found to be light yellow viscous liquids (solid, when R = *n*-C_3H_7), moisture-sensitive and having poor solubility in common organic solvents. The reactants, N-alkyl-2-mercaptoacetamides and $Sb(OPr^i)_3$ were highly soluble in benzene but the complexes were insoluble, hence the complexes were purified by repeated washings with benzene. Azeotrope (Pr^iOH), Sb, N and S estimations (Table 3) and spectral (^{1}H, ^{13}C and IR) studies confirm the purity of the complexes.

Infrared spectra

In the infrared spectra of the complexes, disappearance of a weak intensity band at 2500-2520 cm^{-1} ν(SH), observed in parent ligands and appearance of a new band in the region 360-380 cm^{-1} ν(Sb-S)[5,8], indicate the deprotonation of −SH proton and formation of Sb-S bond.

A shift of ~ 25 cm^{-1} in the position of ν-NH band (3076-3275 cm^{-1} in ligand) towards lower wave numbers indicates the coordination of amide nitrogen with antimony. This has been further supported by the appearance of a new band in the region 405-420 cm^{-1}, assigned to νSb−N[9].

A comparison of IR spectra of ligand with those of the corresponding complexes indicates a shift of ~ 40 cm^{-1} towards lower wave numbers, of various amide modes observed at ~ 1560, ~ 1270, ~ 700 and ~ 600 cm^{-1} in parent ligands[10]. The lower shift further supports the involvement of nitrogen atom in bond formation. No significant shift in ν C=O band (~ 1640 cm^{-1}) indicates the non-involvement of carbonyl oxygen in bonding.

^{1}H NMR spectra

The ^{1}H NMR spectra of the complexes have been recorded in DMSO-d_6 solution (Table 1). The disappearance of the signal for −SH proton, observed in the parent ligand at ~ δ 3.5 ppm, confirms the deprotonation of −SH group and the formation of Sb−S bond. A shift of ~ 0.2-1.2 ppm in the position of both −NH proton signals in the spectra of complexes as compared to their position in ligands further supports the involvement of nitrogen atom in bonding.

Table 2 — ^{13}C NMR data of antimony(III) complexes of N-alkyl-2-mercaptoacetamides (~ δppm)

Sl.No.	Complex	$-CH_3$	$=CH_2$	$-CH=$	$-C=O$	$-CH_2S-$
1.	$(CH_3CH_2NHC(O)CH_2S)_3Sb$	13.09,14.87 (12.40,12.68)	32.49,33.57 (27.80,29.50)	—	170.40,182.02 (169.50,175.10)	35.00(34.40) 35.15(34.68)
2.	$(CH_3\overset{a}{C}H_2\overset{b}{C}H_2NHC(O)CH_2S)_3Sb$	12.02,13.80 (10.40,10.89)	a 22.27,23.25 (20.80,21.21) b 32.49,34.30 (28.15,28.40)	—	171.34,182.02 (169.50,174.50)	45.80(40.26) 45.90(41.26)
3.	$(CH_3\underset{\underset{CH_3}{\vert}}{C}HNHC(O)CH_2S)_3Sb$	19.71,21.49 (18.80,20.38)	—	42.64,44.64 (43.00,43.45)	170.14,181.71 (169.80,174.20)	32.83(30.95) 33.07(31.80)
4.	$(CH_3\overset{a}{C}H_2\overset{b}{C}H_2\overset{c}{C}H_2NHC(O)CH_2S)_3$	13.20,13.98 (13.00,13.28)	a 19.45,20.07 (19.20,19.40) b 28.16,29.89 (27.90,28.10) c 31.59,33.64 (30.90,31.20)	—	170.40,181.13 (169.40,175.40)	43.30(39.00) 43.40(39.30)
5.	$(\overset{a}{C}H_3\overset{b}{C}H_2\underset{\underset{CH_3}{\vert}}{C}HNHC(O)CH_2S)_3Sb$	a 12.00,13.78 (7.50,7.80) b 17.35,19.13 (13.00,14.00)	31.30,33.97 (27.00,27.50)	42.20,43.98 (40.00,40.59)	170.30,181.10 (169.80,174.20)	47.50(46.00) 47.60(47.00)
6.	$(\overset{a}{CH_2}=\overset{b}{C}HCH_2NHC(O)CH_2S)_3Sb$	—	a 32.48,33.57 (27.72,28.50) b 138.09,138.98 (136.31,137.20)	121.50,122.98 (116.73,117.62)	174.00,181.10 (169.81,171.92)	44.80(40.83) 44.90(41.97)

Values in parentheses indicate values for the ligands

Table 3—Analytical data of antimony(III) complexes of N-alkyl-2-mercaptoacetamides

Sl. No.	Reaction of $Sb(OPr')_3$ with	Product Mol. form. (yield %)	Found (Calc), %				
			C	H	N	S	Sb
1.	$C_2H_5NHC(O)CH_2SH$	$(C_2H_5NHC(O)CH_2S)_3Sb$ 96	30.1 (30.2)	5.0 (5.0)	8.7 (8.8)	20.0 (20.1)	25.3 (25.5)
2.	n-$C_3H_7NHC(O)CH_2SH$	$(n$-$C_3H_7NHC(O)CH_2S)_3Sb$ 93	27.6 (27.8)	4.5 (4.6)	8.0 (8.1)	18.3 (18.5)	23.3 (23.5)
3.	i-$C_3H_7NHC(O)CH_2SH$	$(i$-$C_3H_7NHC(O)CH_2S)_3Sb$ 97	—	—	7.9 (8.1)	18.3 (18.5)	23.4 (23.5)
4.	n-$C_4H_9NHC(O)CH_2SH$	$(n$-$C_4H_9NHC(O)CH_2S)_3Sb$ 95	—	—	7.3 (7.5)	16.9 (17.1)	21.6 (21.7)
5.	sec-$C_4H_9NHC(O)CH_2SH$	$(sec$-$C_4H_9NHC(O)CH_2S)_3Sb$ 98	25.5 (25.7)	4.1 (4.2)	7.4 (7.5)	16.9 (17.1)	21.5 (21.7)
6.	$CH_2=CH-CH_2NHC(O)CH_2SH$	$(CH_2=CH-CH_2NHC(O)CH_2S)_3Sb$ 95	28.0 (28.1)	4.5 (4.6)	8.0 (8.2)	18.5 (18.7)	23.5 (23.7)

The appearance of two $-NH$ proton signals in antimony(III) complexes indicates that the isomeric forms of ligands interact individually and resulted in the formation of two isomeric metal complexes (Structure IIa and IIb).

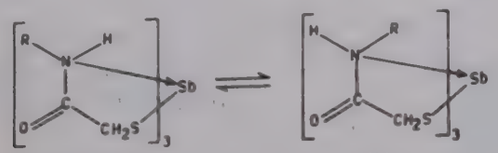

II

^{13}C NMR spectra

The existence of two isomeric forms for these complexes has been further confirmed by the appearance of two signals for carbonyl and alkyl carbon atoms in ^{13}C NMR spectra. A downfield shift in $-CH_2S$ carbon signal indicates the involvement of sulphur atom in complexation. The carbon atoms of alkyl group, attached to nitrogen atom, also experience a downfield shift indicating the involvement of nitrogen in the bonding (Table 2).

In view of the above, the central antimony atom may be proposed to acquire a capped octahedral geometry in which the stereochemically active lone pair of electrons present on the antimony atom occupies the capping position.

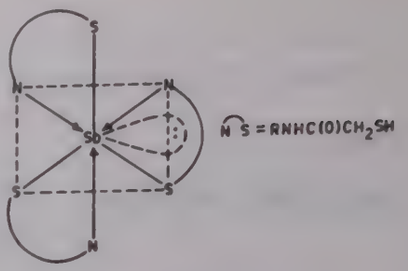

Acknowledgement

One of the authors (Ajay Kaushik) is thankful to the Govt. of Rajasthan and the UGC, New Delhi, for financial support under the Special Assistance Programme.

References

1 Mehrotra R C, Sharma H, Kumar A, Sharma V & Bachlas B P, *Indian J Chem*, 21A (1982) 1074.
2 Ray C & Das J, *Indian J Chem*, 24A (1985) 40.
3 Singh Y, Sharan R & Kapoor R N, *Indian J Chem*, 25A (1986).
4 Karra R, Singh Y P & Rai A K, *Main Group Metal Chemistry*, (1990) (In press).
5 Brill T B & Campbell N C, *Inorg Chem*, 12 (1973) 1884.
6 Mishra R N & Sircar S S, *J Indian chem Soc*, 32 (1955) 127.
7 Vogel A I, *A text book of quantitative inorganic analysis* (The ELBS & Longman's green), 1978.
8 Shindo M, Matsumura Y & Okawara R, *J organometal Chem*, 11 (1968) 299.
9 Chremos G N & Zingaro R A, *J organometal Chem*, 22 (1970) 647.
10 Bellamy L J, *The infrared spectra of complex molecules* (Chapman & Hall, London), 1975.

Indian Journal of chemistry
Vol. 31A, April 1992, pp. 285-287

Anion exchange selectivities of Zn(II), Cd(II), Hg(II) and Ba(II) in KI solutions

Mohd. Ibrahim Nasir* & Ashok Mahan
Department of Chemistry, University of Allahabad, Allahabad 211 002

Received 9 September 1991; revised and accepted 20 December 1991

Potassium iodide provides a suitable medium for the anion exchange separation of a number of binary, ternary and quaternary metal ion mixtures. The procedure is rapid, convenient and is based on the quantitative formation of the anionic species $[MI_4]^{2-}$, in which Cd(II) and Hg(II) separations have been achieved from other metal ions. The separations are clear cut and the method can be applied for the removal and isolation of mercury by the conventional anion exchanger instead of using a chelating type where the elution process is rather difficult.

A large number of anions have been used as complexing agents for the separation of metal ions on ion exchange resin[1]. Halides, (specially chloride) have been widely used for the ion exchange separations of metal ions[2], and some efforts have been made with solutions containing iodide[3,4]. However, no attempt has been made to investigate systematically the anion exchange behaviour of the elements in aqueous potassium iodide solution. Therefore, an investigation of the anion exchange characterization of a number of cations has been undertaken. Moreover, anion exchange appeared to be quite promising, as zinc, cadmium and mercury are reported[5-7] to form iodide complex of the type MI_4^{2-}. The present work relates to separation of Mg(II), Ca(II), Sr(II), Ba(II), Al(III), Mn(II), Co(II), Ni(II), Zn(II), Cd(II), Hg(II), ZrO(II), and Th(IV) with the anion exchanger, Amberlite IRA-400 at thirteen different concentrations (0.16-2.08 *M* KI).

Experimental

Stock solutions (0.05-0.10 *M*) of various metals were prepared by dissolving their chlorides, sulphates or nitrates in doubly distilled water. The samples were either B.D.H. (AR) or E. Merck or S. Merck (G.R.) reagents, while zirconium solution was prepared using $ZrOCl_2.H_2O$ (Johnson Matthey, London) and thorium solution from its nitrate (Harrington Brothers, London). A little acid (HCl) was added to check the hydrolysis. Subsequently, the solutions were standardized by the complexometric methods. An aqueous solution of 4.0 *M* KI (E. Merck, G.R.) was prepared and was standardized.

The anion exchange resin, Amberlite IRA-400 (8% cross-linking, 50-100 mesh, chloride-form, LOBA analytical grade) was pretreated, standardized and air-dried before use. The resin capacity and the moisture content were determined by the usual methods, and were found to be 1.14 meq/g and 22%, respectively.

Procedure

Determination of distribution coefficients (D) was carried out by the batch equilibration technique. Weighed amounts of the air-dried resin (1.000 g each) were added to the solution containing the metal ion and the iodide in 100 cm^3 glass-stoppered flasks, which were agitated for 48 hr. It was ascertained previously that this time was adequate for the attainment of equilibrium. The resin was filtered off and the metal content was estimated in an aliquot of the filtrate employing the EDTA titration. The distribution coefficients were calculated using the relation,

$$D = \frac{\text{meq of the metal ion per g of resin}}{\text{meq of the metal ion per cm}^3 \text{ of solution}}$$

All the experiments were performed at the ratio of total amount of cation to total resin capacity ≈ 0.4, using varying KI concentrations, and at room temperature ($30 \pm 2°C$). The total volume of aqueous phase was 25 cm^3. The result obtained are given in Table 1. Each set of experiments was carried out at least in duplicate and the average values were taken.

Accumulative exeprimental errors are estimated to be less than 2-5% of the results of D-values between 10 and 500, but are higher for very low D-values. The main sources of errors are inhomogeneity and the water content of the resin as the dry resin is a strong desiccant. Generally, D-values determined at relatively higher resin loadings, as in these experiments, provide more practical results than those determined at the tracer concentrations.

A slurry of 5 g air-dried resin (Cl^--form) in water was poured into a column (internal diameter 10 mm, bed height 9 cm). The column was saturated by the passage of 30 cm^3 of 0.60 *M* KI. Then the mixture of Zn, Cd and Hg in 0.60 *M* KI (15 cm^3) was poured into the column. The column was washed with 25 cm^3 of 0.60 *M* KI solution to remove the ad-

herent Zn completely as Zn exhibits almost no sorption by the resin at this concentration of KI. Cd and Hg were eluted successively by the eluants as reported in Table 2. After the elution of Cd, the resin column was washed with distilled water (40 cm^3) and then Hg was eluted. The eluants were collected in 10 cm^3 fractions, and the flow rate was 1.5 ± 0.2 cm^3/min. Quaternary mixture of Mn, Zn, Cd and Hg in 2.08 *M* KI (feed volume = 20 cm^3) was separated under similar conditions and sorbed metals were eluted as given in Table 2.

Results and discussion

The eluant, 1.5 *M* NH_4Cl-10% NH_3 (v/v), was found to be quite efficient and selective for the elution of Cd without disturbing Hg, leading to clearcut separation. Earlier workers[10] have used nitric acid to elute Cd, which could affect Hg present in the same solumn. A comparison of elution results provided in Table 2 shows that a lesser volume of eluant was consumed to desorb Cd in 0.60 *M* KI compared to that used in the case of 2.08 *M* KI. For Hg, 3*M* HNO_3 was used instead of 2*M* HNO_3. This deviation in the desorption with respect to KI concentration indicates that in dilute KI solutions Cd and Hg are weakly sorbed compared to their sorption in highly concentrated KI solutions. This behaviour has also been observed in the case of Zn sorption, which passed through the resin without being sorbed at 0.60 *M* KI, but was retained by the resin at 2.08 *M* KI. Moreover, at high concentrations of KI sorbable species probably occupy the upper part of the column due to strong tendency of exchange, while at lower [KI] the opposite happens and so lesser amount of the eluting agent is required. This is in agreement with the observations of Baggott and Willcocks[10].

While Zn, Cd, Hg and Ba ions showed sorption on the resin in the invetigated concentration range of iodide, no significant sorption was observed in the cases of Mg, Ca, Sr, Al, Mn, Co, Ni, Th and zirconyl cations (non-sorbable cations). At higher iodide concentrations, Zn, Cd and Hg showed strong tendency towards the resin. The loadings of these cations were selectively increased with the increase in KI concentration in the aqueous phase. This gradual enhancement is observed due to the formation of anionic iodato complexes[11], predominantly the species, $[MI_4]^{2-}$. The reported[5-7] comparative pattern of the orders of the metal halide stabilities for these anionic species is:

$[ZnCl_4]^{2-} > [ZnBr_4]^{2-} > [ZnI_4]^{2-}$,
$[CdI_4]^{2-} > [CdBr_4]^{2-} > [CdCl_4]^{2-}$,
$[HgI_4]^{2-} > [HgBr_4]^{2-} > [HgCl_4]^{2-}$ and
$[HgI_4]^{2-} > [CdI_4]^{2-} > [ZnCl_4]^{2-}$,

which clearly indicates and justifies the observed sorption trends in the iodide medium, i.e., DHg > DCd > DZn. In addition, because of the wider differences in the stability constants[7] of iodide

Table 1—Distribution coefficients (D) of Zn, Cd, Hg and Ba at varying [KI] (*M*) with Amberlite IRA-400

[KI](*M*)	Zn	Cd	Hg	Ba
0.16	NS	3.3	4.2	NS
0.32	NS	5.2	6.0	NS
0.48	NS	6.9	10.1	NS
0.64	0.6	10.5	14.6	0.4
0.80	2.0	12.6	21.0	1.2
0.96	3.3	15.7	27.8	2.0
1.12	4.5	19.2	35.5	2.9
1.28	5.9	22.6	45.7	3.9
1.44	7.9	28.1	57.1	3.2
1.60	11.5	35.0	81.9	2.5
1.76	20.1	49.2	110.0	1.1
1.92	34.8	65.1	174.9	0.1
2.08	51.1	101.2	486.0	NS

NS : Almost no sorption, i.e., D ≈ 0.

Table 2—Separation of Zn, Cd and Hg on Amberlite IRA-400 column

Mixture	Metal ion	Eluting agent	Vol. used (cm^3)	Introduced (mg)	Found (mg)	Error(%)
1	Zn	0.6 *M* KI	40	6.54	6.41	−1.98
	Cd	1.5 *M* NH_4Cl − 10% NH_3 (v/v)	80	11.24	11.46	+1.95
	Hg	2.0 *M* HNO_3	100	20.06	20.16	+0.49
2	Mn	2.08 *M* KI	30	5.15	5.15	0.0
	Zn	0.2 *M* NaCl	150	6.54	6.48	−0.90
	Cd	1.5 *M* NH_4Cl − 10% NH_3(v/v)	110	11.24	11.35	+0.97
	Hg	3.0 *M* HNO_3	110	20.06	20.26	+0.99

complexes of these cations in comparison to the stability constant of chloride and bromide complexes, the iodide is found to be a superior and an advantageous medium to obtain the successful separation of Zn, Cd, Hg and other metal ions. So at higher concentrations of iodide (1.90-2.10 *M*) a number of separations of Zn, Cd and Hg from other metal ions can be achieved. At lower KI concentrations (0.50-0.60 *M*), Zn also passes through resin bed unsorbed due to its weak tendency to form anionic iodide complexes[5,6], while Cd and Hg are retained by the resin and eluted by suitable eluants as shown in Table 2. In addition to the ternary and quaternary separations shown in Table 2, a number of binary separations can be achieved using selective KI concentrations.

At lower KI concentrations, the formation of the mononegatively charged species $[MI_3]^-$ appears less quantitative though Cyr[12] and Soe *et al.*[13] reported the existence of $[CdI_3]^-$ in aqueous and mixed methanol-KI solutions, respectively. Also, the iodide ion, being mononegatively charged as well as smaller in size compared to the complex species, exchanges in preference to $[MI_3]^-$ leading to low metal ion uptake by the resin. Marcus *et al.*[14] have reported that the complex species $[MI_3]^-$ is not preferred by the resin and this contributes towards the decrease in the metal ion sorption.

The relatively low metal ion sorption, at low KI concentrations is also due to the poor formation of divalent negatively charged species though the molar ratio of the metal ion to the iodide was 1:8 at lowest KI concentration taken, i.e., 0.16 *M*. Therefore, it appears that the iodide is not able to replace the coordinated water of the metal ion completely at these low KI concentrations to facilitate the greater formation of higher negatively charged complex species. The formation of neutral species MI_2 cannot be ruled out, but as HgI_2 is insoluble in water its existence is almost nil in the chosen range of KI concentrations.

In case of Ba(II), it seems that above 1.28 *M* KI, the iodide anion starts competing with or replacing the barium iodide complex species in the resin. Other non-sorbed metal ions have poor tendency to form the anionic species to be taken up by the resin as in case of Mn[15].

The study of the effect of *p*H on D-values is not possible as KI decomposes in acid. The observation that is general D-values decrease with the decrease of *p*H and vice-versa[16], is not applicable in the case of present iodide system.

References

1 Mahan A, Ghose A K & Dey A K, *Separtion Sci*, 6 (1971) 781.
2 Marinsky J A & Marcus Y, *Ion exchange and solvent extraction*, Vol. 5 (Marcel Dekker, New York), 1973.
3 Raptis S & Muller K, *Clin chim Acta*, 88 (1978) 393.
4 Kumagai T, *Bull chem Soc Jpn*, 57 (1984) 2738.
5 Stocks R H, *Trans Faraday Soc*, 44 (1948) 137.
6 Stock R H & Levien B J, *J Am chem Soc*, 68 (1946) 1852.
7 Cotton F A & Wilkinson G, *Advanced inorganic chemistry* (Wiley Eastern, New Delhi), 1984, 514, 1093.
8 Flaschka H A, *EDTA titrations* (Pergamon, New York) 1964.
9 Vogel A I, *A text book of quantitative inorganic analysis* (ELBS, London) 1985.
10 Baggot E R & Willcocks R G W, *Analyst*, 80 (1955) 53.
11 Nanjundiah C & Narayan R, *Trans SAEST*, 16 (1981) 233.
12 Cyr H M, *Comprehensive inorganic chemistry*, edited by M C Sneed & R C Brasted (Van Nostrand, New York) 1955.
13 Soe K N, Doe H & Kitagawa T, *Bull chem Soc Jpn*, 61 (1988) 2981.
14 Marcus Y & Eliezer I, *J inorg nucl Chem*, 25 (1963) 867.
15 Misumi S & Aihara M, *Talanta*, 19 (1972) 549.
16 Jensen B S & Jensen H, *Europ Appl Res Rept Nucl Sci Technol*, 6 (1985) 1493.

Indian Journal of chemistry
Vol. 31A, April 1992, pp. 288-290

Separation and recovery of vanadium from a chelating ion exchanger containing N-benzoylphenyl hydroxylamine as a functional group

Maya Pobi* & (Late) Jyotirmoy Das
Department of Chemistry, University of Burdwan, Burdwan 713 104

Received 21 October 1991; revised 4 December 1991; accepted 13 January 1992

A chelating resin containing N-benzoylphenylhydroxyl amine as the functional group has been synthesised and characterised by its water regain value, stability towards acids, alkali, heating and γ-radiation. The resin is highly selective for vanadium and it is also possible to carry out the quantitative recovery of vanadium from the resin without destruction of the resin.

Many chelating resins containing N-BPHA group have been utilised for the separation of a large number of cations[1-4]. Though they have been tested for their selectivity towards vanadium(V), none of them is known to have reported the complete recovery of vanadium. The high affinity of the resin containing N-substituted functional group for vanadium poses a problem, as the only method for complete recovery of vanadium is by the destruction of the resin. Several eluting agents were tested for vanadium, but in each case residual metal ion was found by wet ashing. In this note we describe the selective absorption of V(V) for the recovery of vanadium from a chelating resin containing N-BPHA group and also the separation of vanadium from uranium.

Experimental

The metal ions were detected and/or determined by a double beam UV-visible spectrophotometer (UV-190). Infrared measurements were carried out in KBr matrix. A gravity flow glass column with appropriate reservoir was used to hold the chelating resin. All the chemicals used were of AR grade. The buffer solutions sodium chloride-hydrochloric acid (*p*H 0.5-3.9) and sodium acetate-acetic acid (*p*H 4.0-6.0) were used. For buffer solutions above *p*H 6 disodium hydrogen phosphate and potassium dihydrogen phosphate were used.

A stock solution of vanadium was prepared from vanadyl sulphate in dilute acid medium. The metal content of the solution was determined by complexometric titration[5].

Synthesis of the resin

Styrene DVB polymer beads (80-100 mesh) (Thermax, Poona, India) with 8% cross linking (5 g) were swollen in chloroform for 30 min. The solvent was then removed and beads were nitrated with concentrated nitric acid-sulphuric acid mixture at 60°-70°C. The nitrated polymer was suspended in 1.5% solution of ammonium chloride (200 ml) with vigorous stirring and reduced by the batchwise addition of zinc powder (1.5 g total). The temperature was increased to 55-60°C and the mixture stirred for 1 h after the complete addition of zinc powder.

Finally, the phenylhydroxylamine resin beads were separated from zinc dust and the benzoyl group was introduced by the addition of benzoyl chloride in presence of pyridine[6].

Determination of capacity of resin

The exchange capacities of resin for different metal ions were studied both by batch and column operation methods.

In the batch technique, the metal ion was in excess of the chelate function. Dry resin (0.5 g) was suspended in a metal ion solution of known strength (0.1 *M*) at the required *p*H. The mixture was stirred magnetically for 24 h, filtered, and the resin was washed with the appropriate buffer solution. The metal ions sorbed were released from the resin with 1,2,3-phenyloxyamidine (1%) and their concentration was determined. Vanadium was determined by a spectrophotometric method[7].

For column studies, a 30×1 cm column of the N-BPHA containing resin was used. For the recovery of trace metals, the samples were passed through the resin column at a flow rate 0.5-1.0 ml min^{-1}. The complexed metals were stripped from the column with 1,2,3-phenyloxyamidine (1%) solution.

The sorption pattern of the different metal ions as a function of *p*H is shown in Fig. 1.

For the separation of vanadium(V) from a mixture containing different allied cations, the resin column was preequilibrated at *p*H 6.8. The *p*H of the mixture containing vanadium(V) and one or more of the ions like Ti(IV), Hf(IV), Fe(III), Co(II) and Cu(II) was adjusted to *p*H 6.8 and it was passed through the column. Vanadium(V) was eluted with 1,2,3-

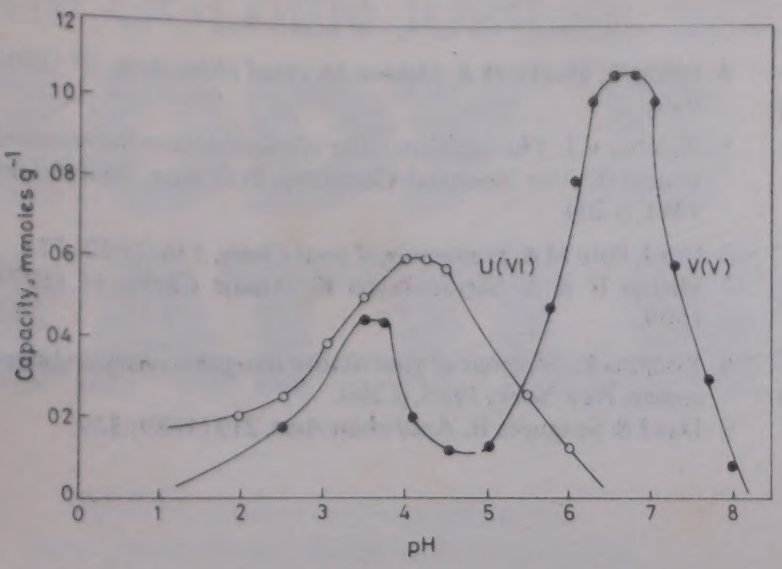

Fig. 1 – Sorption capacity of U(VI)and V(V) at different *p*H values

phenyloxyamidine (1%) solution and determined; over 99% of vanadium was recovered from several synthetic mixtures.

Vanadium(V) could easily be separated from uranium(VI) using a similar procedure. The percentage recovery of vanadium in presence of uranium was ~99%.

Samples containing vanadium (~0.2 g) were treated with HCl and HNO_3 and evaporated to white fumes with H_2SO_4. The residue was extracted with 25% ammonium acetate-ammonium hydroxide buffer and ignited. The solution was prepared by a standard procedure[8] and vanadium was separated and compared with the standard value. The results are presented in Table 1.

An aliquot of each of the solutions was fed into the resin column maintaining *p*H at 6.8 and the sorbed metal ions were then eluted with different eluting agents and percentage recovery was found as follows: 2 *M* H_2SO_4 (71.2), 4 *M* H_2SO_4 (69.0), 5 *M* HCl (73.2), 4 *M* $HClO_4$ (2.5), 0.5 *M* NaOH (14.0), 1,2,3-phenyloxyamidine (1%) (100.0).

Results and discussion

The resin was characterised by determining its water regaining value following a standard procedure[9]. The value was found to be 0.56 g g^{-1}. Elemental analysis of the resin gave 57.6% C, 4.5% H and 10.65% N. The incorporation of the N-BPHA group in the resin was confirmed from its infrared spectrum in KBr matrix. The bands at 3300 cm^{-1} and 2500 cm^{-1} were assigned to the N–OH and that at 1640 cm^{-1} to C=O stretching. Another band characteristic of hydroxamic acid near 1550 cm^{-1} was also present. The resin was stable in acids e.g., upto 4 *M* sulphuric acid, 6 *M* hydrochloric acid and 4 *M* perchloric acid. However, it could tolerate only upto 0.5 *M* sodium hydroxide. The resin decomposed at higher *p*H, as was indicated by the appearance of blue colour. Common organic solvents such as benzene, chloroform, diethyl ether and carbon tetrachloride did not affect the resin but dimethylformamide decomposed it. The density of the resin particles is 0.0051 gm cm^{-3}.

Table 1—Determination of vanadium in vanadinite and vanadium steel

Sample taken (mg)	Vanadium found (mg)	Found (Calc) (%)
	128.5	31.7 (32.0)
Vanadinite (404)	128.7	
	128.5	
	92.34	28.5 (29.0)
Vanadium steel (324)	92.40	
	92.40	

*Average of three determinations

Thermogravimetric analysis showed that the resin was stable upto 110°C. It could also tolerate γ-radiation doses upto 12.93 *M* rad for 72 h. The stability in all the cases was confirmed by determination of its capacity for metal ions.

The capacity of metal absorption (vanadium) on resin column was slightly lower than that in batch operation. The resin exhibits high selectivity towards vanadium as shownin Fig. 1. Absorption of vanadium(V) starts from *p*H 1.0 followed by a peak at *p*H 3 and then it decreases. But at *p*H 6.8, the capacity of vanadium is very high (1.2 m mol g^{-1}). Again the capacity for uranium(VI) was ~0.45 m mol g^{-1} at *p*H 4.0. Among the other metal ions studied titanium(IV), zirconium(IV), hafnium(IV), iron(III), copper(II) and cobalt(II) sorbed only below *p*H 3.0. Cobalt is absorbed in small amounts in the working range for vanadium. Thus, a clean separation of vanadium(V) from uranium(VI) and also from other elements is possible.

The rates of absorption of the metal ions were also determined. The time taken for 50% uptake of vanadium(V), titanium(IV), zirconium(IV) and hafnium(IV) varied between 1 and 6 h.

Acknowledgement

The authors gratefully acknowledge financial support of CSIR, New Delhi, and Dr S Basu for his val-

uable suggestions. They are also indebted to Thermax (P), Poona, for gift samples of styrene DVB and Prof R K Mishra for their gift samples of 1,2,3-phenyloxyamidine.

References

1 Majumdar A K, *N-Benzoylphenylhydroxylamine and its analogues* (Pergamon Press Ltd, Oxford) 1972.
2 Shome S C, *Analyst*, 75 (1960) 27.
3 Cornaz J P, Hutschnekar K & Duel H, *Helv chim Acta*, 40 (1957) 2015.
4 Petrie G, Hocke D & Meloan D, *Anal chim Acta*, 37 (1965) 919.
5 Welcher F J, *The analytical uses of ethylenediamine tetraacetic acid* (D Van Nostrand Company, Princeton, New Jersey) 1961, p 204.
6 Das J, Pobi M & Frescenius, *Z anal Chem*, 336 (1990) 578.
7 Mishra R K & Satyanarayan K, *Analyt Chem*, 46 (1974) 1609.
8 Kodama K, *Methods of quantitative inorganic analysis* (Interscience, New York) 1963, p 290.
9 Das J & Sengupta B, *Anal chim Acta*, 219 (1989) 339.

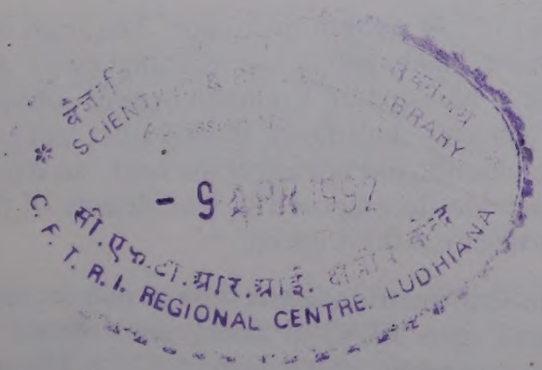

CSIR GOLDEN JUBILEE SERIES

BODY'S BATTLES

BAL PHONDKE

WAR makes rattling good history", said Oscar Wilde referring to the struggles of nations to capture new and to retain old territories. But other battles not visible to the naked eye are equally fascinating. An account of the miniscule wars fround within the confines of the human body is breathtaking if only for the fact that these are being fought every single living moment. The human body is continually besieged and attacked by a multitude of microbial enemies of great cunning and guile. However, nature has endowed the human body with an unique built-in defence organization that can be envy of the most modern technologically advanced nation.

This attractive and lavishly illustrated book, written especially for the non-specialist, unfolds the dramatic story of this inner defence organization, the diversity and specificity of its armament, and the methodical way in which it maintains a round the clock vigil to meet squarely every imaginable threat to the human body and also how it wins the body's battles most of the time.

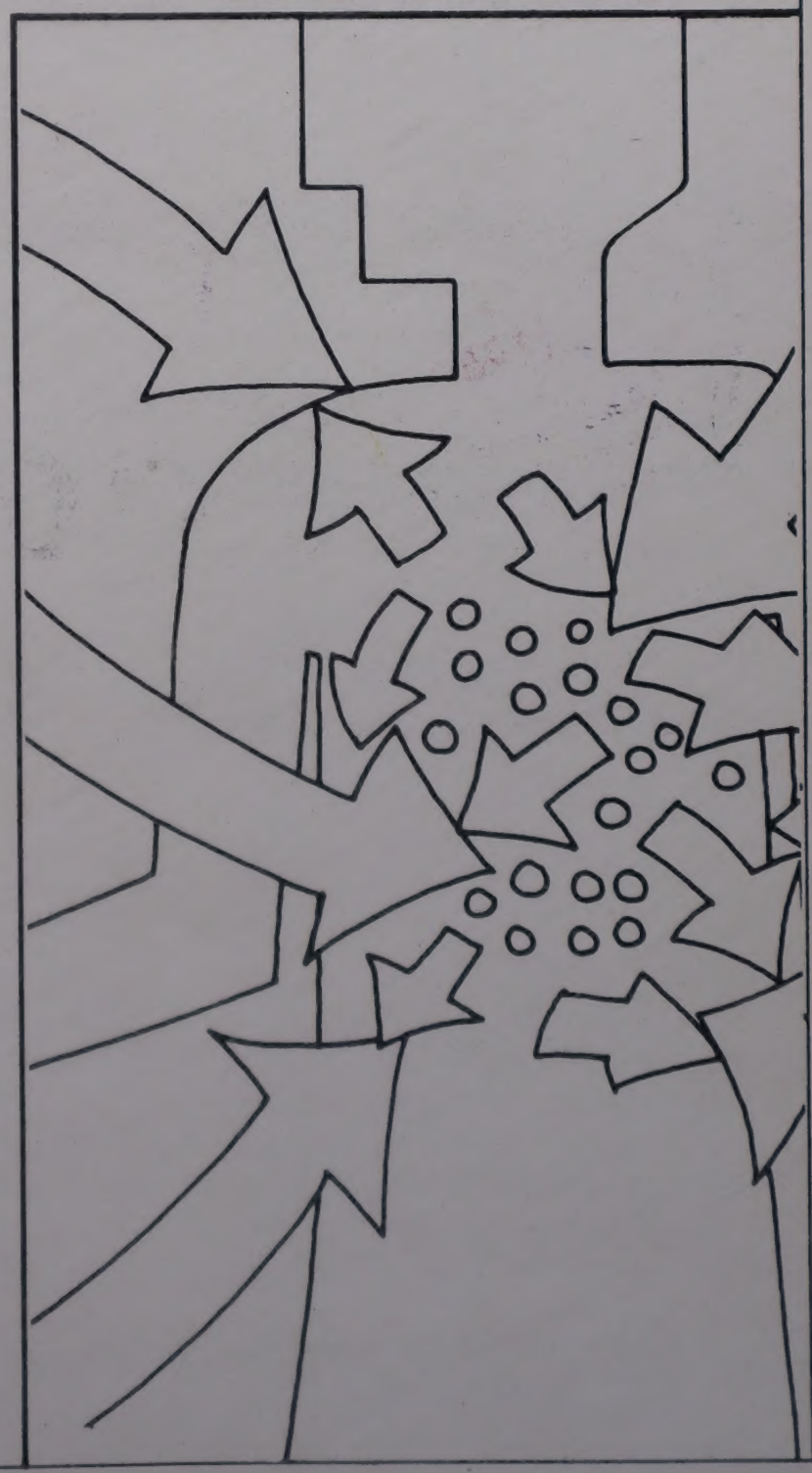

Price : Rs.9/- Paper back
:Rs.18/- Hard Bound

Orders should be accompanied by money order or Demand Draft made payable to PUBLICATIONS & INFORMATION DIRECTORATE, NEW DELHI and sent to:

The Senior Sales & Distributions Officer,
Publications & Information Directorate, CSIR
Dr K.S. Krishnan Marg,
New Delhi - 110 012

Printed & Published by Dr G.P. Phondke, Publications & Information Directorate (PID)
Dr K.S. Krishnan Marg, New Delhi 110 012, at PID Printing Unit

CLOSE ENCOUNTERS

Smoo ....ch. Slu ....rp. Sma ....ck.
Be it those naughty-haughty moments in campus, jive sessions at your favourite discotheque or those moments of leisure and pleasure with your spouse.
YES. For that real thing, Real comfort. Real thrill, Real quality and Real style.
Wear'em on and get going. Indulge in close encounters of action kind.

action®

★ Snooker ★ Nice time ★ Free line

DL-18023/92
RN 7090/63